

Modelling of combustion processes and NO formation with reduced reaction mechanisms

Citation for published version (APA):

Eggels, R. L. G. M. (1996). *Modelling of combustion processes and NO formation with reduced reaction mechanisms*. [Phd Thesis 1 (Research TU/e / Graduation TU/e), Mechanical Engineering]. Technische Universiteit Eindhoven. <https://doi.org/10.6100/IR450240>

DOI:

[10.6100/IR450240](https://doi.org/10.6100/IR450240)

Document status and date:

Published: 01/01/1996

Document Version:

Publisher's PDF, also known as Version of Record (includes final page, issue and volume numbers)

Please check the document version of this publication:

- A submitted manuscript is the version of the article upon submission and before peer-review. There can be important differences between the submitted version and the official published version of record. People interested in the research are advised to contact the author for the final version of the publication, or visit the DOI to the publisher's website.
- The final author version and the galley proof are versions of the publication after peer review.
- The final published version features the final layout of the paper including the volume, issue and page numbers.

[Link to publication](#)

General rights

Copyright and moral rights for the publications made accessible in the public portal are retained by the authors and/or other copyright owners and it is a condition of accessing publications that users recognise and abide by the legal requirements associated with these rights.

- Users may download and print one copy of any publication from the public portal for the purpose of private study or research.
- You may not further distribute the material or use it for any profit-making activity or commercial gain
- You may freely distribute the URL identifying the publication in the public portal.

If the publication is distributed under the terms of Article 25fa of the Dutch Copyright Act, indicated by the "Taverne" license above, please follow below link for the End User Agreement:

www.tue.nl/taverne

Take down policy

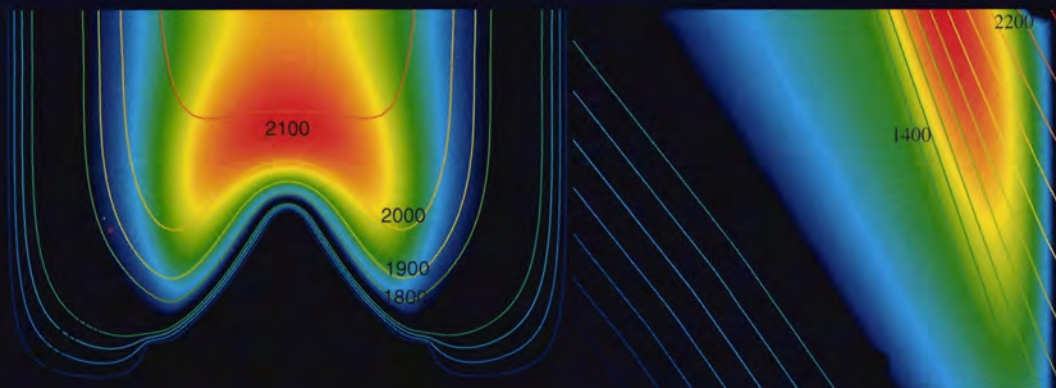
If you believe that this document breaches copyright please contact us at:

openaccess@tue.nl

providing details and we will investigate your claim.

Modelling of Combustion Processes and NO Formation with Reduced Reaction Mechanisms

R.L.G.M. Eggels



Modelling of Combustion Processes
and NO Formation with
Reduced Reaction Mechanisms

PROEFSCHRIFT

ter verkrijging van de graad van doctor aan de
Technische Universiteit Eindhoven, op gezag van
de Rector Magnificus, prof.dr. J.H. van Lint, voor
een commissie aangewezen door het College van
Dekanen in het openbaar te verdedigen op vrijdag
29 maart 1996 om 16.00 uur

door

Rudolf Leonardus Gerardus Maria Eggels

geboren te Wessem

Dit proefschrift is goedgekeurd door de promotoren:

prof.ir. J.K. Nieuwenhuizen

prof.dr. R.M.M. Mattheij

en de copromotor:

dr. L.P.H. de Goeij

Dit proefschrift is mede tot stand gekomen door de financiële bijdrage van GASTEC N.V. te Apeldoorn en NOVEM te Utrecht.

CIP-DATA KONINKLIJKE BIBLIOTHEEK, DEN HAAG

Eggels, Rudolf Leonardus Gerardus Maria

Modelling of combustion processes and NO formation with reduced reaction mechanisms / Rudolf Leonardus Gerardus Maria Eggels. - Eindhoven : Eindhoven University of Technology

Thesis Technische Universiteit Eindhoven. - With ref. - With summary in Dutch.

ISBN 90-386-0007-0

Subject headings: chemical kinetics / NO_x formation / reduced reaction mechanics.

Copyright ©1995 by R.L.G.M. Eggels

All rights reserved.

No part of the material protected by this copyright notice may be reproduced or utilized in any form or by any means, electronic or mechanical, including photocopying, recording or by any information storage and retrieval system, without permission from the publisher.

Printed in the Netherlands.

Contents

1	Introduction	1
1.1	Chemical Reacting Flows	4
1.2	Chemistry	7
1.3	Composition Space	9
1.4	Modelling of Flames with Complex Chemistry	12
1.5	Reduced Chemical Models	12
1.5.1	Partial-Equilibrium Assumptions	14
1.5.2	Steady-State Assumptions for Radicals	14
1.5.3	Mathematical Reduction Technique	15
1.5.4	Complete Decoupling of a Group of Species	15
1.6	The Application of Reduced Reaction Mechanisms	15
2	Mathematical Reduction Technique	19
2.1	Mathematical Reduction Technique	20
2.1.1	Complex Eigenvalues	23
2.1.2	Orthonormal Basis	24
2.1.3	Solution Method	25
2.2	Application of the Mathematical Reduction Technique to Flat Flames	27
2.2.1	Differential Equations for the Specific Element Mole Numbers	28
2.2.2	Differential Equations for the Reduced Reaction Mechanism	29
2.2.3	Projection Methods	33
2.3	Numerical Methods	37
2.3.1	Solution Strategy to Obtain a Manifold Point	37
2.3.2	Gridding Strategy	39
2.3.3	Parallel Processing	41
2.3.4	Linearization and Discretization of Flame Equations	41
2.3.5	Interpolation	45
2.3.6	Mesh Generation for One-Step Reduced Mechanism	49
2.4	The Application of Reduced Schemes in Turbulent Flames	49
2.4.1	Turbulent Combustion Modelling	50
2.4.2	Steady-States for Species	51
2.4.3	Partial-Equilibrium of Reactions	52

3 Applications of Reduction Methods	53
3.1 Adiabatic Hydrogen Air Flames	54
3.1.1 Results of Manifold Calculations	55
3.1.2 Flat Flame Calculations	58
3.1.3 Time Scale Analysis of the Full system	61
3.1.4 Two-Step Reduced Mechanism	64
3.2 Burner-Stabilized Flames	67
3.2.1 Results	68
3.3 Reduced Schemes for Carbon Monoxide- Hydrogen/Air Mechanisms	75
3.3.1 Introduction	75
3.3.2 Results	76
3.3.3 Influence on NO Formation	79
3.4 Mathematically Reduced Methane-Air Reaction Schemes.	80
4 Post-Processing Method for Modelling NO Formation	87
4.1 Thermal and Prompt NO Mechanisms	88
4.2 Flat Flame Computations using Various Reaction Mechanisms	92
4.3 Post-Processing Method	95
4.3.1 Steady-State Equations	96
4.3.2 Discretization	97
4.4 One-Dimensional Flames	100
4.4.1 Comparison of Post-Processor Results with Detailed Computations . .	101
4.4.2 Comparison of the Discretization Methods	103
4.4.3 Reaction Paths of NO	103
4.4.4 Adiabatic Flames	111
4.4.5 Comparison of Computations and Measurements	113
4.5 Two-Dimensional Flames	115
4.6 Empirical Model for Prompt NO Formation.	121
A Example Mathematical Reduction Technique	125
B Reaction schemes	133
Summary	137
Samenvatting	139
References	141
Acknowledgements	145
Curriculum Vitae	147

Chapter 1

Introduction

Combustion processes play a major role in energy conversion. Most of the energy necessary for transport and manufacturing is obtained through combustion of organic fuels. The use of combustion processes has a history of several thousands years, the development of the mathematical description, however, started much later. Due to the non-linear behaviour of the governing equations it is not possible to solve these equations analytically. Only recently, when fast computers and kinetic data became available, modelling of combustion processes is possible. The kinetics of hydrogen and methane combustion is well understood by now. Progress in developing reaction mechanisms of heavier hydrocarbons and soot formation is also being achieved. However, accurate predictions are still difficult due to the relatively large uncertainties in reaction rate data.

Although the chemical kinetics of simple hydrocarbons is reasonably well understood and the speed and storage capability of modern computers is increasing continuously, it is still impossible to model practical furnaces and burners using complex reaction mechanisms. Especially the modelling of turbulent flames is tremendously complicated, due to the large range of time and length scales. The modelling of laminar flames is easier since the flow is relatively simple. Nevertheless, even the application of detailed reaction schemes for laminar flames is limited to one- and simple two-dimensional geometries. To model more practical burners and to reduce the computational effort, reduced chemical reaction mechanisms are required.

Since a number of years, much research is spent in the development of reduced chemical models. The development of 'ad-hoc' one-step reduced models started already before detailed reaction mechanisms became available. Fuel and oxygen are assumed to be converted into combustion products in one step only. The reaction rate of such a reaction model is described by a small number of parameters. These parameters are obtained by fitting them to experiments or computations using detailed reaction mechanisms. Effects caused by complex transport processes, however, cannot be modelled adequately. It is also impossible to get information about the composition of exhaust gases. To limit environmental pollution, knowledge of CO and NO_x emission is essential. Therefore, more attention is focussed on the development of reduced chemical reaction models which are able to predict the detailed structures of flames appropriate. These models are based on the detailed reaction mechanisms, but reduce the computational effort considerably without losing too much accuracy.

Several approaches can be distinguished to reduce the full complex reaction mechanisms. In the first place, a reaction mechanism can be reduced straightforwardly by omitting less important species and reactions. Further reduction can be achieved by introducing algebraic equations for intermediate species instead of differential equations. This is the main objective of modern systematical reduction methods. The so-called Conventional Reduction Methods (CRM) are based on steady-state assumptions for intermediate species and partial-equilibrium assumptions for certain reactions. This method is introduced by Peters et al. first [Pet87], [Pet93]. The strategy applied to find out which species and reactions may be considered as steady-state or partial-equilibrium ones, however, requires much understanding of chemical kinetics. Nevertheless, this Conventional Reduction Method can be used successfully for modelling flames [Smo91], [Pet93], [Som94] as well as for modelling *NO* formation [Gla92], [Egg92].

Another method to simplify chemical kinetics is to separate the reaction system into fast and slow reaction groups, which are linear combinations of elementary reactions. The reactions which are fast and slow change during the combustion process. Therefore, it is complicated to find out the various reaction groups. It is, however, possible to separate the fast and slow the reaction groups automatically, so that less insight in chemical kinetics is required. Having determined the groups of fast and slow reactions, various approaches can be followed. Lam and Goussis [Lam88], [Gou92] use the information to find out which steady-state assumptions for the species and partial-equilibrium assumptions for a set of elementary reactions can be applied locally. This CSP (Computational Singular Perturbation) method can be used to solve the full set of differential equations of the complex reaction system fast and accurately. Furthermore, the knowledge of reaction groups with various time scales can also be used by applying partial-equilibrium assumptions for the fastest reaction groups [Maa92] [Egg95]. This method will be used in this thesis and will be referred to as Mathematical Reduction Technique (MRT) or Intrinsic Low-Dimensional Manifold (ILDM) method. The difference with the previously mentioned Conventional Reduction Methods is that the reaction groups are not related to individual species or elementary reactions. It has been shown [Maa92], [Maa93], [Egg94] that this (ILDM) method gives accurate results if it is used for a perfectly stirred reactor and flame calculations. As most reduction methods are developed only recently, still much research has to be invested in the application of reduced reaction mechanisms to model practical burner geometries.

At the Eindhoven University of Technology laminar and turbulent combustion processes are studied. The research on laminar flames was initiated by the VEG-Gasinstituut¹ and is supported by NOEM. The aim of the present project is to investigate the influence of variations in the composition of natural gas on the combustion process in domestic applications. Subjects such as flame stability and prediction of the composition of the exhaust gases are of main importance. In order to predict the effects of variations in gas composition on these properties, numerical tools for simulating combustion processes are needed. The development of these tools requires much knowledge of combustion processes. Initially, the chemistry was described in a rather simple way by an 'ad-hoc' one-step reaction mechanism (Fuel + Oxygen → Products) [Lan92]. To model various kinds of fuels, the chemical reaction parameters of the one-step model have been determined by use of measurements or computations using detailed reaction mechanisms. The burners chosen for the experiments and detailed computations should be sim-

¹Presently Gastec N.V.

ple and well defined for obtaining these parameters fast and efficiently. Flat-flame burners can be used successfully for this purpose [Mav94].

The one-step reduced reaction mechanisms are subsequently used for simulating flames on simple practical burners [Lan92], [Mal95]. It appeared that these models are suitable for modelling flame shape, stability and flashback behaviour reasonably well. One-step reaction models, however, cannot predict all aspects of the combustion process. Therefore, more detailed and systematic reduced reaction mechanisms have been considered instead [Som94]. The systematic reduced reaction mechanisms are based on the Conventional Reduction Method, as mentioned before. Starting with a detailed flame computation, it is studied for which species the steady-state assumptions are most accurate by applying a first order sensitivity analysis [Som94]. It appears that the use of detailed reaction mechanisms is practical for one-dimensional flames only. If simplified reaction mechanisms² are used, the simulation of two-dimensional flames is also possible, as long as the use is limited to simplified burner geometries. These simplified reaction mechanisms, however, do not include *NO* formation.

The aim of the research presented in this thesis is to develop methods to predict flames and *NO* formation using reduced chemical models. For the modelling of the flames, the recently developed Mathematical Reduction Technique, based on Intrinsic Low-Dimensional Manifolds is used, while relatively simple reaction mechanisms are used. Much effort has been given to the development and application of this reduction technique. Most attention will be paid to the application of the reduced reaction mechanisms to laminar flames. However, the reduced reaction mechanisms can also be used for turbulent flames. The reduction method is presented in chapter 2. Results of the Mathematically Reduced Technique applied to hydrogen/air, carbon monoxide-hydrogen/air and methane/air reaction are presented in chapter 3.

Furthermore, a method to model *NO* formation in laminar methane/air flames is developed. The reaction mechanisms which include *NO* reactions consist of at least 27 species³. One of the objectives of the present research is to develop a method for performing detailed *NO* computations, with a computational effort not much larger than needed for a detailed flame computation using a simple reaction mechanism. It will be shown that this can be achieved by decoupling the main combustion species from species involved in the nitrogen chemistry. The main combustion species are solved together with the flow equations, while the other are computed in a post-processing step. Furthermore, steady-state assumptions are introduced in the post-processing step for many intermediates. The method is presented in chapter 4. Post-processors for one-dimensional as well as for two-dimensional flames are developed. The results of the one-dimensional flames are compared with detailed computations and are compared with measurements on a ceramic foam surface burner.

In the remainder of this chapter, the conservation equations which describe chemical reacting flows are presented. As for non-reacting flows, transport equations for mass, momentum and energy are considered. For modelling chemical reacting flows, additional conservation equations for the various chemical components have to be taken into account. Further, the chemistry is described and the basics of the methods to reduce a chemical reaction mechanism are treated.

²The reaction mechanism consists of a minimum number of species, which is roughly equal to 10 to 16, depending on the kind of fuel.

³The most detailed reaction mechanism which is considered includes 51 species

1.1 Chemical Reacting Flows

The conservation of mass is expressed by the continuity equation:

$$\frac{\partial \rho}{\partial t} + \nabla \cdot (\rho \mathbf{v}) = 0, \quad (1.1)$$

where ρ denotes the mixture density and \mathbf{v} the flow velocity. The mixture density is the sum of the densities of the various species: $\rho = \sum_{i=1}^n \rho_i$, with n the number of species. The conservation equation for a species which we shall denote by an index i , is given by:

$$\frac{\partial \rho_i}{\partial t} + \nabla \cdot (\rho_i \mathbf{v}_i) = \dot{\rho}_i, \quad (1.2)$$

with \mathbf{v}_i the specific velocity of species i and $\dot{\rho}_i$ the chemical source term. How this source term is obtained from a detailed reaction mechanism will be described in section 1.2. After defining the mass fractions of the species by $Y_i = \rho_i / \rho$ and introducing the diffusion velocity $\mathbf{V}_i = \mathbf{v}_i - \mathbf{v}$, with \mathbf{v} the mass averaged velocity given by:

$$\rho \mathbf{v} = \sum_{i=1}^n \rho_i \mathbf{v}_i, \quad (1.3)$$

we obtain the following form for the continuity equation for the species (1.2):

$$\frac{\partial \rho Y_i}{\partial t} + \nabla \cdot (\rho Y_i \mathbf{v}) + \nabla \cdot (\rho Y_i \mathbf{V}_i) = \dot{\rho}_i. \quad (1.4)$$

With the use of the continuity equation (1.1), this can be rewritten as:

$$\rho \frac{\partial Y_i}{\partial t} + \rho \mathbf{v} \cdot \nabla Y_i + \nabla \cdot (\rho Y_i \mathbf{V}_i) = \dot{\rho}_i. \quad (1.5)$$

For multi-component mixtures the diffusion flux of species i depends on the concentration gradients of all species except for the concentration gradient of species i [Dix68], [Pet91], [Som94]. If one component is present in large amounts, which is the case for nitrogen for combustion processes with air as oxidator, the diffusion flux may be assumed to be proportional to the concentration gradient of species i , leading to Fick's law (Fick's law states that the diffusion flux $Y_i \mathbf{V}_i$ is proportional to the concentration gradient). If the gradient in the averaged molar mass is neglected, the diffusion flux is linear with the gradient in the mass fractions. If thermal diffusion, which is proportional to the temperature gradient, is also included the diffusion flux is given by:

$$Y_i \mathbf{V}_i = -D_i \nabla Y_i - \frac{D_i^T}{\rho T} \nabla T, \quad (1.6)$$

with D_i the diffusion coefficient and D_i^T the thermal diffusion coefficient of species i in the mixture. Thermal-diffusion is neglected in most cases, since it is relatively small. By substituting (1.6) and neglecting thermal diffusion we obtain the following convection diffusion equations for the species:

$$\rho \frac{\partial Y_i}{\partial t} + \rho \mathbf{v} \cdot \nabla Y_i - \nabla \cdot (\rho D_i \nabla Y_i) = \dot{\rho}_i, \quad (1.7)$$

Conservation of momentum is described by the Navier-Stokes equation:

$$\frac{\partial \rho \mathbf{v}}{\partial t} + \nabla \cdot (\rho \mathbf{v} \mathbf{v}) = -\nabla \cdot \mathbf{P} + \rho \mathbf{g}, \quad (1.8)$$

where \mathbf{P} denotes $p\mathbf{I} + \boldsymbol{\tau}$, with the pressure p , the identity matrix \mathbf{I} , the stress tensor $\boldsymbol{\tau}$ and \mathbf{g} denotes the gravitational acceleration.

The conservation of energy is described by:

$$\frac{\partial \rho u}{\partial t} + \nabla \cdot (\rho \mathbf{v} u) = -\nabla \cdot \mathbf{q} - \nabla \cdot (\mathbf{P} \cdot \mathbf{v}) + \rho \mathbf{v} \cdot \mathbf{g}, \quad (1.9)$$

with $u = \frac{1}{2}v^2 + \hat{u}$ the total energy density, \hat{u} the internal energy density and \mathbf{q} the heat flux vector. The term $\frac{1}{2}v^2$ represents the kinetic energy density. The conservation equation for the internal energy \hat{u} is obtained by subtraction of the dot product of \mathbf{v} with eq. (1.8) from eq. (1.9):

$$\frac{\partial \rho \hat{u}}{\partial t} + \nabla \cdot (\rho \mathbf{v} \hat{u}) = -\nabla \cdot \mathbf{q} - \mathbf{P} : (\nabla \mathbf{v}), \quad (1.10)$$

The internal energy is related to the enthalpy h by:

$$\hat{u} = h - p/\rho. \quad (1.11)$$

After substituting (1.11) into eq. (1.10) and writing $\mathbf{P} : (\nabla \mathbf{v})$ as $\boldsymbol{\tau} : (\nabla \mathbf{v}) + \rho \nabla \cdot \mathbf{v}$, the energy equation can be rewritten in terms of the enthalpy:

$$\rho \frac{\partial h}{\partial t} + \rho \mathbf{v} \cdot \nabla h - \frac{\partial p}{\partial t} - \mathbf{v} \cdot \nabla p = -\nabla \cdot \mathbf{q} - \boldsymbol{\tau} : (\nabla \mathbf{v}). \quad (1.12)$$

Fourier's law of thermal conductivity states that the heat flux is proportional to the temperature gradient. Furthermore, the heat flux vector includes the transport of specific species enthalpy by diffusion, leading to:

$$\mathbf{q} = -\lambda \nabla T + \rho \sum_{i=1}^n Y_i \mathbf{V}_i h_i, \quad (1.13)$$

where λ denotes the thermal conductivity and h_i the specific enthalpy of species i . The total enthalpy h is the mass weighted sum of the specific enthalpy of all species:

$$h = \sum_{i=1}^n Y_i h_i. \quad (1.14)$$

The specific enthalpy h_i is a function of the temperature given by:

$$h_i = h_i^0 + \int_{T_0}^T c_{p,i}(T') dT', \quad (1.15)$$

where h_i^0 is the heat of formation per unit mass at reference temperature T_0 and c_{p_i} is the specific heat at constant pressure per unit mass of species i . In order to rewrite the heat flux vector in terms of the enthalpy gradient, we introduce the mass weighted specific heat by:

$$c_p = \sum_{i=1}^n Y_i c_{p_i}. \quad (1.16)$$

Using the definition of the enthalpy (1.14) and the definition of the specific enthalpy (1.15) we may write:

$$dh = c_p dT + \sum_{i=1}^n h_i dY_i, \quad (1.17)$$

and thus:

$$\nabla h = c_p \nabla T + \sum_{i=1}^n h_i \nabla Y_i, \quad (1.18)$$

so that the heat flux vector \mathbf{q} becomes:

$$\mathbf{q} = -\frac{\lambda}{c_p} \nabla h - \sum_{i=1}^n h_i \left(\rho D_i - \frac{\lambda}{c_p} \right) \nabla Y_i, \quad (1.19)$$

where we substituted Fick law's for the diffusion flux (1.6) and neglected thermal diffusion. Since energy dissipation by viscous forces is relatively small, the term $\tau : (\nabla \mathbf{v})$ in the differential equation for the enthalpy (1.12) is neglected. Furthermore, pressure gradients are of minor importance in the energy balance because flow velocities are much lower than the speed of sound. As pressure variations are small compared to the atmospheric pressure, the pressure may therefore be assumed to be constant and may be derived from the ideal gas law:

$$p = \rho RT / \bar{M}, \quad (1.20)$$

with \bar{M} the average molar mass and R the universal gas constant. Pressure effects can be neglected in the energy equation since they are expected to be small due to the low flow velocity, the differential equation for the enthalpy reads:

$$\rho \frac{\partial h}{\partial t} + \rho \mathbf{v} \cdot \nabla h = \nabla \cdot \left(\frac{\lambda}{c_p} \nabla h \right) + \nabla \cdot \left(\sum_{i=1}^n h_i \left(\rho D_i - \frac{\lambda}{c_p} \right) \nabla Y_i \right). \quad (1.21)$$

The diffusion term can be simplified by introducing Lewis numbers Le_i , defined by:

$$Le_i = \frac{\lambda}{c_p \rho D_i}. \quad (1.22)$$

If the Lewis numbers are assumed to be constant, the ratio of heat and mass transport by diffusion is constant. Substitution of (1.22) in eq. (1.21) yields:

$$\rho \frac{\partial h}{\partial t} + \rho \mathbf{v} \cdot \nabla h - \nabla \cdot \left(\frac{\lambda}{c_p} \nabla h \right) = \nabla \cdot \left(\frac{\lambda}{c_p} \sum_{i=1}^n h_i \left(\frac{1}{Le_i} - 1 \right) \nabla Y_i \right). \quad (1.23)$$

This is a non-stationary convection diffusion equation for the enthalpy with a source term in the right-hand-side. If the convection diffusion equations of the species (1.7) are substituted in the right-hand-side of eq. (1.23) it can be seen that the source term of the enthalpy contains the chemical source terms of the species. If all Lewis numbers are equal to one, the source term is equal to zero. Then the heat flux due to temperature gradients is cancelled by the heat flux due to enthalpy transport through diffusion of the species. In reality the Lewis numbers of most species are close to unity, only the Lewis numbers of H and H_2 deviate strongly from 1.

This set of equations complete the set of equations which describe the transport of mass, momentum and energy in chemically reacting flows.

1.2 Chemistry

If a mixture contains chemically reacting species, conservation equations for each of the components have to be considered. These equations are coupled by the chemical source terms. Before presenting the general expression for the chemical source term, the contribution of only one specific reaction is considered. The following reaction is chosen as an example:



As a result of this reaction, concentrations of species O_2 and H will decrease and the concentrations of OH and O will increase in time. The number of molecules that react depends on the concentrations of species O_2 and H . The forward reaction rate r_1^f of reaction (1.24) is defined by:

$$r_1^f = k_1^f [O_2][H], \quad (1.25)$$

where $[O_2]$ denotes the concentration of species O_2 and k_1^f the elementary reaction rate coefficient. The index f indicates that the forward reaction is considered.

For a homogeneous system, the concentrations of the species considered here change in time due to this reaction according to:

$$\frac{d[OH]}{dt} = \frac{d[O]}{dt} = -\frac{d[O_2]}{dt} = -\frac{d[H]}{dt} = r_1^f \quad (1.26)$$

The elementary reaction rate coefficient is usually written in a so-called Arrhenius form:

$$k_1^f = A_1^f T^{b_1^f} \exp(-E_1^f/RT), \quad (1.27)$$

where A_1^f and b_1^f are reaction constants and E_1^f the activation energy. In general, the species may react also in opposite direction:



The reaction rate of this backward reaction is given by r_1^b and the net reaction rate of reactions (1.24) and (1.28) is given by $r_1 = r_1^f - r_1^b$:

$$r_1 = k_1^f [O_2][H] - k_1^b [OH][O]. \quad (1.29)$$

If the reaction is in chemical equilibrium the reaction rate r_j is zero, so that:

$$\frac{[OH][O]}{[O_2][H]} = \frac{k_1^f}{k_1^b} = K_1, \quad (1.30)$$

with K_1 the equilibrium constant of the reaction. The equilibrium constant can be derived from the thermo-dynamic properties of the species O_2 , O , OH and O . How this is done for a general reaction is explained later on.

In general a chemical reaction j can be written as follows:



where A_i represents the symbol of species i and $\nu_{ij} = \nu_{ij}'' - \nu_{ij}'$ are the stoichiometric coefficients of reaction j . If they are negative, they indicate the number of particles that disappear in the elementary reaction, otherwise they indicate the number of particles that are formed. If the concentration of species i is not changed by reaction j , the stoichiometric coefficient is equal to zero. For reaction (1.24) the stoichiometric coefficients ν_{ij} for O_2 , H , OH and O are equal to -1 , -1 , 1 , 1 , respectively.

The reaction rate for the general reaction (1.31) is given by:

$$r_j = k_j^f \prod_{i=1}^n ([A_i])^{\nu_{ij}'} - k_j^b \prod_{i=1}^n ([A_i])^{\nu_{ij}'}, \quad (1.32)$$

where $[A_i]$ denotes the concentration of species A_i .

In a chemically reacting system the source term, as it appears in the conservation equations of the species (1.2), contains the contributions of all chemical reactions:

$$\dot{\rho}_i = M_i \sum_{j=1}^{n_r} r_j \nu_{ij}, \quad (1.33)$$

with M_i the molar mass of species i and n_r the number of chemical reactions in the system.

For most reactions the reaction constants and activation energy which appear in the Arrhenius expressions (1.27) for the forward and backward reaction rate coefficients k_j^f and k_j^b can be found in literature. However, the equilibrium constants $K_j = k_j^f / k_j^b$ are well defined by thermo-dynamic properties of the species which are involved in the reaction [Str84]. The computation of the reverse reaction rate by $k_j^b = k_j^f / K_j$ gives a much more accurate prediction of the chemical equilibrium composition. The equilibrium constants are given by [Kee91]:

$$K_j = K_j^p \left(\frac{p}{RT} \right)^{\sum_{i=1}^n \nu_{ij}}, \quad (1.34)$$

where K_j^p is given by the change in entropy $\Delta \bar{s}_j$ and enthalpy $\Delta \bar{h}_j$ by reaction j , where we introduced \bar{s} and \bar{h} denoting the entropy and enthalpy given in Joule per mole, to distinguish them from s and h denoting the entropy and enthalpy given in Joule per unit mass.

$$K_j^p = \exp \left(\frac{\Delta \bar{s}_j}{R} - \frac{\Delta \bar{h}_j}{RT} \right), \quad (1.35)$$

where

$$\begin{aligned}\frac{\Delta \hat{s}_j}{R} &= \sum_{i=1}^n \nu_{ij} \frac{\hat{s}_i}{R}, \\ \frac{\Delta \hat{h}_j}{RT} &= \sum_{i=1}^n \nu_{ij} \frac{\hat{h}_i}{RT}.\end{aligned}\quad (1.36)$$

The enthalpies and entropies of the individual species are approximated by a sum of log-functions and polynomials in T , whose coefficients can be found in tables [Kee91]. This also holds for the specific heat. The expressions are given by:

$$\begin{aligned}\frac{\hat{h}_i}{RT} &= \sum_{k=1}^5 \frac{e_{ki}}{k} T^{k-1} + \frac{e_{6,i}}{T}, \\ \frac{\hat{s}_i}{R} &= e_{1,i} \ln(T) + \sum_{k=2}^5 \frac{e_{ki}}{k-1} T^{k-1} + e_{7,i}, \\ \frac{\hat{c}_{p,i}}{R} &= \sum_{k=1}^5 e_{ki} T^{k-1}.\end{aligned}\quad (1.37)$$

The coefficients are well tabulated in a thermodynamic database.

1.3 Composition Space

Until now, we used concentrations and mass fractions to describe the composition of the mixture. Instead of these variables, mole fractions and specific mole numbers are often used. The mole fractions X_i are given by:

$$X_i = [A_i] \bar{M} / \rho, \quad (1.38)$$

and the specific mole numbers by:

$$\phi_i = Y_i / M_i = X_i / \bar{M}. \quad (1.39)$$

The specific mole numbers denote the number of moles of species i per unit mass of the mixture. We use the specific mole numbers throughout this thesis. The use of specific mole numbers has the advantage that the molar masses do not appear explicitly in the differential equations for the species. Furthermore, the conservation equations for the chemical elements have a simplified form in terms of specific mole numbers. The elements are the atoms from which the molecules of the various species are composed. Similarly as done for the species we can define specific element mole numbers:

$$X_j = \frac{z_j}{W_j}, \quad (1.40)$$

where z_j indicates the mass fraction of element j and W_j the molar mass of element j . The hydrocarbon/air mixtures discussed in this thesis consist of only four elements: C , H , O and

N . In general, the number of elements is given by n_e . The specific element mole numbers are obtained from the specific mole numbers of the species by:

$$\chi_j = \sum_{i=1}^n \mu_{ji} \phi_i, \quad (1.41)$$

where the μ_{ji} denote the element composition coefficients. These element composition coefficients denote the number of atoms of kind j in species i . From the definition of μ_{ji} it is clear that the molar mass M_i of species i is given by:

$$M_i = \sum_{j=1}^{n_e} \mu_{ji} W_j. \quad (1.42)$$

As the mass fractions of all species sum to one, the following relation for the specific element mole numbers can be derived:

$$\sum_{i=1}^n Y_i = \sum_{i=1}^n M_i \phi_i = \sum_{i=1}^n \sum_{j=1}^{n_e} \mu_{ji} W_j \phi_i = \sum_{j=1}^{n_e} W_j \chi_j = 1, \quad (1.43)$$

which states that $\sum_{j=1}^{n_e} z_j = 1$. If equation (1.41) would be written in terms of mass fractions, the element composition coefficients would be equal to the ratio of the molar masses of the species and the elements. The use of specific mole numbers, however, provides that the coefficients μ_{ji} have integer values.

The composition of a mixture is given by the specific mole numbers of all species: ϕ_1, \dots, ϕ_n . In vector notation this can briefly be written as $\phi = (\phi_1, \dots, \phi_n)^T$. The differential equations for a homogeneous system in vector notation read:

$$\rho \frac{d\phi}{dt} = \text{diag}(1/M_1, \dots, 1/M_n) \dot{\rho} \quad (1.44)$$

with chemical source term $\dot{\rho} = (\dot{\rho}_1, \dots, \dot{\rho}_n)^T$. This source term itself can be written in terms of reaction vectors ν_k , using (1.33):

$$\dot{\rho} = \text{diag}(M_1, \dots, M_n) \begin{pmatrix} | & & | \\ \nu_1 & \dots & \nu_n \\ | & & | \end{pmatrix} \begin{pmatrix} r_1 \\ \vdots \\ r_n \end{pmatrix}. \quad (1.45)$$

The vector notation is associated with the description of the mixture in the so-called composition space. Defining basis vectors which correspond to the species, the specific mole numbers (ϕ_1, \dots, ϕ_n) are the coordinates in this composition space. A reaction vector indicates in which direction the composition will change by that reaction. How fast a composition will change in the direction of such a reaction vector is indicated by the reaction rate r_i . A complex reaction process will be controlled by many reactions as given by (1.45). The direction in which the composition will change depends on the magnitude of the reaction rates r_1, \dots, r_n . As these

reaction rates change in time or space, also the reactions that determine the progress of the process and the direction of the process change. Therefore, the reaction path may have a complex shape.

In vector notation the conservation equations of elements (1.41) becomes:

$$\chi_j = (\mu_j, \phi), \quad (1.46)$$

with μ_j the element composition vectors. As the elements are conserved in elementary reactions it can be shown that:

$$(\mu_j, \nu_k) = 0. \quad (1.47)$$

This holds for all reactions k and elements j . Equation (1.47) indicates that all reaction vectors are perpendicular to all element composition vectors. The reaction source term vector $\dot{\rho}$ is a linear combination of elementary reaction vectors, as given by (1.33), and is also perpendicular to the element composition vectors:

$$(\mu_j, \dot{\rho}) = 0. \quad (1.48)$$

As the chemical source term vector is perpendicular to the element composition vectors, the element composition vectors define directions in composition space in which no movements due to chemical reactions are possible. Only diffusion effects may change the specific element mole numbers. Therefore, movements in composition space due to chemical reactions are restricted to a lower $(n - n_e)$ dimensional subspace, the so-called reaction space. The complementary part of this reaction space in composition space is spanned by the element composition vectors.

Example

We end this section with an example in which the properties defined above are illustrated. Suppose we have the following species: O_2 , H , OH , O , H_2 , H_2O , HO_2 so that the number of species n is 7. The species are composed of two elements O and H , thus $n_e = 2$. The natural basis vectors of the composition space are ordered in the same way as the species are presented. Furthermore, if we consider the following reaction:



the specific mole number vector ϕ , reaction vector ν and the element composition vectors μ_O and μ_H are given by:

$$\phi = \begin{pmatrix} \phi_{O_2} \\ \phi_H \\ \phi_{OH} \\ \phi_O \\ \phi_{H_2} \\ \phi_{H_2O} \\ \phi_{HO_2} \end{pmatrix}, \quad \nu = \begin{pmatrix} -1 \\ -1 \\ 1 \\ 1 \\ 0 \\ 0 \\ 0 \end{pmatrix}, \quad \mu_O = \begin{pmatrix} 2 \\ 0 \\ 1 \\ 1 \\ 0 \\ 1 \\ 2 \end{pmatrix}, \quad \mu_H = \begin{pmatrix} 0 \\ 1 \\ 1 \\ 0 \\ 2 \\ 2 \\ 1 \end{pmatrix}. \quad (1.50)$$

It is easy to see that $(\mu_O, \nu) = 0$ and $(\mu_H, \nu) = 0$, as required by (1.47).

1.4 Modelling of Flames with Complex Chemistry

To model laminar combustion processes the previously presented conservation equations for mass, momentum and energy for the averaged mixture properties have to be solved. Furthermore, for each species a conservation equation has to be considered. Solving this set of equations is the key problem in combustion modelling. As the number of species for methane/air flames is at least 16, these are not only a lot of equations, but the equations for the various species are also strongly coupled by the chemical source terms. The chemical source term contains a wide range of time scales $\tau_k = \frac{\rho}{M r_k}$ arising from the various chemical reactions. This implies that the set of equations is stiff. In practice, this means that the differential equations for the species have to be solved by use of implicit techniques, which leads to a large set of linearized algebraic equations. An often used technique to solve the set of non-linear equations is Newton's method. This method requires the computation of a Jacobian matrix which is a very CPU intensive task. The computational effort to compute a Jacobian matrix is proportional to the square of the number of variables. In spite of the increasing speed of computers it is still not possible to compute flames in more-dimensional practical burner geometries using complex reaction schemes within reasonable time. Therefore, much attention has been devoted recently to the development of methods to reduce the number of variables that have to be solved together with the flow equations. Several approaches to reduce the reaction mechanism are described in the next section. In section 1.6 the approach which will be followed and problems encountered with the application of the various techniques will be sketched.

1.5 Reduced Chemical Models

The easiest way to reduce the reaction system is the elimination of less important species and reactions, by which the reaction path is hardly influenced. The gain of this elimination, however, is limited. For instance, the minimum number of species of a methane/air reaction mechanisms that gives appropriate results is 16. If, however, information about *NO* formation is desired, the number of species is much larger (about 27). To reduce the number of variables further, other reduction methods have to be used.

The computational effort can be reduced further by splitting the reaction mechanism into two groups of species. One part of the reaction mechanism is solved together with the flow equations. The second part can be treated in a variety of ways. In fact, splitting the reaction mechanism and decoupling of one part, is the basis of all subsequent reduction techniques. The differences between the various approaches are found in the method to separate the reaction mechanism. It is clear that the computational effort depends on the number of species which are solved together with the flow equations and on the computational effort necessary to solve the second group of species. If, for example, the equations of the second group of species are solved by using an implicit method, the maximal reduction of the computational effort to obtain the Jacobian matrices is a factor of two⁴. Such a decoupling of species could, however, imply an

⁴Note that the computational effort is proportional to the number of species squared. If the reaction mechanism is split into two groups of the same size, the computational effort is proportional to $2 * (n/2)^2 = n^2/2$

increase of the number of necessary iterations. Therefore, decoupling the species and solving the equations, by an implicit method does not give much computational benefits. More sophisticated reduction methods which decouple a special part of the full system will be considered in the following.

As the original set of differential equations is stiff, the best way to reduce the reaction mechanism is to remove part of the stiffness. This, however, implies a modification of the equations. To remove fast time scale processes and therefore also to reduce the stiffness of the equations, we have to study the reaction system in more detail.

The stiffness of a chemical reaction system finds its origin in the wide range of time scales of the system. In a chemical reacting system many species and reactions are involved and the reaction rates may differ several orders of magnitude. The progress of a combustion processes is determined by indispensable slow reactions. If the time scales of the chemical source term are compared with the range of physical time scales, observed in real combustion processes, it is seen that the range of physical time scales associated with convection and diffusion processes is much smaller than the range of chemical time scales. The range of physical and chemical time scales is sketched in Figure 1.1. The chemical source term contains some fast time scale

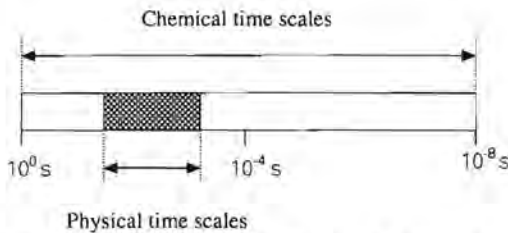


Figure 1.1: Typical ranges of chemical and physical time scales

processes, whereas in practice the entire reaction process is much slower. This means that reactions which correspond to small time scales will be in partial-equilibrium soon after initiation and will remain in partial-equilibrium during the subsequent combustion process. This implies that movements in certain directions in reaction space are more or less frozen. As soon as the fastest reaction groups are relaxed towards a steady-state situation, the combustion process will effectively take place in a low-dimensional manifold. If we could describe this manifold, a reduced model of the chemical system could be associated with movements on this manifold. This model describes the evolution corresponding to relatively large time scales, while processes associated with small time scales are assumed to be in steady-state. As this manifold is a subspace of the reaction space it can be described by a reduced number of variables.

The key problem of reducing reaction mechanisms is to identify the fast and slow processes. Several approaches will be considered in the next subsections. First, Conventional Reduction Methods, as introduced by Peters et al. [Pet91] to reduce a reaction system will be considered. These methods are based on partial-equilibrium assumptions for some reactions and steady-state assumptions for some intermediate species. A Mathematical Reduction Method will also

be treated. This method, developed by Maas and Pope [Maa92], separates the chemical source term in fast and slow reaction groups and assumes fast reaction groups in steady-state. The decoupling in fast and slow reaction groups is obtained by using an eigenvector analysis of the Jacobian matrix of the source term. The last reduction method which will be presented is based on the fact that it is sometimes possible to decouple a group of species which are associated with slow processes of the reaction mechanism, totally. These species can subsequently be modelled in a post-processing method.

1.5.1 Partial-Equilibrium Assumptions

The most straightforward approach to identify the fast processes is to associate them with elementary reactions with large reaction rates. It is relatively easy to define a time scale for a specific reaction. This time scale may be written as: $\tau_k = \rho / (\bar{M}r_k)$. The progress of the reaction process will be limited by slow reactions so that fast reactions will be in partial-equilibrium. This means that the net reaction rate of the fast reactions is small, whereas the forward and backward reaction rates are large. If the fastest reactions are known, the reaction rates can be set to zero, leading to algebraic equations. However, an important drawback of this method is that the reactions which are important during the combustion process change in time and space. Radicals are formed in an early stage of the combustion process, whereas they recombine in later stages. The reactions by which radicals are formed and recombined are generally different. Furthermore, in general there are more reactions than species, so that the application of partial-equilibriums assumptions involves a selection of reactions. Knowledge of chemical kinetics is essential to choose the partial equilibrium assumptions appropriately.

1.5.2 Steady-State Assumptions for Radicals

In another approach the fast time scales are not associated with elementary reactions, but with species. Since radicals are formed and recombined fast, it is likely to associate fast processes with a group of reactions which form or destruct a radical. If a radical is formed by a certain reaction, the effect of this reaction will be cancelled immediately by an other reaction which removes the radical. This means that the net source term of a species will be small compared to the 'production' $\dot{\rho}_i^{(+)}$ and 'consumption' part $\dot{\rho}_i^{(-)}$ (the net source term is given by $\dot{\rho}_i = \dot{\rho}_i^{(+)} - \dot{\rho}_i^{(-)}$). The reaction mechanism can be simplified by introduction of steady-state relations $\dot{\rho}_i = 0$. Introduction of steady-state assumptions for several intermediate species means that the chemical source term vector $\dot{\rho}$ is frozen in certain directions.

The application of partial-equilibrium and steady-state assumptions has been used in many applications [Smo91], [Pet93], [Som94]. In this thesis, steady-state assumptions for radicals are applied in a post-processing method which is used to model the formation of *NO* in laminar premixed methane/air flames. This post-processing method will be considered in subsection 1.5.4 and is described in detail in chapter 4.

1.5.3 Mathematical Reduction Technique

A recently developed method to reduce a reaction mechanism [Maa92] tries to find out in which directions the source term vector will reach a steady-state rapidly. The directions are not associated with individual species or elementary reactions and are not fixed throughout the combustion process as for the Conventional Reduction Method. These directions are obtained from the chemical reaction system itself. The dynamic behaviour of the chemical source term is studied by perturbing the composition in all possible directions. The specific mole numbers for each species are changed and the effect on the chemical source term is examined. In this way the Jacobian matrix of the source term $\frac{dP}{d\phi}$ is evaluated and in chapter 2 it will be shown that the eigenvalues of this Jacobian matrix are associated with the typical chemical time scales of the chemistry. The corresponding eigenvectors are associated with reaction groups. Subsequently, steady-state assumptions are introduced for fast reaction groups; only slow reaction processes remain. The method estimates the fast and slow reaction groups, locally. Therefore, the reduced reaction mechanism will be optimal at every stage in the reaction process. This Mathematical Reduction Technique (which determines Intrinsic Low-Dimensional Manifolds) is more complicated than Conventional Reduction Methods because of the fact that the eigenvectors, the reaction groups and the steady-state equations are not constant throughout the combustion process.

1.5.4 Complete Decoupling of a Group of Species

In the previous subsections, we considered methods to reduce the stiffness of the reaction system by applying partial-equilibrium or steady-state assumptions for either reactions, radicals or reaction groups. If a reaction mechanism contains a large number of species, the computational effort for solving a combustion process with a detailed reaction mechanism can also be reduced considerably by decoupling a group of species from the mechanism. One group of major combustion species is first solved together with the flow equations, while the second group of species is solved in a post-processing step. If this strategy is followed, the influence of the second group on the first group should be small. This means that at least the mass fractions of the species which are solved in a post-processing step must be small. Moreover, these species may not be essential for the combustion process. However, the question arises which species are suitable to be decoupled. Furthermore, why should species with very low mass fractions, which are not essential for the combustion process, be modelled at all? The answer can be found from the fact that some species are associated with pollutant emission and accurate prediction of the mass fractions of these species is essential to design clean burners. For instance, complex reaction mechanisms are necessary for an accurate prediction of NO_x formation. The concept of solving NO formation in a post-processing step is used in chapter 4.

1.6 The Application of Reduced Reaction Mechanisms

In the following chapters the above mentioned reduction methods will be discussed in more detail. To give the reader an impression of the approach which is followed and the problems

encountered, a brief outline of the approach and problems associated with the application of the methods will be given finally.

The use of reduced reaction mechanisms implies that the differential equations for a reduced number of variables have to be solved in flame calculations. Furthermore, the steady-state or equilibrium relations have to be treated mathematically and numerically. In principle, the entire set can be solved by an implicit method, like Newton. However, not much computational gain can be achieved. Since the reduction method implies a decrease of the stiffness of the system, the steady-state equations can be solved by faster explicit methods. However, the equations are still non-linear and convergence depends on the specific combustion problem considered. Furthermore, an often observed additional problem is that the steady-state or partial equilibrium assumptions are not well defined for low temperatures. This may cause computational problems: some radical concentrations tend to become infinite or to have negative values.

Sometimes it is possible to truncate the set of steady-state assumptions. This means that the steady-state relation of one species is rewritten so that it depends on previous computed species only. The set of steady-state species can be solved in one computational step so that the computational gain is large [Pet93] [Som94]. A drawback is that the truncation of the set of steady-state relations is a complicated task and is often not possible. A truncation can then be enforced, by modifying the steady-state equations. However, this introduces inaccuracies in the solution.

In turbulent combustion modelling it is common practice to solve the steady-state equations as a function of some progress variables and store the solution in look-up tables. The progress or control variable should be a variable that changes monotonously during the combustion process. For instance, the mass fractions of the fuel, H_2O , CO_2 are suitable control variables. For an n_c reduced scheme, n_c progress variables are introduced. This approach of using look-up tables is also applied in the Mathematically Reduction Technique, because a relatively large amount of time is necessary to obtain the fast and slow reaction groups from an eigenvector analysis of the chemical source term.

The drawback of look-up tables is that they can become very large if the dimension of the reduced scheme increases. However, the storage capacity of modern computers increases continuously while the price per mega-byte decreases rapidly.

In order to model flames with the reduced mechanism, differential equations have to be derived from the complete set of differential equations. As the reduced scheme may be considered as a low-dimensional manifold in the higher dimensional reaction space, the transformation from n differential equations of the species into n_c differential equations for the control variables is a projection method. For conventional reduced mechanisms, with steady-state assumptions, the projection is easy. In this case no variations in the direction of the steady-state species are possible and these directions remain constant throughout the combustion process. Therefore, the projection filters the effect of steady-state species out. The remaining differential equations are the differential equation for the non steady-state species. If the Mathematical Reduction Technique is used, the projection is more complicated because the slow reaction groups are not constant. How these differential equations for the control variables are derived, can be found in chapter 2.

Finally, one may wonder how accurate these reduced mechanisms are. In principle, the di-

mension (number of differential equations) of the reduced scheme is chosen beforehand. Note that it is not possible to determine the most appropriate dimension of the reduced mechanism in advance. This holds for conventional (CRM) as well as for the mathematical (MRT) reduction methods. Comparison with detailed computations for simple burner geometries should prove that the reduced scheme is appropriate. The Mathematical Reduction Technique, however, makes it possible to examine the eigenvalues on the manifold, which are representing the chemical time scales. These time scales can be compared with the time scales of convection and diffusion. This gives an indication whether the reduced scheme will be appropriate or not.

Chapter 2

Mathematical Reduction Technique

Several techniques to reduce chemical reaction mechanisms have been introduced in chapter 1. In the present chapter, we focus on the Mathematical Reduction Technique. This method, introduced by Maas and Pope [Maa92] is based on the existence of Intrinsic Low-Dimensional Manifolds (ILDM) in reaction space. These manifolds are subspaces in composition space where only slow processes take place: the fast processes are in steady-state. As a result these manifolds will have the property that they attract reaction trajectories. Reaction paths found from detailed computations of reaction processes will proceed towards this manifold fast, while the subsequent movement on the manifold is much slower. A reduced model of a complex reaction mechanism is associated with movements within this manifold. As mentioned before, the manifold is characterized by slow reaction groups of the chemical source term. The full chemical source term is separated into fast and slow reaction groups using an eigenvector analysis of the Jacobian matrix of the chemical source term. As this eigenvector analysis is a computationally intensive task, the manifold is computed before the actual flame modelling. To this end, the manifold is parameterized by a number of control or progress variables. For discrete values of these control variables, manifold compositions are computed and stored in a data base. For the actual modelling of the combustion processes, differential equations for the control variables are solved together with the flow equations. These equations are derived from the complete set of differential equations for the species. During the flame computation the manifold map is used to obtain the mixture composition by use of an interpolation method.

The mathematical basis of the reduction technique is presented in section 2.1. The governing equations which define the manifold, are derived from the steady-state relations. Next, the solution method used for solving these equations is treated. The application of the mathematically reduced reaction mechanism is presented in section 2.2. Differential equations for the control variables and the specific element mole numbers are derived. Numerical aspects applied for the computation of the manifold data base are presented in section 2.3. In this section the solution procedure and the generation of the locally refined grid for the manifold and the extension of the algorithm for implementation on parallel computers is treated. Furthermore, the linearization, discretization and interpolation methods, which are used to model flat flames, are also presented in section 2.3. As the mathematically reduced reaction mechanisms can be used for modelling turbulent combustion problems too, the concept of modelling turbulent flames is

explained briefly in section 2.4. Results of a number of applications of the reduction method are presented in chapter 3. An example where the Mathematical Reduction Technique is applied to a simple reaction mechanism is presented in Appendix A.

2.1 Mathematical Reduction Technique

To reduce the chemical reaction system, it is sufficient to consider the differential equations of the various species. The conservation equations of the species (1.7) in terms of specific mole numbers ($\phi_i = Y_i/M_i$) are given by:

$$\rho \frac{\partial \phi_i}{\partial t} + \rho v \cdot \nabla \phi_i - \nabla \cdot (\rho D_i \nabla \phi_i) = \rho w_i, \quad (2.1)$$

The chemical source term of species i is now written as: $w_i = \frac{\rho}{M_i}$. To study the chemical nature of the reaction system the convective and diffusive terms in eq. (2.1) can be omitted for the time being, so that the differential equations for a homogeneous time-dependent system remain:

$$\frac{d\phi_i}{dt} = w_i. \quad (2.2)$$

To obtain knowledge about fast and slow processes, the source term $\mathbf{w} = (w_1, \dots, w_n)^T$ is linearized around a reference composition ϕ^0 :

$$\mathbf{w} \approx \mathbf{w}(\phi^0) + \mathbf{J}(\phi - \phi^0), \quad (2.3)$$

where $\mathbf{J} = \left(\frac{\partial w_i}{\partial \phi_j} \right)_{\phi^0}$ denotes the Jacobian matrix of the source term. Substitution of (2.3) in eq. (2.2) gives:

$$\frac{d\phi}{dt} \approx \mathbf{w}(\phi^0) + \mathbf{J}(\phi - \phi^0). \quad (2.4)$$

The local characteristics of the system can be examined by transforming these equations into the basis of eigenvectors of the Jacobian matrix. The eigenvectors \mathbf{s}_i are defined by:

$$\mathbf{J}\mathbf{s}_i = \lambda_i \mathbf{s}_i, \quad (2.5)$$

with λ_i the eigenvalues of the Jacobian matrix. If we define the transformation matrix by $\mathbf{S} = (\mathbf{s}_1, \dots, \mathbf{s}_n)$, assuming that \mathbf{J} is diagonalisable, we obtain from the definition of the eigenvectors:

$$\mathbf{J}\mathbf{S} = \mathbf{S}\mathbf{\Lambda}, \quad (2.6)$$

where $\mathbf{\Lambda} = \text{diag}(\lambda_1, \dots, \lambda_n)$, only the diagonal elements of the latter matrix are non-zero. Multiplication of (2.6) on the left by \mathbf{S}^{-1} yields:

$$\mathbf{\Lambda} = \mathbf{S}^{-1}\mathbf{J}\mathbf{S}. \quad (2.7)$$

Note that the eigenvalues and eigenvectors may be complex quantities in general. We will associate reaction groups with eigenvectors and define steady-state relations in terms of eigenvectors, which is only meaningful if these reaction groups are real. In the next section we will discuss how a modified eigenvector basis, consisting of real valued vectors, is constructed. Here, however, the eigenvectors may be complex.

Writing the specific mole numbers in the eigenvector basis as $\hat{\phi}_i$ and using the transformation $\phi = S\hat{\phi}$, the linearized equations for the homogeneous system in the basis of eigenvectors are given by:

$$\frac{d\hat{\phi}}{dt} \approx \hat{w}(\hat{\phi}^0) + \Lambda(\hat{\phi} - \hat{\phi}^0). \quad (2.8)$$

Note that the time dependency of the eigenvectors is not taken into account, since we consider the linearized system. As a result of the transformation into the basis of eigenvectors, the differential equations in eq. (2.8) are decoupled and the solutions are given by:

$$\hat{\phi}_i = \hat{\phi}_i^0 + \frac{\hat{w}_i(\hat{\phi}^0)}{\lambda_i} (\exp(\lambda_i t) - 1). \quad (2.9)$$

Considering (2.9) we may conclude the following about the typical time scales of the reaction system. If the absolute value of an eigenvalue is small, thus ($|\lambda_i| \ll 1$), the exponent may be written as $\exp(\lambda_i t) = 1 + \lambda_i t$, so that:

$$\hat{\phi}_i - \hat{\phi}_i^0 = w_i t, \quad (2.10)$$

indicating that the typical scales are given by $1/w_i$. On the other hand, if the absolute value of the real part of an eigenvalue is large, the typical time scale is found from the exponent:

$$\tau_i = 1/|\Re(\lambda_i)|. \quad (2.11)$$

From the expressions (2.10) and (2.11) for the typical time scales of the chemical source term the following can be concluded. If the magnitude of an eigenvalue is large, movements in the direction of the corresponding eigenvector will proceed fast. The larger the magnitude of the eigenvalue, the faster the process will be. Further we can distinguish different ways of behaviour. First, processes which correspond to negative eigenvalues will extinguish and will arrive in a steady-state situation finally. Processes which correspond to eigenvalues with a large imaginary part have an oscillating behaviour and processes which correspond to positive eigenvalues will not relax towards a steady-state situation either. Finally, some eigenvalues may be equal to zero. The corresponding eigenvectors are associated with conserved quantities (we show this is the next paragraph).

Having considered the behaviour of the reaction groups depending on the eigenvalues, it can be concluded that the introduction of steady-state equations is most suitable for reaction groups corresponding to eigenvalues with large negative real parts. Note that all eigenvalues must be zero or negative at the equilibrium point, where $\frac{d\phi_i}{dt} = 0$. When combustion processes are studied, it can be observed that most eigenvalues have negative real parts while the magnitude is large. This was shown by Maas and Pope for carbonmonoxide/hydrogen-air reaction systems

[Maa92] and will be shown in chapter 3 for hydrogen/air reaction systems. The existence of many eigenvalues with large negative real parts is essential in order to reduce the reaction mechanism by the Mathematical Reduction Technique.

In the following, we show that conserved quantities correspond to eigenvalues which are zero. As indicated by eq. (1.48) the specific element mole numbers are conserved quantities. The element composition vectors μ_i are left eigenvectors of the Jacobian matrix; this can be seen by considering:

$$\begin{aligned} (\mu_i)^T \mathbf{J} &= (\mu_{i1}, \dots, \mu_{in}) \begin{pmatrix} \frac{\partial w_1}{\partial \phi_1} & \dots & \frac{\partial w_1}{\partial \phi_n} \\ \vdots & & \vdots \\ \frac{\partial w_n}{\partial \phi_1} & \dots & \frac{\partial w_n}{\partial \phi_n} \end{pmatrix} = \\ &= \left((\mu_i, \frac{\partial w}{\partial \phi_1}), \dots, (\mu_i, \frac{\partial w}{\partial \phi_n}) \right) = \left(\frac{\partial}{\partial \phi_1} (\mu_i, w), \dots, \frac{\partial}{\partial \phi_n} (\mu_i, w) \right) = \mathbf{0}^T, \end{aligned} \quad (2.12)$$

which is the definition of a left eigenvector with $\lambda_i = 0$. As there are n_e elements there have to be at least n_e eigenvalues which are equal to zero.

If the eigenvalues are arranged in such a way that the eigenvalues with the highest index correspond to fastest damping reaction processes, the steady-state equations can be formulated easily as:

$$\frac{d\phi_i}{dt} = 0, \quad i = n_c + n_e + 1, \dots, n, \quad (2.13)$$

where n_c denotes the dimension of the reduced reaction mechanism. This can be achieved by ordering the eigenvalues in descending order of real part: $\Re e(\lambda_1) \geq \dots \geq \Re e(\lambda_n)$. Note that this ordering implies that only fast processes which correspond to negative eigenvalues are assumed to be in steady-state. Moreover, we assume that there are enough eigenvalues with large negative real parts.

To obtain the steady-state relations in the original basis we transform Eq. (2.13) using the transformation matrix \mathbf{S}^{-1} which may be written as:

$$\mathbf{S}^{-1} = \begin{pmatrix} - & (s_1^L)^T & - \\ & \vdots & \\ - & (s_n^L)^T & - \end{pmatrix}, \quad (2.14)$$

where obviously the s_i^L denote the left eigenvectors of the Jacobian matrix, i.e.,

$$(s_i^L)^T \mathbf{J} = \lambda_i (s_i^L)^T. \quad (2.15)$$

so that:

$$\mathbf{S}^{-1} \mathbf{J} = \Lambda \mathbf{S}^{-1}. \quad (2.16)$$

From \mathbf{S} and \mathbf{S}^{-1} we obtain the following relation for the right and left eigenvectors:

$$(s_i, s_j^L) = \delta_{ij}. \quad (2.17)$$

The transformation from the basis of eigenvectors to the original basis is given by $\hat{\phi} = S^{-1} \phi$, so that the steady-state equations (2.13) become:

$$(s_i^L, \mathbf{w}) = 0, \quad i = n_e + n_c + 1, \dots, n, \quad (2.18)$$

These steady-state relations define a low-dimensional manifold in composition space in terms of the left eigenvectors of the Jacobian matrix of the chemical source term, where only slow reaction processes take place. Note that the definition of the manifold is only meaningful if the Jacobian matrix, and therefore also the eigenvectors, will not change too much if the system is disturbed.

The formulation of the steady-state assumptions (2.18) is different from the definition of Maas and Pope [Maa92], who use an orthonormal basis to define the steady-state equations. In section 2.1.2 it will be shown that both approaches will lead to the same results. First, the treatment of complex eigenvalues and eigenvectors will be considered in more detail.

2.1.1 Complex Eigenvalues

As already mentioned, the eigenvalues are complex in general. When a pair of complex eigenvalues is detected, a slightly different approach will be followed. The real and imaginary parts of the complex eigenvectors are used to create a modified real basis (\tilde{S}). This modified basis is composed as follows.

Splitting the complex eigenvalues and eigenvectors in real and imaginary parts $\tilde{\lambda}_i + i\tilde{\lambda}_{i+1}$ and $\tilde{s}_i + i\tilde{s}_{i+1}$ with $\tilde{\lambda}_i, \tilde{\lambda}_{i+1}, \tilde{s}_i$ and \tilde{s}_{i+1} real, we may write:

$$\mathbf{J}(\tilde{s}_i + i\tilde{s}_{i+1}) = (\tilde{\lambda}_i + i\tilde{\lambda}_{i+1})(\tilde{s}_i + i\tilde{s}_{i+1}). \quad (2.19)$$

It should be noted that the complex conjugate of an eigenvector of the Jacobian matrix is also an eigenvector of the Jacobian matrix. Also the corresponding eigenvalue of the latter eigenvector is the complex conjugated of the original. Therefore, we also have:

$$\mathbf{J}(\tilde{s}_i - i\tilde{s}_{i+1}) = (\tilde{\lambda}_i - i\tilde{\lambda}_{i+1})(\tilde{s}_i - i\tilde{s}_{i+1}). \quad (2.20)$$

Equations (2.19) and (2.20) may be combined into the following real equations:

$$\mathbf{J}\tilde{s}_i = \tilde{\lambda}_i\tilde{s}_i - \tilde{\lambda}_{i+1}\tilde{s}_{i+1},$$

and

$$\mathbf{J}\tilde{s}_{i+1} = \tilde{\lambda}_i\tilde{s}_i + \tilde{\lambda}_{i+1}\tilde{s}_{i+1}. \quad (2.21)$$

If the i^{th} eigenvalue is complex, we rearrange the eigenvectors so that the $(i+1)^{\text{th}}$ eigenvector is the complex conjugate of the i^{th} eigenvector. In the modified eigenvector basis \tilde{S} , defined by the basis vectors $(\tilde{s}_1, \dots, \tilde{s}_n)$, the Jacobian matrix has the following form:

$$\mathbf{J}\tilde{S} = \begin{pmatrix} \ddots & & & 0 \\ & \tilde{\lambda}_i & -\tilde{\lambda}_{i+1} & \\ & \tilde{\lambda}_{i+1} & \tilde{\lambda}_i & \\ 0 & & & \ddots \end{pmatrix} \tilde{S}, \quad (2.22)$$

with 2×2 blocks on the diagonal for every pair of complex eigenvalues. We can do the same for left eigenvectors to construct the matrix S^{-1} as given by (2.14). This, however, does not guaranty that $S^{-1}S = I$. Therefore, the right and left eigenvectors are redefined in such a way that $(s_i^L, s_j) = \delta_{ij}$. In the remainder of this thesis the eigenvalues and eigenvectors are denoted by λ_i and s_i instead of $\bar{\lambda}_i$ and \bar{s}_i for reasons of simplicity. Then λ_i is either a real eigenvalue or the real or imaginary part of a complex eigenvalue.

2.1.2 Orthonormal Basis

Instead of the basis of left eigenvectors an orthonormal basis, called Schur basis, can be used to define the steady-state equations for the fast reaction groups. This is the approach followed by Maas and Pope [Maa91]. An orthogonal transformation (real) matrix Q is defined in such a way that the Jacobian matrix in the new basis $Z = Q^T J Q$ becomes an upper-triangular matrix, with 2×2 blocks on the diagonal, in case of complex eigenvectors:

$$Z = \begin{pmatrix} z_{11} & z_{12} & \dots & z_{1n} \\ 0 & z_{22} & \dots & z_{2n} \\ \vdots & \vdots & \ddots & \vdots \\ 0 & 0 & \dots & z_{nn} \end{pmatrix}, \quad (2.23)$$

with $z_{ij} = 0$ for $j < i$. Note that $Q^{-1} = Q^T$ because Q is orthogonal. For real eigenvalues the diagonal elements are equal to the eigenvalues: $z_{ii} = \lambda_i$. The eigenvalues are ordered in the same way as described in the previous section and the steady-state equations are defined similarly:

$$(q_i^T, w) = 0, \quad i = n_e + n_c + 1, \dots, n. \quad (2.24)$$

The steady-state equations for the orthogonal reaction groups give the same low-dimensional manifold as the steady-state eqs. (2.18) for the basis of eigenvectors. I.e. one can go from (2.18) to (2.24) by merely changing basis. To show this, we construct an orthonormal basis using the left eigenvectors and will show that this basis is the Schur basis.

An orthonormal basis $Q = (q_1, \dots, q_n)$ can be constructed from the left eigenvectors by using the Gramm-Schmidt orthogonalisation method:

$$q_n = s_n^L, \quad (2.25)$$

$$q_i = \frac{s_i^L - \sum_{j=i+1}^n (s_i^L, q_j) q_j}{\left| s_i^L - \sum_{j=i+1}^n (s_i^L, q_j) q_j \right|}, \quad i = n-1, \dots, 1.$$

The construction of the orthonormal basis in this way implies that the vectors of this basis q_i may be written as a linear combination of the $(n-i+1)$ last left eigenvectors s_i^L, \dots, s_n^L :

$$q_i = a_{i1} s_i^L + \dots + a_{in} s_n^L. \quad (2.26)$$

The coefficients a_{ij} can be derived from eq. (2.25). Substitution of eqs. (2.26) into eqs. (2.24) shows that $(\mathbf{q}_i, \mathbf{w}) = 0$, for $i > n_c + n_e$, so that the steady-state relations for the orthonormal reaction groups lead to the same result as the steady-state relations for the left eigenvectors.

Next, we have to prove that $\mathbf{Z} = \mathbf{Q}^T \mathbf{J} \mathbf{Q}$ is an upper-triangular matrix. From (2.26) it follows that \mathbf{Q}^T is given by:

$$\mathbf{Q}^T = \mathbf{T} \mathbf{S}^{-1}, \quad (2.27)$$

with \mathbf{T} a upper-triangular matrix, so we may write:

$$\mathbf{Q}^T \mathbf{J} \mathbf{Q} = \mathbf{T} \mathbf{S}^{-1} \mathbf{J} \mathbf{Q}, \quad (2.28)$$

which becomes using (2.16):

$$\mathbf{T} \mathbf{A} \mathbf{S}^{-1} \mathbf{Q} = \mathbf{T} \mathbf{\Lambda} \mathbf{T}^{-1}, \quad (2.29)$$

with $\mathbf{Z} = \mathbf{T} \mathbf{\Lambda} \mathbf{T}^{-1}$ an upper-triangular matrix.

This proves that the orthonormal basis as used by Maas and Pope may be derived from eqs. (2.25) and that both definitions of the steady-state relations (2.24) and (2.18) lead to the same results.

2.1.3 Solution Method

Since the steady-state equations (2.18) depend on the local composition of the mixture, their solution has to be calculated many times during flame calculations leading to a high computational cost. This can be avoided by solving equations (2.18) beforehand and making a parameterization of the manifold in the form of control variables $\alpha_1, \dots, \alpha_{n_c}$, which describe the progress of the process on the manifold. In principle, the control variables may be any linear combination of the specific mole numbers of the species $\alpha_i = (\xi_i, \phi)$, with ξ_i a given vector. However, the control variables must be chosen in such a way that there exists only one manifold composition for each combination of the control variables. In Figure 2.1 e.g., the specific mole number ϕ_{H_2O}

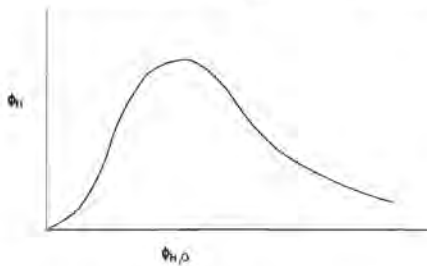


Figure 2.1: The control variables should be chosen carefully to have only one manifold composition for every value of the control variables. In the example of this figure ϕ_{H_2O} is a good choice and ϕ_H is a bad one.

of H_2O would be an appropriate control variable. However, if the specific mole number ϕ_H of H would be used as control variable this would not lead to an unique mapping.

It has to be kept in mind that the specific element mole numbers ($\chi_1, \dots, \chi_{n_e}$), enthalpy h and the pressure p appear as additional degrees of freedom of the manifold as these may change by transport processes in the flame. In general therefore, the number of degrees of freedom of the manifold is equal to $(n_c + n_e + 2)$, with n_c the chosen number of control variables.

Manifold compositions are calculated within a range of physically reasonable values of the parameters introduced above. The set of equations to be solved to calculate one point on the manifold for control variables $\alpha_1 \dots \alpha_{n_c}$, specific element mole numbers $\chi_1 \dots \chi_{n_e}$, enthalpy h_{ref} and pressure p_{ref} , is formally given by the equation $\mathbf{g} = \mathbf{0}$, defined as:

$$\begin{aligned} g_i &= (\xi_i, \phi) - \alpha_i = 0, & i &= 1, \dots, n_c, \\ g_i &= (\mu_{(i-n_c)}, \phi) - \chi_{(i-n_c)} = 0, & i &= n_c + 1, \dots, n_c + n_e, \\ g_i &= (s_i^L, \mathbf{w}) = 0, & i &= n_c + n_e + 1, \dots, n_t \\ g_{n+1} &= \sum_{i=1}^n M_i \phi_i \left(h_i^0 + \int_{T_0}^T c_{p_i} \tau d\tau \right) - h_{ref} = 0, \\ g_{n+2} &= p - p_{ref} = 0. \end{aligned} \quad (2.30)$$

The first n_c equations define the values for the control variables on the manifold, the subsequent n_e equations indicate that the specific element mole numbers are fixed. The next n_c equations are the steady-state equations for the fastest reaction groups. The last equations fix the enthalpy and pressure to the preselected values.

To solve the set of equations (2.30) a modified Newton's method is used. If this method is applied, the set of equations (2.30) is linearized around composition ϕ_0 :

$$\mathbf{g}(\phi) \approx \mathbf{g}(\phi_0) + \mathbf{G}(\phi - \phi_0) = 0, \quad (2.31)$$

where \mathbf{G} is the Jacobian matrix of the set of equations given by:

$$\mathbf{G} = \left(\frac{\partial \mathbf{g}}{\partial \phi} \right)_{\phi_0}. \quad (2.32)$$

This matrix can be derived from eqs. (2.30). According to these equations, the first n_c rows of \mathbf{G} , denoted as \mathbf{t}_i , are given by:

$$\mathbf{t}_i = \xi_i, \quad i = 1, \dots, n_c. \quad (2.33)$$

The next n_e rows of \mathbf{G} are given by:

$$\mathbf{t}_i = \mu_{i-n_c}, \quad i = n_c + 1, \dots, n_c + n_e. \quad (2.34)$$

The last rows of \mathbf{G} are given by:

$$\mathbf{t}_i = (s_i^L)^T \mathbf{J}, \quad i = n_c + n_e + 1, \dots, n_t. \quad (2.35)$$

where the Jacobian matrix J of the source term is used. The approximated solution of (2.31) is updated according to:

$$\phi = \phi_0 - \beta G^{-1} g(\phi_0), \quad (2.36)$$

where β denotes a damping coefficient ($0 < \beta \leq 1$). For a linear set of equations one Newton step with ($\beta = 1$) would be sufficient to obtain the solution. The set of equations (2.30), however, is strongly non-linear. Therefore, an iteration processes is needed. Since the convergence region of Newton's method is rather small in practice, convergence can be enhanced by adding a pseudo-transient term to the equations. Note that not the full transient term is taken into account as we do not want to solve the evolution of the system; we only want to solve the steady-state relations for the fastest reaction groups. In fact only a transient term for the fastest reaction groups is added. Hence, a time-stepping procedure will be followed for compositions ϕ^0 outside the convergence region of Newton's method. That the steady-state equations of (2.30) extended by a time-dependent term become:

$$g_i = \left(s_i^L, w - \frac{\phi - \phi^0}{\Delta t} \right) = 0 \quad \text{for } i = n_c + n_e + 1, \dots, n, \quad (2.37)$$

where Δt denotes a (small) time step. This implies that the rows of G are changed into:

$$t_i = (s_i^L)^T J - (s_i^L, \delta_i) / \Delta t, \quad i = n_c + n_e + 1, n, \quad (2.38)$$

with δ_i a vector with Kronecker delta functions δ_{ij} as coefficients. The other equations in eq. (2.30) (for $i = 1, \dots, n_c + n_e$) are not modified. This set of equations is also solved with Newton's method for every time step.

The strategy which is followed to extend the damped Newton method with a pseudo-transient term and the choice of the damping coefficient β and time-step magnitude Δt is explained in more detail in section 2.3. There, we also explain how the locally-refined mesh for the manifold is constructed.

2.2 Application of the Mathematical Reduction Technique to Flat Flames

In this section we describe how the reduction method is applied to premixed flat flames. Since only stationary flames are considered, all time dependent terms are omitted from the governing differential equations. The continuity equation states that:

$$\rho u = \dot{M}, \quad (2.39)$$

where u is the flow velocity and \dot{M} is the constant mass flow rate. Equation (2.39) eliminates the flow velocity as independent variable.

As indicated in chapter 1, the flow-velocities are generally much lower than the speed of sound for deflagration processes, so that the pressure may be assumed to be constant. Hence, the pressure is eliminated from the set of dynamic variables. The assumption that the pressure is

considered to be constant, eliminates the Navier-Stokes equation (1.8) from the set of equations to be solved.

The transport equations for the species in stationary flat flames are derived from eq. (1.7):

$$\dot{M} \frac{d\phi_i}{dx} - \frac{d}{dx} \left(\rho D_i \frac{d\phi_i}{dx} \right) = \rho w_i \quad \text{for } i = 1, \dots, n. \quad (2.40)$$

We use the energy equation in terms of the enthalpy, given by eq. (1.23).

$$\dot{M} \frac{dh}{dx} - \frac{d}{dx} \left(\frac{\lambda}{c_p} \frac{dh}{dx} \right) = \frac{d}{dx} \frac{\lambda}{c_p} \sum_{i=1}^n h_i \left(\frac{1}{Le_i} - 1 \right) M_i \frac{d\phi_i}{dx}, \quad (2.41)$$

Hence, the number of independent variables for flat flames is $n + 1$ (the specific mole numbers of the species ϕ_i and enthalpy h).

For the reduced scheme, the independent variables are the control variables, the specific element mole numbers and the enthalpy, so that the number of degrees of freedom reduces to $n_c + n_e + 1$. The specific element mole numbers appear now as additional degrees of freedom although they can not change due to chemical reactions. This implies that the change of the specific element mole numbers can not be predicted by the reduced reaction mechanism. They can, however, change through diffusion processes. The equations for these specific element mole numbers are derived in the next subsection. The equations for the control variables are derived in section 2.2.2. In section 2.2.3 we treat the projection of the differential equations of the species on the manifold, in detail.

2.2.1 Differential Equations for the Specific Element Mole Numbers

The differential equation for the specific element mole numbers are obtained from the definition of the specific element mole numbers eq. (1.41) and the differential equations for the species (2.40).

$$\dot{M} \frac{d\chi_j}{dx} = \dot{M} (\mu_j, \frac{d}{dx} \phi) = \sum_{i=1}^n \mu_{ji} \frac{d}{dx} (\rho D_i \frac{d\phi_i}{dx}) + \rho (\mu_j, \mathbf{w}). \quad (2.42)$$

The term $\rho (\mu_j, \mathbf{w})$ is equal to zero because elements are conserved in chemical reactions as indicated by (1.48). After integration of (2.42) from x_{ref} to x we arrive at:

$$\dot{M} (\chi_j(x) - \chi_j(x_{ref})) = \left(\sum_{i=1}^n \mu_{ji} \rho D_i \frac{d\phi_i}{dx} \right)_x - \left(\sum_{i=1}^n \mu_{ji} \rho D_i \frac{d\phi_i}{dx} \right)_{x_{ref}}. \quad (2.43)$$

If we substitute the Lewis numbers, defined by eq. (1.22), equation (2.43) may be written as:

$$\begin{aligned} \dot{M} (\chi_j(x) - \chi_j(x_{ref})) = & \left(\sum_{i=1}^n \mu_{ji} \frac{\lambda}{c_p} \frac{d\phi_i}{dx} \right)_x + \left(\sum_{i=1}^n \mu_{ji} \frac{\lambda}{c_p} \frac{d\phi_i}{dx} \left(\frac{1}{Le_i} - 1 \right) \right)_x - \\ & \left(\sum_{i=1}^n \mu_{ji} \frac{\lambda}{c_p} \frac{d\phi_i}{dx} \right)_{x_{ref}} - \left(\sum_{i=1}^n \mu_{ji} \frac{\lambda}{c_p} \frac{d\phi_i}{dx} \left(\frac{1}{Le_i} - 1 \right) \right)_{x_{ref}}. \end{aligned} \quad (2.44)$$

Using $\sum_{i=1}^n \mu_{ji} \frac{d\phi_i}{dx} = (\mu_j, \frac{d\phi}{dx}) = \frac{d\chi_j}{dx}$, we can rewrite eq. (2.44) as:

$$\begin{aligned} \dot{M}\chi_j(x) - \frac{\lambda}{c_p} \frac{d\chi_j(x)}{dx} &= \frac{\lambda}{c_p} \sum_{i=1}^n \mu_{ji} \left(\frac{1}{Le_i} - 1 \right) \left[\left(\frac{d\phi_i}{dx} \right)_x - \left(\frac{d\phi_i}{dx} \right)_{ref} \right] + \\ &\dot{M}\chi_j(x_{ref}) - \frac{\lambda}{c_p} \frac{d\chi_j(x_{ref})}{dx}, \end{aligned} \quad (2.45)$$

i.e. we obtain a first-order differential equation for χ_j . The right-hand-side of this equation appears as a source term. Furthermore, these differential equations for elements have the same form as the enthalpy equation (2.41). If all Lewis numbers are equal to one (2.45) becomes:

$$\dot{M}\chi_j(x) - \frac{\lambda}{c_p} \frac{d\chi_j(x)}{dx} = \dot{M}\chi_j(x_{ref}) - \frac{\lambda}{c_p} \frac{d\chi_j(x_{ref})}{dx}. \quad (2.46)$$

These differential equations have an exponential solution. The specific element mole numbers must be finite at $x \rightarrow \infty$ and $x \rightarrow -\infty$ which implies that the specific element mole numbers have to be constant throughout the entire domain; hence $\chi_j(x) = \chi_j(x_{ref})$. The specific element mole numbers also remain constant through the entire domain if all Lewis numbers are equal (not necessary equal to one). Furthermore, if all Lewis numbers of species which include the element i ($\mu_{ji} \neq 0$) are equal, the specific element mole number of that element does not change. If the Lewis numbers of species which include the element i are not equal, the specific element mole number of that element may change. However, if the specific element mole number of k elements are constant because of equal Lewis numbers, there are only $n_e - k - 1$ additional degrees of freedom. This is due to the fact that sum of the element mass fractions equals one ($\sum_{j=1}^{n_e} W_j \chi_j = 1$), as given by equation (1.43). Thus if only the Lewis of species with include one specific element deviate from the Lewis numbers of the other species, all specific element mole numbers remain constant. E.g. $\chi_j = \chi_j(x_{ref})$, for $j = 1, \dots, n_e$ if $Le_i = c$, for $i = 1, \dots, n$, except $Le_H \neq c$ and $Le_{H_2} \neq c$.

Thus if equal Lewis numbers are used, the specific element mole numbers disappear as independent variables, so that $n_c + 1$ independent variables remain. In chapter 1 we have already seen that the enthalpy remains constant if all Lewis numbers are equal, but the enthalpy still remains an independent variable for burner-stabilized flames, since the flame is cooled at the burner. The enthalpy will remain constant in the down-stream part of the burner, but is not equal to the enthalpy of the unburned mixture. For adiabatic flames the number of degrees of freedom is also $n_c + 1$ as the mass flow rate \dot{M} appears as independent variable.

2.2.2 Differential Equations for the Reduced Reaction Mechanism

Finally, we derive differential equations for the control variables for flat flames. First, the equations that describe the composition are described by a reduced number of variables. Subsequently, the differential equations for the species are projected on the manifold.

To describe the evolution of the process, the n_c control variables, n_e specific element mole numbers and the enthalpy are sufficient as the manifold gives the relation with the other variables. Therefore we may write: $\phi = \phi(\alpha_1, \dots, \alpha_{n_c}, \chi_1, \dots, \chi_{n_e}, h)$. Using this, the derivatives $\frac{d\phi_i}{dx}$, which appear in eq. (2.40) can also be written as

$$\frac{d\phi_i}{dx} = \sum_{j=1}^{n_c} \frac{\partial \phi_i}{\partial \alpha_j} \frac{\partial \alpha_j}{\partial x} + \sum_{j=1}^{n_e} \frac{\partial \phi_i}{\partial \chi_j} \frac{\partial \chi_j}{\partial x} + \frac{\partial \phi_i}{\partial h} \frac{\partial h}{\partial x}. \quad (2.47)$$

Since we consider a stationary one-dimensional system (flat flames), all variables α_i , χ_i and h depend on the spatial coordinate x only. Suppose that all suitable control variables α_j increase or decrease monotonously with x . Then, all variables may be considered as a function of α_j also, for any fixed j . This means that we may write $\frac{\partial \alpha_j}{\partial x} = \frac{\partial \alpha_i}{\partial \alpha_j} \frac{\partial \alpha_j}{\partial x}$, $\frac{\partial \chi_i}{\partial x} = \frac{\partial \chi_i}{\partial \alpha_j} \frac{\partial \alpha_j}{\partial x}$ and $\frac{\partial h}{\partial x} = \frac{\partial h}{\partial \alpha_j} \frac{\partial \alpha_j}{\partial x}$. If we substitute these relations into eq. (2.47) we arrive at:

$$\frac{d\phi_i}{dx} = \frac{d\phi_i}{d\alpha_j} \frac{d\alpha_j}{dx}. \quad (2.48)$$

Note that we have to use monotonously increasing or decreasing control variables, otherwise $\frac{d\phi_i}{d\alpha_j}$ could be zero. The second-order derivatives are treated similarly: For the second-order derivative of ϕ_i we obtain, after substitution of eq. (2.48):

$$\frac{d^2 \phi_i}{dx^2} = \frac{d}{dx} \left(\frac{d\phi_i}{d\alpha_j} \frac{d\alpha_j}{dx} \right) = \left(\frac{d}{dx} \left(\frac{d\phi_i}{d\alpha_j} \right) \right) \frac{d\alpha_j}{dx} + \frac{d\phi_i}{d\alpha_j} \frac{d^2 \alpha_j}{dx^2}. \quad (2.49)$$

The factor $\frac{d\phi_i}{d\alpha_j}$ may be considered as a function of α_j only, so that we may write:

$$\frac{d}{dx} \left(\frac{d\phi_i}{d\alpha_j} \right) = \frac{d^2 \phi_i}{d\alpha_j^2} \frac{d\alpha_j}{dx}. \quad (2.50)$$

If we substitute eqs. (2.48), (2.49) and (2.50) into the differential equations (2.40), we obtain:

$$M \frac{d\phi_i}{d\alpha_j} \frac{d\alpha_j}{dx} - \frac{d\rho D_i}{d\alpha_j} \frac{d\phi_i}{d\alpha_j} \left(\frac{d\alpha_j}{dx} \right)^2 - \rho D_i \left(\frac{d^2 \phi_i}{d\alpha_j^2} \left(\frac{d\alpha_j}{dx} \right)^2 + \frac{d\phi_i}{d\alpha_j} \frac{d^2 \alpha_j}{dx^2} \right) - \rho w_i = 0. \quad (2.51)$$

Since equation (2.51) holds for all i , we have n equations and only n_c independent variables α_j . This is not a contradiction, because variations of the composition are restricted; the composition vector has to be in the manifold.

Furthermore, the combustion process of the one-dimensional flame is a path in composition space. It starts at a position denoting the unburned mixture composition and ends at the equilibrium point. An example of a reaction path describing a flat flame on a two-dimensional manifold is given in Figure 2.2. The direction of the path changes continuously during the combustion process. However, at every stage there is only one direction vector in which the composition changes. In other words, the process will change in the direction of the tangential direction vector $\frac{d\phi}{dx}$ (see Figure 2.3). Disturbances introduced for instance by diffusion processes may

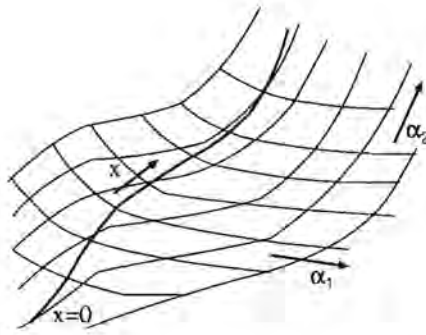


Figure 2.2: Flat flame path on a two-dimensional manifold in composition space

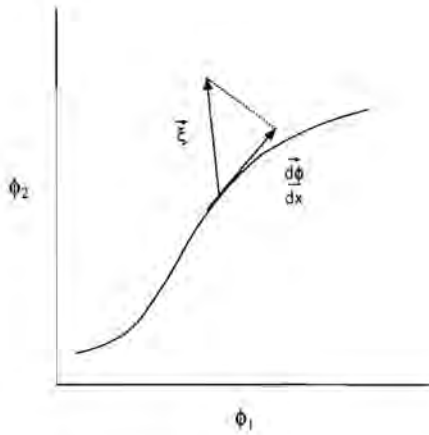


Figure 2.3: A disturbance will be projected on the tangential direction vector.

have a different direction. However, only the contribution of the disturbance in the direction of the tangential direction vector is relevant. Moving in any other direction is not allowed. Therefore, only the contributions of all terms in the differential equation within the manifold will be considered. One possible approach (which we followed) is to project the differential equations using the local tangential direction vector. Writing the differential equations as $\mathbf{r} = \mathbf{0}$, with residuals $r_i = \dot{M} \frac{d\phi_i}{dx} - \frac{d}{dx} (\rho D_i \frac{d\phi_i}{dx}) - \rho w_i$, the projection of the residuals in the direction of the local direction vector is defined by: $r_j = (\mathbf{r}, \frac{d\phi}{d\alpha_j}) \frac{d\phi}{d\alpha_j} / |\frac{d\phi}{d\alpha_j}|^2$, for $j = 1, \dots, n_c$. Note that this is a perpendicular projection. This projection method projects disturbances on the manifold along the shortest path, which will be perpendicular to the manifold. This projection method will be studied in more detail in section 2.2.3.

Since all variables may be written as function of only one variable (for flat flames), the tangential direction vectors are given by $\frac{d\phi}{d\alpha_j}$, for any choice of j . The differential equations for the control variables are found by taking the inner-product of \mathbf{r} , where $r_i = 0$ is given by eqs. (2.51), with each vector $\frac{d\phi}{d\alpha_j}$ leading to:

$$\begin{aligned} \dot{M} \frac{d\alpha_j}{dx} \sum_{i=1}^n \left(\frac{d\phi_i}{d\alpha_j} \right)^2 - \sum_{i=1}^n \left[\left(\frac{d\phi_i}{d\alpha_j} \right)^2 \frac{d(\rho D_i)}{d\alpha_j} \left(\frac{d\alpha_j}{dx} \right)^2 + \frac{d\phi_i}{d\alpha_j} \rho D_i \frac{d^2\phi_i}{d\alpha_j^2} \left(\frac{d\alpha_j}{dx} \right)^2 \right. \\ \left. + \left(\frac{d\phi_i}{d\alpha_j} \right)^2 \rho D_i \frac{d^2\alpha_j}{dx^2} \right] - \rho \sum_{i=1}^n \frac{d\phi_i}{d\alpha_j} w_i = 0, \quad j = 1, \dots, n_c. \end{aligned} \quad (2.52)$$

These equations are the differential equations which will be used for flat flame computations with reduced mechanism. Note that these equations are obtained by projecting the original differential equation of the control variables on the local tangential direction vector of the manifold, since there is only one local direction vector for flat flames. If the reduced reaction mechanism is applied to more dimensional flames the projection is more complicated.

The projection used here, is not the only possible projection. The definition of the manifold eq. (2.18),

$$(s_i^L, \mathbf{w}) = 0, \quad i = n_e + n_c + 1, \dots, n, \quad (2.53)$$

implies that all variations in the direction of the fastest reaction groups will be damped out immediately. Similarly, we can enforce the convection term and the diffusion term not to induce variations in the direction of the fast reaction groups. This means that disturbances in the direction of the fast reaction groups, caused by convection and diffusion effects will immediately relax towards a steady-state situation due to fast reactions. For the diffusion term this implies:

$$(s_i^L, \boldsymbol{\pi}) = 0, \quad i = n_e + n_c + 1, \dots, n, \quad (2.54)$$

with $\boldsymbol{\pi}$ the diffusion vector, with $\pi_i = \frac{d}{dx} (\rho D_i \frac{d\phi_i}{dx})$. The physical picture of this projection is that disturbances will relax fast towards the manifold parallel to the fast eigenvectors. As the reaction groups are not orthogonal, this is not a perpendicular projection in contrast with the first presented projection method based on the tangential direction method. Therefore, the two projection methods may give different results.

In the next section, the two projection methods are considered in more detail.

2.2.3 Projection Methods

In this section two projection methods to transform the differential equations for the species (2.51) into differential equations for the control variables (2.52) are considered. The projection method used for the applications presented in chapter 3, makes use of the tangential direction vectors of the manifold. As indicated before, an other projection method based on the eigenvectors can also be derived. We will show that the projection of the convection and the source term are identical for both methods. Furthermore, we will show that the projections of these terms are identical to the corresponding terms in the initial equations (2.40) of those species which are used as control variables. This means that only the diffusion term in the reduced scheme equations differs from the diffusion term of equation (2.40).

Projection Method Based on Tangential Direction Vectors

For a flat flame and also for a homogeneous time-dependent system there is only one direction vector, as the combustion process proceeds following a one-dimensional path on the manifold. Therefore, we may write:

$$\frac{d\phi}{d\alpha_1} = \frac{d\phi}{d\alpha_2} \frac{d\alpha_2}{d\alpha_1}, \quad (2.55)$$

if α_2 is a monotonous function of α_1 . Note that $\frac{d\phi}{d\alpha_j}$ denotes the total derivative (see eq. (2.47)). A projection operator which transforms the n differential equations of the species into n_c differential equations for the control variables is given by the $n \times n_c$ matrix \mathbf{P}' :

$$\mathbf{P}' = \begin{pmatrix} - & p_1 & - \\ & \vdots & \\ - & p_{n_c} & - \end{pmatrix}, \quad (2.56)$$

with p_i given by:

$$p_i = \frac{d\phi}{d\alpha_i} / \left| \frac{d\phi}{d\alpha_i} \right|^2. \quad (2.57)$$

We will show that the projected convection and chemical source terms are identical to the terms in the initial species equation (2.40) for the control variable.

First, the convection term $M \frac{d\phi_j}{d\alpha_j} \frac{d\alpha_j}{dx}$ is considered. The j^{th} component of the projection of the tangential direction vector $\frac{d\phi}{d\alpha_i}$ is given by:

$$\left(\mathbf{P}' \frac{d\phi}{d\alpha_i} \right)_j = \left(\frac{d\phi}{d\alpha_j}, \frac{d\phi}{d\alpha_i} \right) / \left| \frac{d\phi}{d\alpha_j} \right|^2 = \left(\frac{d\phi}{d\alpha_j}, \frac{d\phi}{d\alpha_j} \right) / \left| \frac{d\phi}{d\alpha_j} \right|^2 \frac{d\alpha_j}{d\alpha_i} = \frac{d\alpha_j}{d\alpha_i}, \quad (2.58)$$

leading to:

$$\mathbf{P}' \begin{pmatrix} \frac{d\phi_1}{d\alpha_i} \\ \vdots \\ \frac{d\phi_{n_c}}{d\alpha_i} \end{pmatrix} = \begin{pmatrix} \frac{d\alpha_1}{d\alpha_i} \\ \vdots \\ \frac{d\alpha_{n_c}}{d\alpha_i} \end{pmatrix}. \quad (2.59)$$

When we apply this projection operator on the convection term $\dot{M} \frac{d\phi}{dx}$, we obtain for the j^{th} control variable:

$$\dot{M} \left(\mathbf{P} \frac{d\phi}{d\alpha_i} \right)_j \frac{d\alpha_i}{dx} = \dot{M} \frac{d\alpha_j}{dx}, \quad (2.60)$$

which is equal to the convective term in the differential equation of ϕ_i corresponding to control variable $\alpha_j = \phi_i$.

Now, let us consider the projection of the source term \mathbf{w} . As the eigenvectors s_i form a basis of composition space, the source term may be written as:

$$\mathbf{w} = \sum_{i=1}^n \beta_i s_i. \quad (2.61)$$

Using the definition of the manifold $(s_i^t, \mathbf{w}) = 0$, for $i = n_c + n_e + 1, \dots, n$ and $(s_i^t, s_j) = \delta_{ij}$, where δ_{ij} denotes the Kronecker delta, we obtain:

$$\mathbf{w} = \sum_{i=1}^{n_c} \beta_i s_i. \quad (2.62)$$

The tangential direction vectors are parallel to the manifold. The manifold, however, is also spanned by the first n_c eigenvectors so that we may write:

$$\frac{d\phi}{d\alpha_i} = \sum_{j=1}^{n_c} a_{ij} s_j. \quad (2.63)$$

From (2.62) and (2.63) it can be seen that the number of degrees of freedom is n_c . The equation used to define the manifold and the time scales is given by:

$$\frac{d\phi}{d\alpha_i} \frac{d\alpha_i}{dt} = \mathbf{w} \quad (2.64)$$

Although this is a set of n equations, the vectors $\frac{d\phi}{d\alpha_i}$ and \mathbf{w} are restricted to a n_c dimensional subspace, so that there are only n_c degrees of freedom. Therefore, we may conclude from (2.64) that the tangential direction vectors and the source term are parallel, so that the source term may be written as:

$$\mathbf{w} = \frac{d\phi}{d\alpha_j} (\xi_j, \mathbf{w}). \quad (2.65)$$

With the use of (2.58) it easily follows that:

$$\mathbf{P}' \mathbf{w} = ((\xi_1, \mathbf{w}), \dots, (\xi_{n_c}, \mathbf{w}))^T, \quad (2.66)$$

which is again the source term of the differential equation for the species corresponding to the control variable.

Eigenvector Projection

The manifold is defined by steady-state equations for fast reaction groups, which are found from an eigenvector analysis. In the eigenvector basis the eigenvalues are ordered from large to small real parts (Note that most real parts of the eigenvalues are negative). Therefore, the reaction groups which correspond to fast damping processes have the highest index. These processes will be assumed to be in steady-state for the reduced reaction mechanism. To obtain the evolution equations for the remaining processes, we make use of the following ($n \times n$) projection matrix F' , defined in the basis of eigenvectors:

$$F' = \begin{pmatrix} \mathbf{I} & \mathbf{0} \\ \mathbf{0} & \mathbf{0} \end{pmatrix}. \quad (2.67)$$

with \mathbf{I} the $n_c \times n_c$ identity matrix. All other matrix elements are zero. For the original basis this becomes:

$$F = S \begin{pmatrix} \mathbf{I} & \mathbf{0} \\ \mathbf{0} & \mathbf{0} \end{pmatrix} S^{-1}, \quad (2.68)$$

The next step transforms the differential equations into differential equations for the control variables. This gives the following transformation matrix:

$$P = KS \begin{pmatrix} \mathbf{I} & \mathbf{0} \\ \mathbf{0} & \mathbf{0} \end{pmatrix} S^{-1}, \quad (2.69)$$

where \mathbf{K} is a $n \times n_c$ matrix, so that \mathbf{P} is also a $n \times n_c$ matrix. Since the control variables are given by $\alpha_i = (\xi_i, \phi)$, the elements of \mathbf{K} are given by $k_{ij} = \xi_{ij}$. For example, if the specific mole numbers of species with index 5 and index 1 ($\alpha_1 = \phi_5$ and $\alpha_2 = \phi_1$) are used as control variables in a 2-D ($n_c = 2$) reduced reaction mechanism and the number of species is $n = 7$, the matrix \mathbf{K} has the following form:

$$\mathbf{K} = \begin{pmatrix} 0 & 0 & 0 & 0 & 1 & 0 & 0 \\ 1 & 0 & 0 & 0 & 0 & 0 & 0 \end{pmatrix}. \quad (2.70)$$

Let us now consider the projection of the source term $F\mathbf{w}$ in more detail. For $\mathbf{w} - F\mathbf{w}$ we may write:

$$(\mathbf{I} - F)\mathbf{w} = S \left(\mathbf{I} - \begin{pmatrix} \mathbf{I} & \mathbf{0} \\ \mathbf{0} & \mathbf{0} \end{pmatrix} \right) S^{-1}\mathbf{w} = S \begin{pmatrix} \mathbf{0} & \mathbf{0} \\ \mathbf{0} & \mathbf{I} \end{pmatrix} S^{-1}\mathbf{w} = 0, \quad (2.71)$$

since $(s_i^t, \mathbf{w}) = 0$ for $i = n_c + n_e + 1, \dots, n$ by definition of the manifold. We have found that \mathbf{w} is not changed by the projection operator F :

$$F\mathbf{w} = \mathbf{w}. \quad (2.72)$$

Applying the projection and transformation to the source term gives:

$$P\mathbf{w} = ((\xi_1, \mathbf{w}), \dots, (\xi_{n_c}, \mathbf{w}))^T. \quad (2.73)$$

leading to the same result as the projection method based on the tangential direction vectors (eq. 2.66).

Now, consider the convection term $M \frac{d\phi}{d\alpha_i} \frac{d\alpha_i}{dx}$. Using (2.63) and $(s_i^l, s_j) = \delta_{ij}$ gives:

$$\mathbf{F} \frac{d\phi}{d\alpha_j} = \frac{d\phi}{d\alpha_j}, \quad (2.74)$$

further we get:

$$\mathbf{P} \begin{pmatrix} \frac{d\phi_1}{d\alpha_1} \\ \vdots \\ \frac{d\phi_n}{d\alpha_1} \end{pmatrix} = \begin{pmatrix} \frac{d\alpha_1}{d\alpha_1} \\ \vdots \\ \frac{d\alpha_n}{d\alpha_1} \end{pmatrix}. \quad (2.75)$$

This agrees with the result we have found for the other projection method (2.58). From this we may conclude that \mathbf{P} and \mathbf{P}' give identical results for the convective and source terms in the differential equations (2.40).

Now, let us turn to the projection of the diffusive terms. For a stationary flat flame the differential equations are given by:

$$M \frac{d\phi}{d\alpha_i} \frac{d\alpha_i}{dx} - \pi = w, \quad (2.76)$$

where π represents the diffusion term, with $\pi_i = \frac{d}{dx} (\rho D_i \frac{d\phi_i}{dx})$. Projection of this equation on the manifold gives:

$$M \frac{d\alpha_i}{dx} - \mathbf{P} \pi = (\xi_i, w)^T \quad (2.77)$$

According to equation (2.52) the diffusion term may be written as:

$$\pi_i = -\frac{d(\rho D_i)}{d\alpha_j} \frac{d\phi_i}{d\alpha_j} \left(\frac{d\alpha_j}{dx} \right)^2 - \rho D_i \frac{d^2 \phi_i}{d\alpha_j^2} \left(\frac{d\alpha_j}{dx} \right)^2 - \rho D_i \frac{d\phi_i}{d\alpha_j} \frac{d^2 \alpha_j}{dx^2}. \quad (2.78)$$

For equal diffusion coefficients ($D_i = D$), the first and the third terms of the right-hand side of (2.78) are thus parallel to $\frac{d\phi}{d\alpha_j}$. Note that terms parallel to $\frac{d\phi}{d\alpha_j}$ give identical results for both projection methods. The only term which is not parallel to the manifold in case of identical D_i is the second term of the right-hand side of (2.78). Differences between the two mentioned projection methods arise if this term is large.

Summarizing we may conclude that from a mathematical point of view the eigenvector projection is most accurate. The projection based on the tangential direction vector is a simplified method. We have implemented the projection method based on the tangential direction vectors because for the projection method based on the eigenvectors, the eigenvectors have to be stored, which leads to significantly larger look-up tables. It is to be expected that the inaccuracies introduced by the projection method \mathbf{P}' are of minor importance compared to the inaccuracies introduced by the reduction of the reaction mechanisms. This supports the choice to employ the projection method based on the tangential direction vector for the application of the reduced reaction mechanism.

2.3 Numerical Methods

In the previous sections the equations defining the reduced reaction mechanism and the equations applying the reduced mechanism to flat flame computations are presented. The numerical methods and strategies used to implement these equations are presented in the subsections below.

The strategy used to find a manifold point is considered in the following subsection. As explained before, manifold compositions are computed either using a damped Newton method or with a pseudo-time-step procedure. The procedure which applied is to switch from the damped Newton to the pseudo-time-step algorithm. In a subsequent section the gridding strategy is explained. Finally, the extension of the algorithm for implementation on parallel computers is treated.

2.3.1 Solution Strategy to Obtain a Manifold Point

As explained in section 2.1.3 Newton's method is used to solve the set of equations for obtaining a manifold point. Here, we focus our attention on the procedure to compute a manifold point. To compute a single manifold point, the enthalpy and pressure are constant as they are not changed by the chemical source term. Further, nitrogen can be considered inert so that the set of equations (2.30) can be reduced to $(n - 1)$ equations. This implies that the size of the Jacobian matrix is smaller than (2.30) suggests. For the computation of \mathbf{g} and the Jacobian matrix the temperature must be obtained from the specific mole numbers. This is done by using the $(n + 1)^{st}$ equation of (2.30). As the temperature depends on the specific enthalpies of the species which on their turn are temperature-dependent, this can not be done in one step. Therefore, the temperature is solved in an inner-iteration loop by using a Newton's method. The enthalpy equation can be written as:

$$h_{ref} = h(\phi) + \left(\frac{\partial h}{\partial T} \right)_{\phi} (T - T_0), \quad (2.79)$$

where T_0 is an initial guess for the temperature. The temperature is then obtained from:

$$T = T_0 + (h_{ref} - h(\phi)) / \left(\frac{\partial h}{\partial T} \right)_{\phi}. \quad (2.80)$$

As $\frac{\partial h}{\partial T}$ is not very sensitive for temperature fluctuations only a few Newton steps are necessary.

The procedure which is used to switch from the damped Newton to the pseudo-transient method is schematically presented in Figure 2.4. Initial values for the specific mole numbers are necessary to start Newton's method. How this initial composition is obtained is described in the next subsection.

The damping coefficient β is set to 1 initially and the code iterates with decreasing values for β until the norm of the vector \mathbf{g} , defined by: $|\mathbf{g}| = \sum_{i=1}^n |g_i|$ is decreased. If the norm $|\mathbf{g}|$ does not decrease, the damping coefficient is decreased by a factor 2. This is repeated until Newton's method is successful or until the damping coefficient is smaller than 0.001. After a number of damped Newton steps (up to 20, if Newton's method continues to decrease the norm and the

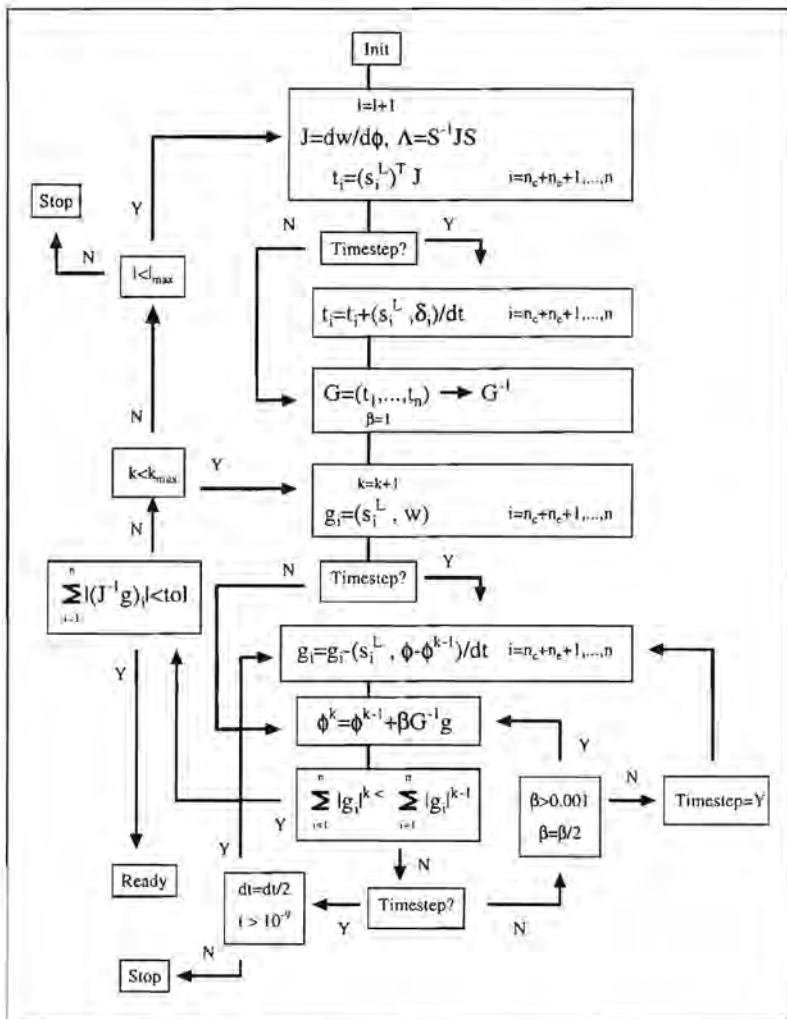


Figure 2.4: A flow diagram of the procedure to solve a manifold point.

norm is larger than the desired value) the Jacobian matrix of the chemical source term and the eigenvectors of the Jacobian matrix are updated.

If the norm of \mathbf{g} can not be reduced by a very low damping coefficient the pseudo-transient method is invoked to the equations. This procedure is started with a time step magnitude of $1 \cdot 10^{-6} s$. If a time-step does not lead to a decreasing norm, the time-step magnitude is decreased. After a successful time-step, the time-step magnitude is slightly increased. If a number of successful time-steps is performed, Newton's method without the pseudo-transient term is tried again. If even the time-step method fails to reduce the norm of the vector \mathbf{g} with time-steps as low as $1 \cdot 10^{-9}$, the computation of the manifold point is stopped.

The procedure is repeated until $\mathbf{J}^{-1}\mathbf{g}$ is small enough.

2.3.2 Gridding Strategy

The set of equations (2.30) defines a point on the manifold for given values of the control variables. To obtain the entire manifold the set is solved within a range of physically reasonable values of the control variables. The minimum value of a control variable is zero. The maximum value is limited by conservation of elements and is given by:

$$\max(\alpha_i) = \min(\chi_1/(\xi_i, \mu_1), \dots, \chi_{n_c}/(\xi_i, \mu_{n_c})). \quad (2.81)$$

The specific element mole numbers χ_j are obtained from the unburned mixture composition. The unburned mixture is supposed to contain only stable species as CH_4 , CO , CO_2 , H_2 , O_2 , H_2O and N_2 .

The procedure followed to make a grid for the manifold starts from an equidistant coarse grid mapped on the region between the minimum and maximum values of the control variables. Then a starting point on the manifold is chosen. This point is chosen close to the equilibrium position. In the neighborhood of the equilibrium point, the temperature is high and the reaction rates are large. Reaction processes, however, will proceed slowly. This makes it relatively easy to find reaction groups which are in steady-state. Furthermore, the equilibrium point is well defined; there is only one solution possible. If the manifold of the first point is solved, the surrounding points are treated, using the composition of the previous point as initial composition. For one-dimensional manifolds there are only two surrounding points: one on the right and one on the left side. For two-dimensional manifolds the order in which the points are treated is shown in Figure 2.5. The points are treated in this order by starting at the lower left corner of the grid and proceeding in vertical direction on each line from left to right, in the meanwhile checking whether a neighbouring point has already been solved before, so that the solution of this point can be used as initial composition.

If all points on the coarse grid have been treated, the grid is refined if the relative difference of one of the species or the source term of one of the control variables between two neighbouring points is larger than a prescribed value. Usually, we employ a value of 0.03 as maximum relative difference. The relative differences are obtained by dividing the absolute difference by the maximum value of this variable in already computed manifold points on a lower refinement level. For the two-dimensional manifold we can identify three different kinds of refinement points (see Figure 2.6). There are points which are situated between the north and south points,

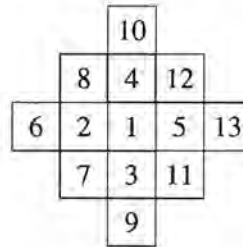


Figure 2.5: The manifold solution of the points is generated in the order as indicated by the numbers. The first point is chosen close to the equilibrium point.

others between the east and west points, the third kind of points is situated in the middle of four surrounding points. The last point is refined if one of the relative differences between points in the diagonal directions is too large.

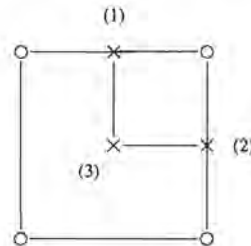


Figure 2.6: If the grid is refined, three kinds of points can be identified. Type (1): point on the fine grid which has equal y -values as its east and west neighbours. Type (2): point on the fine grid which has equal x -values as north and south neighbours. Type (3): the point is situated in the middle of four surrounding points. Circles denote coarse grid points.

The region where physically reasonable solutions for the specified specific mole numbers are generated is restricted. Some values of the control variables are not allowed due to conservation of elements. These points can easily be detected by computation of the specific element mole numbers from the values of the control variables. If these values are higher than the required values for specific mole numbers, that point is omitted. Furthermore, for certain values of the control variables the set of equations may lead to solutions with negative specific mole numbers. From a physical point of view it is not possible that the specific mole numbers of a species is negative. The mathematical description of the manifold, however, does not guaranty that only positive values are found. If this occurs, i.e. if a manifold point is solved successfully whereas the specific mole number of a species is negative, the specific mole number of that species is set to zero and a steady-state equation for that species is introduced instead of a steady-state assumption for a reaction group. Subsequently, the point is computed once

again, with the modified set of equations. During the computation of a manifold point, however, (small) negative values for the specific mole number are allowed.

2.3.3 Parallel Processing

As the computation of two neighbouring points is independent, manifold points can be computed simultaneously i.e. parallel. However, to compute a point on the manifold efficiently, an accurate estimate of the solution is necessary, which is available when the solution in neighbouring points is used. Considering Figure 2.5 it can be seen that if the solution in point (1) is known, points (2, ..., 5) can be computed simultaneously. If the solutions of these points are available, points (6, ..., 13) can be computed simultaneously. The number of points that can be solved simultaneously increases, until almost all points are solved. The code developed to compute manifolds, has been implemented on parallel computers with up to 16 processors located in workstations connected by ethernet (extension to 32 processors is possible). To start the computations, one processor calculates the first point. Four processors treat the next four points. If these are solved, all eight processors perform separate tasks. The code is based on a master-slave approach. The master program decides which points have to be computed and distributes the points among the slave programs. Most of the time (up to 98%) this program is waiting until a slave process finishes the computation of a point and gives it a new point to solve immediately. The communication between the computers is performed by using PVM software [Gei94] and the already available ethernet connections.

To check whether much time is lost with the communication between the workstations, the time between the send commands (about which point has to be treated) and the receive commands (the calculation is finished) is determined, on the master machine. This time is referred to as t_{master} . Furthermore, the time on the slave machine between a receive command and a send command is determined. This time is denoted as t_{slave} . An efficiency is defined as the ratio t_{slave}/t_{master} . If this quantity is large (near to 1) there is not much time spent on the communication between the computers i.e. the latency is small. Furthermore, there is only communication between the master and the slaves programs, which implies that the speed up is equal to the efficiency times the number of computers (if the performance of all computers is the same). This, however, does not apply for the startup and final procedure. For the most inefficient case, a very simple hydrogen/air reaction system, efficiencies as low as 50% are observed, depending on the network load. For larger reaction mechanisms, e.g. for methane efficiencies are generally larger than 99%.

2.3.4 Linearization and Discretization of Flame Equations

Until now, we have presented procedures and methods which are used to compute a manifold data-base. This data-base can be used to model laminar as well as turbulent flames. The application to flat flames will be considered in this section. The equations that have to be solved for flat flames are derived in the section 2.2. Here we treat the numerical methods that are applied to solve these equations. Before the differential equations for the control variables (2.52) can be solved numerically, the equations are linearized and discretized. The linearization and

discretization method are described below. The tabulated manifold can be used to find the specific mole numbers of all species and source terms by interpolation. The interpolation method is explained in the next subsection. Finally, a special mesh generation procedure is presented for a one-step reduced reaction mechanism which eliminates the need for interpolations on the manifold.

Consider the discretization and linearization of the differential equation of one control variable α_i . The differential equations for the other control variables are treated in the same way. The differential equation for the control variable is given by (2.52):

$$c_1 \frac{d\alpha_1}{dx} + c_2 \left(\frac{d\alpha_1}{dx} \right)^2 + c_3 \frac{d^2\alpha_1}{dx^2} + c_4 = 0, \quad (2.82)$$

with

$$\begin{aligned} c_1 &= M \sum_{i=1}^n \left(\frac{d\phi_i}{d\alpha_1} \right)^2, \\ c_2 &= - \left(\sum_{i=1}^n \left(\frac{d\phi_i}{d\alpha_1} \right)^2 \frac{d\rho D_i}{d\alpha_1} + \rho D_i \frac{d\phi_i}{d\alpha_1} \frac{d^2\phi_i}{d\alpha_1^2} \right), \\ c_3 &= - \sum_{i=1}^n \rho D_i \left(\frac{d\phi_i}{d\alpha_1} \right)^2, \\ c_4 &= - \sum_{i=1}^n \rho \frac{d\phi_i}{d\alpha_1} w_i. \end{aligned}$$

It might be clear that the coefficients c_1 , c_2 , c_3 and c_4 depend on the specific mole numbers of all species. The specific mole numbers on the other hand, are functions of the control variables, specific element mole numbers and enthalpy. Eq. (2.82) can be rewritten in the form:

$$\tilde{c}_1 \frac{d\alpha_1}{dx} + \tilde{c}_2 \left(\frac{d\alpha_1}{dx} \right)^2 + \frac{d}{dx} \left(\tilde{c}_3 \frac{d\alpha_1}{dx} \right) + \tilde{c}_4 = 0, \quad (2.83)$$

with

$$\begin{aligned} \tilde{c}_1 &= M \sum_{i=1}^n \left(\frac{d\phi_i}{d\alpha_1} \right)^2, \\ \tilde{c}_2 &= \sum_{i=1}^n \rho D_i \frac{d\phi_i}{d\alpha_1} \frac{d^2\phi_i}{d\alpha_1^2}, \\ \tilde{c}_3 &= - \sum_{i=1}^n \rho D_i \left(\frac{d\phi_i}{d\alpha_1} \right)^2, \\ \tilde{c}_4 &= - \sum_{i=1}^n \rho \frac{d\phi_i}{d\alpha_1} w_i. \end{aligned}$$

which is more suitable for the discretization method. First, the non-linear term $\left(\frac{d\alpha_1}{dx} \right)^2$ is linearized by writing it as $\left(\frac{d\alpha_1}{dx} \right) \left(\frac{d\alpha_1}{dx} \right)$ and including one factor $\frac{d\alpha_1}{dx}$ in the coefficient c_1 . This leads to the following equation:

$$c'_1 \frac{d\alpha_1}{dx} + \frac{d}{dx} \left(c'_2 \frac{d\alpha_1}{dx} \right) + c'_3 = 0, \quad (2.84)$$

with

$$\begin{aligned}c'_1 &= \tilde{c}_1 + \tilde{c}_2 \frac{d\alpha_1}{dx}, \\c'_2 &= \tilde{c}_3, \\c'_3 &= \tilde{c}_4.\end{aligned}$$

The equation is discretized by the finite-difference method of Thiart [Thi90], which will briefly be outlined below, resulting in a set of linear equations for the control variables at the grid points.

The discretization is performed as follows. First, eq. (2.84) is written in terms of fluxes. Next, this equation is integrated over a control volume. The control volume is shown in Figure 2.7. If we define the flux as $\epsilon = c'_1 \alpha_1 + c'_2 \frac{d\alpha_1}{dx}$, the differential equation may be written as:

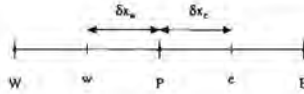


Figure 2.7: Control volume that is used for discretization.

$$\frac{d\epsilon}{dx} + c'_3 = 0. \quad (2.85)$$

Integration of the equation from $x = x_w$ to $x = x_e$ (see Figure 2.7) over the control volume gives:

$$\epsilon_e - \epsilon_w + (c'_3 \delta x_e + c'_3 \delta x_w) = 0, \quad (2.86)$$

where ϵ_e is the flux on the east side of the control volume. The distances δx_e and δx_w are defined as shown in Figure 2.7. The index w denotes the point on the discretization cell boundary between x_{i-1} and x_i on the west side of point i , and the index e denotes the east point between x_{i+1} and x_i . To derive a linear equation for the variables at neighbouring points, an expression for the fluxes ϵ_e and ϵ_w in terms of the values in the grid points W , P and E is required. This can be obtained if a function for α between the grid points can be derived. An analytic solution of (2.84) is available if the coefficients c_i are constant. This analytical solution between points x_l on the left side and x_r on the right side is given by:

$$\alpha_1(x) = \alpha_1(x_l) - \frac{c'_3}{c'_1}(x - x_l) + \frac{\alpha_1(x_r) - \alpha_1(x_l) + \frac{c'_1}{c'_1}(x_r - x_l)}{\exp\left(-\frac{c'_1}{c'_2}(x_r - x_l)\right) - 1} \left(\exp\left(-\frac{c'_1}{c'_2}(x - x_l)\right) - 1 \right). \quad (2.87)$$

If we substitute (2.87) in the equations for the fluxes ϵ_e and ϵ_w on the east and west side of the control volume, equation (2.86) can be rewritten as:

$$a^W \alpha_{1,W} + a^P \alpha_{1,P} + a^E \alpha_{1,E} = b, \quad (2.88)$$

Next we write the control variables as $\alpha_{1,i}$, with i the position index. The coefficients a^W , a^P and a^E depend on the coefficients $c'_{j=1,\dots,3}$ which generally depend on the position and are therefore written as a_i^W , a_i^P and a_i^E respectively, leading to:

$$a_i^W \alpha_{1,i-1} + a_i^P \alpha_{1,i} + a_i^E \alpha_{1,i+1} = b_i, \quad (2.89)$$

The coefficients of eq. (2.89) are given by:

$$a_i^E = \frac{c'_{2,i-1}}{x_i - x_{i-1}} A(-P_i^W),$$

$$a_i^W = \frac{c'_{2,i+1}}{x_{i+1} - x_i} A(P_i^E),$$

$$a_i^P = -(a_i^E + a_i^W),$$

$$b_i = -c_{4,i-1}(x_i - x_{i-1})(1 - W(P_i^W)) - c_{4,i+1}(x_{i+1} - x_i)W(P_i^E),$$

The local Peclet numbers P_i^W and P_i^E are defined by:

$$P_i^W = \frac{-c'_{1,i}}{c'_{2,i}}(x_i - x_{i-1}),$$

$$P_i^E = \frac{-c'_{1,i+1}}{c'_{2,i+1}}(x_{i+1} - x_i).$$

The functions A and W result from the exact exponential solution eq. (2.87). These functions are given by:

$$A(P) = \frac{P}{e^P - 1}, \quad (2.90)$$

$$W(P) = \frac{1 - A(P)}{P}.$$

These functions are often approximated by the following expressions:

$$A^*(P) = \max[0, (1 - 0.1|P|^5)] + \max[0, -P], \quad (2.91)$$

$$W^*(P) = \frac{1 - A^*(P)}{P}.$$

This approximation has the advantage that it is calculated much faster. It has been shown [Thi90] that the exact functions A and W are very well approximated by A^* and W^* .

The discretization finally gives a set of i linear equations for $\alpha_{j,i}$: $\mathbf{A}\alpha_i = \mathbf{b}$ for each control variable, where the matrix \mathbf{A} is a tridiagonal matrix. This matrix equation can simply be solved by using a tridiagonal matrix solver.

Starting with a first estimate for the solution, the equations for α_j , h and χ_j can be considered one after the other. I.e. they are linearized, discretized and solved sequentially by the use of a tridiagonal matrix solver.

Alternatively, all equations can be solved simultaneously. To this end, use has been made of a code developed at the Eindhoven University of Technology by Somers [Som94], which solves all equations simultaneously, using an implicit procedure (Newton's method). To this end, the discretized equations for the control variables (2.89) are written as:

$$g_{ji} = a_{ji}^W \alpha_{j,i-1} + a_{ij}^P \alpha_{j,i} + a_{ij}^E \alpha_{j,i+1} - b_{ji} = 0, \quad (2.92)$$

denoting the residual for the j^{th} control variable at position i . The solution procedure which is followed to solve this set of equations is similar to the procedure applied for the manifold computations. Most results presented in chapter 3 are obtained using the first mentioned explicit method, since the implementation of mathematically reduced mechanisms in the code solving the equations implicitly, is performed in a later stage.

2.3.5 Interpolation

For application of mathematically reduced reaction mechanisms, differential equations are solved for all independent variables. The remaining variables are obtained from the manifold look-up table. Since the manifold look-up table consists of compositions at discrete points, interpolation has to be applied. We describe the interpolation method for one- and two-dimensional manifolds. For a one-dimensional manifold the interpolation is linear. Consider the function f , only known at certain points $x_i, i = 1, \dots, n_p$. The value of f at point x_i is denoted by f_i . The interpolated value of f at position x , situated between x_{i-1} and x_i , is given by:

$$f(x) = (1 - s_x) f_{i-1} + s_x f_i, \tag{2.93}$$

with

$$s_x = \frac{x - x_{i-1}}{x_i - x_{i-1}}.$$

On a two-dimensional manifold, linear interpolations can be used in all directions if an rectangular grid is used. However, in our approach the manifold is locally refined, which makes the interpolation more complicated. First, the domain is divided into triangles (1). Next the position on the manifold of the point that has to be interpolated is searched (2). Then, the actual interpolation can be performed (3). These aspects of the interpolation procedure will be described successively.

(1) The subdivision of the domain in triangles is done by searching the neighbouring points of all points, first. In general, eight kinds of neighbouring points are to be distinguished. These

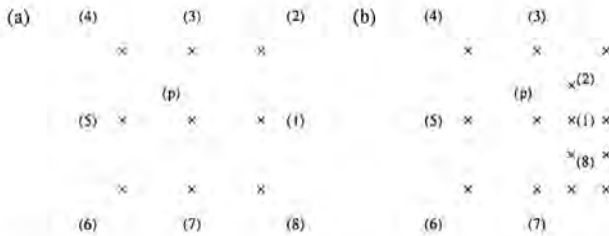


Figure 2.8: Eight points surroundings (p) are searched in the manifold mesh, with an (a) equidistant mesh and (b) a locally refined mesh.

points are shown in Figure 2.8 for an equidistant grid (a) and a refined grid (b). A problem which arises is that the choice of triangles is not unique. This can be seen by considering Figure 2.8. In the north-east corner above point p we can construct four different triangles: $(p, 1, 2)$, $(p, 2, 3)$, $(p, 1, 3)$ and $(1, 2, 3)$. Multiple triangles for a certain position on the manifold have to be avoided or course. If more than one triangle is possible, a disturbance might imply a possible switch to another triangle, leading to a discontinuity in the interpolated function. Therefore, we have to ensure neighbouring points to use the same triangles. In practice this means that some of the surrounding points of a specific point will not be used. We have chosen to

use triangles $(p, 1, 2)$ and $(p, 2, 3)$ in the north-east region. In the north-west region triangles $(p, 3, 5)$ and $(3, 4, 5)$ will be used. Finally, the domain around point (p) is divided into triangles as presented in Figure 2.9. It can be seen that surrounding points (4) and (8) are not

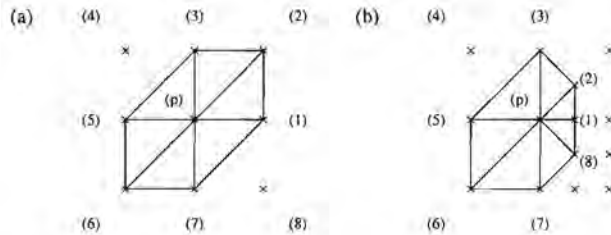


Figure 2.9: The domain is divided into triangles, for an (a) equidistant mesh and (b) a locally refined mesh.

used for the equidistant grid, while for the refined grid only point (4) is not used. An example of a locally refined grid, for a two-step reduced hydrogen-air reaction mechanism, with three refinement levels, and the corresponding triangles is shown in Figure 2.10. It can be seen that there are no points in the upper-right region. Here, the sum of the specific mole numbers of the control variables times the element composition coefficients exceeds the values of the element mole number of H ($\mu_{H, H_2O} \phi_{H_2O} + \mu_{H, H} \phi_H > \chi_H$).

(2) Before the actual interpolation can be performed, the position on the manifold has to be searched. This is done in the following way. First, an initial position is chosen. At first this will be the position corresponding to the unburned mixture. If interpolation is used during an iterative process the previous position on the manifold will be used. Then it is considered whether one of the neighbouring points of the initial position on the manifold is positioned closer to the point I which has to be interpolated. To find the nearest point on the manifold, we compute the relative distances to the surrounding points. However, it should be kept in mind that the maximum values of the control variables are not equal in general. Therefore, relative distances scaled by the maximum value of the control variables are used. Moreover, one should realize that the number of grid points used in the different directions may be different. An example of a situation where the number of grid points in both directions is different is presented in Figure 2.11. The dashed areas in the figures show the regions which use the middle point as reference for the interpolation for (a) as it should be and (b) using normally scaled distances. Therefore, we define a relative difference that is independent of the number of grid points.

If the value of one control variable is given by x , the point will be positioned between the points i and $i + 1$ for an equidistant grid, with i given by $\text{trunc}(i_x^{\max} x / x_{\max})^1$, where i_x^{\max} denoted the number of gridpoints and x_{\max} the maximum value of the control variable. If the grid is refined, we can compute the position on the finest grid level using a numbering as if a full fine grid was used, similarly. Subsequently a relative distance between point I , with coordinates

¹The function *trunc* (entier function) converts real numbers into integer numbers by omitting the digits behind the decimal point: $\text{trunc}(1.8) = 1$

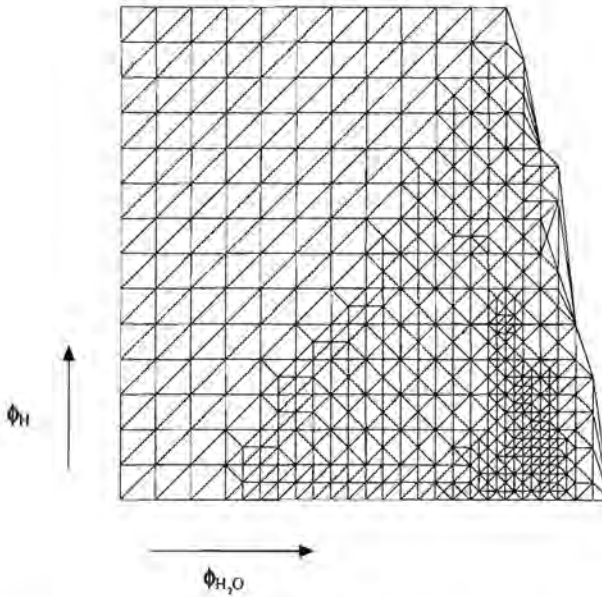


Figure 2.10: Example of a locally refined grid for a two-step reduced hydrogen-air reaction mechanism. In the x -direction the specific mole number of H_2O is used as control variable, in the y -direction the specific mole number of H is used as control variable.

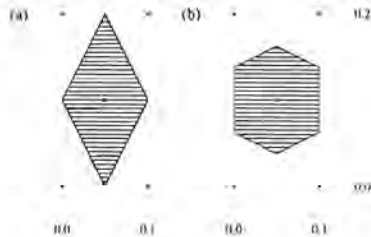


Figure 2.11: The points which have the smallest distance to the point in the middle are within the dashed area. The shape of the area depends on the definition of the relative distances: (a) definition as by (2.94) and (b) normally scaled distances.

(x, y) and point j is defined by:

$$d_j = \sqrt{(i_x^{max} x / x_{max} - i_x^j)^2 + (i_y^{max} y / y_{max} - i_y^j)^2}, \quad (2.94)$$

where i_x^j denotes the index on the finest grid level of point j . Defining the relative distances in this way is independent of the range of a control variable and the maximum number of gridpoints which is used in one direction.

Having defined the relative distances to manifold points, we return to the search of the nearest point on the manifold of point I . Starting at the initial point, the relative distances to the neighbouring points are computed. If the relative distance to one of the surrounding points is smaller than the relative distance to the starting point, then that point will be used as new starting position. The procedure is repeated until all the relative distances to neighbouring points are larger than the relative distance to the point which is considered.

When this point is known, denoted by p , the triangle in which the point I that has to be interpolated is positioned, has to be determined. Therefore, the following procedure is followed for the triangles that surround the point p . Denoting the points of the triangle by p , s_1 and s_2 (see Figure 2.12) the points k_1, \dots, k_4 are determined. These points are situated on the sides of

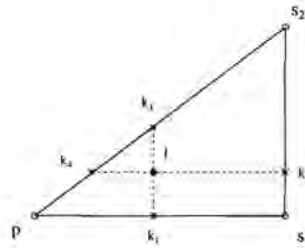


Figure 2.12: The points k_1, \dots, k_4 are used to detect whether the point I is located in the triangle spanned by the points p , s_1 and s_2 .

the triangle and have either equal x - or y -values as the point I . If the x -coordinate of the point I is smaller than the x -coordinate of k_2 and larger than the x -coordinate of k_4 , and the y -coordinate of I is in between the y -coordinates of k_1 and k_3 the point I is situated in the triangle. Now we are ready to interpolate.

(3) The values of the function that is interpolated are written as f_p , f_{s_1} and f_{s_2} , respectively. Then, the interpolation is given by:

$$f = f_p + l_1(f_{s_2} - f_{s_1}) + l_2(f_p - f_{s_2}), \quad (2.95)$$

where l_1 and l_2 are two parameters found from:

$$\begin{aligned} x_I &= x_p + l_1(x_{s_2} - x_{s_1}) + l_2(x_p - x_{s_2}), \\ y_I &= y_p + l_1(y_{s_2} - y_{s_1}) + l_2(y_p - y_{s_2}). \end{aligned} \quad (2.96)$$

Solving this set of equations gives values for l_1 and l_2 , so that the unknown variables can be obtained with (2.95).

In general, the enthalpy and the specific mole numbers may also change, so that there are $n_e + 3$ independent variables for a two-dimensional reduced reaction mechanism. The mesh on the manifold is not locally refined for the enthalpy and specific element mole numbers yet, so that a linear interpolation is sufficient for these variables.

2.3.6 Mesh Generation for One-Step Reduced Mechanism

For applications using a one-step reduced reaction mechanism with a single control variable a special mesh generation procedure is used to reduce the number of interpolations to a minimum. This is done by regridding in such a way, that the values of the control variables at the grid points coincide with manifold (grid) points, so that no interpolation errors are made (see Figure 2.13). The regridding procedure is less expensive than the interpolation procedure: no interpo-

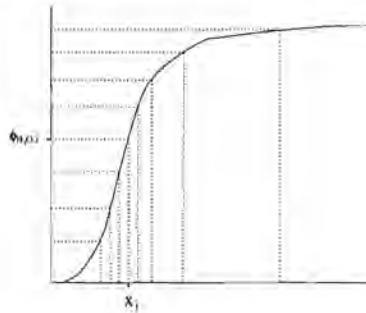


Figure 2.13: Adaptive grid; the grid points x_i are chosen in such a way that the values of the control variables ϕ_{H_2O} in these points (along the vertical axis) coincide with the grid points of the manifold

lations of species and chemical source terms have to be carried out. Also the derivatives $\frac{d\phi}{d\alpha}$ are functions of α only, and are constant if the values of the control variables remain unchanged in the grid points. Note that this regridding procedure becomes complicated if more-dimensional geometries are used. Furthermore, the interpolations can be circumvented only in case of one-dimensional manifolds. For higher-dimensional manifolds a similar procedure can be used to minimize the interpolation errors.

2.4 The Application of Reduced Schemes in Turbulent Flames

The application of the Mathematical Reduction Technique to laminar flame problems has been considered in the previous sections. In turbulent combustion modelling, the need of using reduced reaction mechanisms is even larger. Reduced reaction mechanisms are often used and

compositions are stored as a function of some control variables. These data-bases are made either by using 1-D laminar computations (for flamelet modelling) or by use of Conventional Reduction Methods. The latter approach is followed at the University of Twente (UT). In cooperation with UT we have made a comparative study of various methods to reduce a reaction mechanism. Until now, only Conventional Reduced Methods have been used for modelling turbulent flames (at UT). It is, however, also possible to use data-bases generated by using the Mathematical Reduction Technique. As this method determines the optimal reduced reaction mechanism, it is expected that more accurate results can be obtained.

2.4.1 Turbulent Combustion Modelling

In turbulent combustion modelling, the conservation equations as presented in chapter 1 are valid. However, in turbulent flames the range of time scales and spatial length scales is large. To resolve the smallest fluctuations a very fine grid in time and space would be necessary. Even for flows without combustion processes this requires tremendous large data-storage capacities. The computational effort is very large, even for the fastest super-computers [Egg94]. Therefore, not all fluctuations will be resolved. The variables are split into a mean and a fluctuating part:

$$\Phi = \bar{\Phi} + \Phi' \quad (2.97)$$

Subsequently the conservation equations for mass, momentum and energy are averaged. This leads to equations for the averaged properties. These equations have the same form as the original equations. However, additional terms appear, e.g. in the averaged momentum equation correlations of the type $\overline{v_i'v_j'}$ appear. These so-called Reynolds-stresses have to be modelled. This can be done in several ways. The treatment of these turbulence models, however, is not within the scope of this thesis and will not be considered further. The interested reader is referred to [Bat57], [Ten72]. In the equations for the various chemical components, which have to be solved for combustion problems, additional terms as $\overline{v'Y_i'}$, the so-called Reynolds fluxes, appear. These terms are also modelled. The treatment of these models is described more detail by [Pet92], [San94].

Apart from the fact that several terms have to be modelled, an additional problem may arise. The source terms in the species equations are of Arrhenius type and hence strongly dependent on temperature due to a factor $\exp(-E_A/RT)$ in the kinetic reaction rate. The non-linear behaviour on the temperature could give problems for the computation of the averaged source terms. To see this, the exponential factor in the source term is expanded in a Taylor-series [Lin92].

$$\overline{\exp\left(\frac{-E_A}{RT}\right)} = \exp\left(\frac{-E_A}{R\bar{T}}\right) \left(1 + \frac{1}{2} \left(\frac{E_A}{R\bar{T}}\right)^2 \frac{\overline{T'^2}}{\bar{T}^2} + \dots\right) \quad (2.98)$$

For most reactions, the series in $\overline{T'^2}/\bar{T}^2$ of eq. (2.98) converges. However, convergence is not guaranteed and 10 to 15 terms (i.e. moments) have to be considered to obtain sufficient accuracy, unless the activation energy E_A or the turbulent fluctuations is small. Note that we only considered the consequence of fluctuations of the temperature in (2.98). In general also the influence of fluctuations of reacting species on the averaged source term has to be considered.

The fluctuations of the temperature, however, are the most important ones due the exponential factor. In several important hydrogen reactions the activation energy has a high value, which implies that many terms in (2.98) have to taken into account. This, however, leads to extensive computational effort and should be circumvented.

When a one-step reduced reaction mechanism is used, the problem with the computation of the source term can be circumvented for certain reaction mechanisms. This is done by using a so-called progress variable, which has a source term without contributions of reactions with large activation energies. A combined specific mole number ($\phi_{H_2}^*$) can be defined as follows:

$$\phi_{H_2}^* = \phi_{H_2} + \phi_O + \frac{1}{2}\phi_{OH} + \frac{3}{2}\phi_H - \phi_{HO_2} - \phi_{H_2O_2}. \quad (2.99)$$

The result of this choice of control variable is that the source terms of the reactions r_1 to r_4 of the reaction mechanisms IV and V, presented in section B, cancel in the source term for $\phi_{H_2}^*$. These reactions r_1, \dots, r_4 have large activation energies. Hence, the remaining source term has contributions from the slow reactions having zero or small activation energy only. This progress variable will therefore be used for modelling turbulent H_2 -air as well CO/H_2 -air flames, so that the averaged turbulent composed species source terms can be calculated without problems and the difficulty with the heavily temperature-dependent source terms is avoided.

The Mathematical Reduction Technique has already been described in section 2.1. The conventional reduced mechanisms are constructed in a similar way: the number of steady-state or partial-equilibrium assumptions is equal to $n - n_e - n_c$ (here $n_c = 1$). From the steady-state of partial-equilibrium assumptions, the conservation of elements and the definition of $\phi_{H_2}^*$ (2.99), a set of nonlinear algebraic relations follows.

Because of the similarities between the conventional (CRM) and the mathematical (MRT) reduction methods, the procedure to compute the database is the same for the methods. In fact the reduced mechanisms are obtained from the same code, where only the steady-state equations are different. In the next sections the set of equations that will be solved for the Mathematical Reduction Technique and Conventional Reduction Methods, will be considered briefly to demonstrate the similarities and the differences of the various methods.

2.4.2 Steady-States for Species

The principle of applying steady-state assumptions is already considered in chapter 1. The equations solved to obtain the reduced mechanism are given ones again, to compare them with the equations that are solved for the Conventional Reduction Methods presented in the next sections. A steady-state assumption for species i is given by $w_i = 0$, where w_i is the net chemical source term of species i . If the species are ordered so that the species with the highest index are the steady-state species, this leads to:

$$(\delta_i, \mathbf{w}) = 0, \quad i = n_c + n_e + 1, \dots, n, \quad (2.100)$$

in vector notation, with $\delta_i = (\delta_{i1}, \dots, \delta_{in})$, δ_{ij} being the Kronecker delta. These steady-state equations are solved together with the element conservation equations and control variable $\phi_{H_2}^*$:

$$\begin{aligned} (\xi_i, \phi) - \phi_{H_2}^* &= 0, & i = 1, \dots, n_c, \\ (\mu_{(i-n_c)}, \phi) - \chi_{(i-n_c)} &= 0, & i = n_c + 1, \dots, n_c + n_e, \end{aligned} \quad (2.101)$$

where χ_j denotes the mass fraction of element j , μ_j the element composition vectors, (ξ_i, ϕ) the control variable (see (2.99)).

2.4.3 Partial-Equilibrium of Reactions

The chemical source term can be written in vector notation as:

$$w = \mathbf{V}r, \quad (2.102)$$

with reaction rates r_i and where \mathbf{V} is the transformation matrix with reaction vectors ν_i as column vectors (see (1.45)).

A partial-equilibrium assumption is given by:

$$r_j = 0. \quad (2.103)$$

If the inverse of the matrix \mathbf{V} exists and the reactions are reordered so that the reaction with the highest index are the reactions which are in partial-equilibrium, then the partial-equilibrium assumptions are given by:

$$(\bar{\nu}_i, w) = 0, \quad i = n_c + n_e + 1, \dots, n, \quad (2.104)$$

where $\bar{\nu}_i$ is the i^{th} row-vector of \mathbf{V}^{-1} . The remaining equations for conservation of elements and the progress variable are given by eq. (2.101).

In general, however, there are more reactions than species, which implies that \mathbf{V} is not a square matrix and that the inverse of matrix \mathbf{V} does not exist. Furthermore, the element mass fractions do not change due to chemical reactions. Therefore, the reaction vectors can not form a basis for the entire composition space. However, it is possible to compose a basis from a reduced $(n - n_e)$ number of (independent) reactions vectors and (n_e) element composition vectors. Besides the $(n - n_c - n_e)$ partial-equilibrium reactions (which may not be dependent) and the element composition vectors this basis consists of n_c other reactions vectors. The reactions which are not in steady-state may be chosen arbitrarily because the partial-equilibrium equations do not depend on the reaction rates of these reactions.

Chapter 3

Applications of Reduction Methods

In this chapter applications of the Mathematical Reduction Technique (which determines Intrinsic Low-Dimensional Manifolds in reaction space) as introduced in chapters 1 and 2 are presented. At first, the reduction method is applied to hydrogen/air reaction mechanisms. These reaction mechanisms are relatively simple, due to the relatively small number of species and reactions involved. Furthermore, the reduction method will also be applied to carbon monoxide-hydrogen/air and methane/air reaction mechanisms. The reduced reaction mechanisms are applied to flat flames, because these flames are relatively easy to model. Even computations with the full reaction mechanisms can be performed within reasonable time. This enables us to compare the results of reduced reaction mechanisms with results of detailed computations, giving insight in the performance of the reduction method.

Results of several hydrogen/air reaction mechanisms reduced to one-step schemes and used for modelling adiabatic flames are presented in section 3.1. It will be shown that the most simple hydrogen/air reaction mechanism can be reduced to an accurate one-step scheme. Since we use unit Lewis numbers the specific element mole numbers and enthalpy remain constant and the manifold used is one-dimensional; all species are computed as a function of one control variable. In flame computations one differential equation for the control variable is solved together with an equation for the mass flow rate. The other variables are obtained from the data-base.

A time-scale analysis comparing the chemical time scales with convective and diffusive time scales, is applied to investigate why the reaction mechanisms which include HO_2 cannot be reduced to accurate one-step mechanisms. It is shown that a two-step reduced reaction mechanism improves the results considerably. In the final part of section 3.1, we relax the unit Lewis numbers assumptions for the hydrogen/air reaction mechanism. In section 3.2 the reduced reaction mechanisms are used to model burner-stabilized flat hydrogen flames. As these flames are cooled at the burner edge, the enthalpy appears as an additional variable, for which a differential equation has to be solved. It is studied under which conditions a one-step reduced scheme is still accurate for burner-stabilized flames and under which circumstances a two-step reduced scheme should be used. In section 3.3, databases of carbonmonoxide-hydrogen/air ($CO-H_2$ /air) flames, obtained by the Mathematical Reduction Technique are compared with databases from Conventional Reduction Methods based on steady-state and partial-equilibrium assumptions in order to study the differences between various reduction methods. It is expected that the Math-

emathical Reduction Technique is most accurate, due to the fact that this method determines the fast and slow reaction groups locally.

Since methane is used as fuel in many combustion applications, appropriate reduced reaction mechanisms for methane are required to model such combustion processes fast and efficiently. Therefore, the reduction method is also applied to a methane/air reaction mechanism, finally. In section 3.4 the methane/air reaction mechanism is reduced to a two-step reduced scheme, which is applied to an adiabatic flame. Because we use unit Lewis numbers the manifold used is two-dimensional. The results are compared with computations using detailed reaction mechanisms. The main results presented in this chapter are also published in [Egg95a], [Egg95b] and [Egg95c].

3.1 Adiabatic Hydrogen Air Flames

We start by applying the reduction method to simple reaction mechanisms for adiabatic flat flames. In chapter 2 the differential equations for reduced scheme applications are derived. The solution strategy applied to obtain the manifold data-bases is also discussed there. For the application of reduced schemes presented in this subsection we use unit Lewis numbers (defined by eq. 1.22) and simplified thermodynamic properties: we take constant and equal specific heats $c_{p_i} = c_p$, $i = 1, \dots, n$. These approximations are not essential for the reduction method and are introduced for simplicity.

We have already seen that the unit Lewis number assumption implies that the specific element mole numbers and the enthalpy do not change. This simplifies the system even further. As we consider one-step reduced schemes here, the manifolds are one-dimensional. However, apart from solving a differential equation for the control variable, the mass burning rate has to be determined. The other species are obtained by using the data-base. Here, we take the specific mole number of H_2O as a control variable. We choose this control variable because the specific mole number of H_2O increases continuously during the combustion processes and therefore is a suitable control variable.

To study the performance of the reduction method, we compute one-step reduced mechanisms for three different hydrogen/air reaction systems, with a various number of species. The most simple reaction system, indicated as system I, consists of 6 reacting species (H_2 , O_2 , H , O , OH and H_2O) and nitrogen (N_2), which is assumed to be inert. As HO_2 plays an essential role in hydrogen combustion processes, this most simple reaction mechanism is not physically realistic. The second system II takes HO_2 into account. The third system III additionally includes H_2O_2 . It has to be stressed that it is our primary aim to test the reduction method and that the accuracy of the reaction systems therefore is of minor interest. The reaction mechanisms I, II and III are presented in Appendix B.

To model the structure of more-dimensional flames appropriately, an accurate prediction of the burning velocity is necessary. Therefore, we test whether the reduced schemes predict the burning velocity correctly by comparing the results with computations using detailed mechanisms. Species profiles will also be compared with detailed computations.

Time scales of the reaction system and time scales of convection and diffusion processes

are derived and compared in section 3.1.3. This time scale analysis can be used to predict the accuracy of the reduced scheme.

3.1.1 Results of Manifold Calculations

Scaled mole fractions \tilde{X}_i of the one-dimensional manifold maps for systems I, II and III are given by the solid lines in Figures 3.1, 3.2 and 3.3 as function of the scaled H_2O mole fraction. In these figures, also results of computations using the detailed mechanisms are given for comparison by the dotted lines. The differences between system I and II are small for the species H_2 and

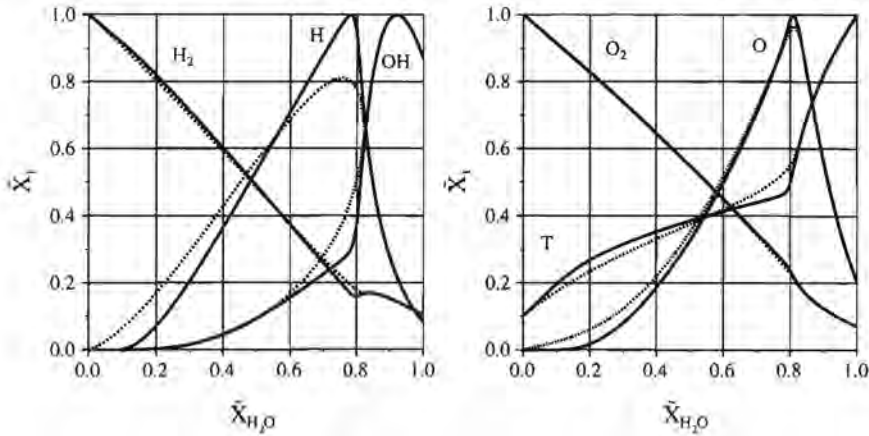


Figure 3.1: Scaled mole fractions and temperature as function of the control variable \tilde{X}_{H_2O} ; comparison of reduced (continuous lines) and full flat-flame calculations (dashed lines), for system I. The maximum values are: O_2 : $1.5 \cdot 10^{-1}$, H : $9.7 \cdot 10^{-2}$, OH : $2.7 \cdot 10^{-2}$, O : $1.7 \cdot 10^{-2}$, H_2 : $3.0 \cdot 10^{-1}$, H_2O : $2.7 \cdot 10^{-1}$ and T : 2750K

O_2 . For the radicals H , O and OH , however, we see that the region where the radical levels are high is smaller for system II. The influence of adding HO_2 to the system is large, especially for low \tilde{X}_{H_2O} values. Since the differences between system I and II are larger than the differences between system II and III, we focus on differences between systems I and II mainly.

The reduction method assumes reaction groups, corresponding to the largest eigenvalues, to be in steady-state. The accuracy of the reduction method increases, if the difference between the time scales of the reaction groups supposed to be in steady-state and the time scale of the remaining slowest process increases. Therefore, it is interesting to consider the magnitude of the real part of the eigenvalues along the manifold, as they represent the inverse of the time scales. Although some eigenvalues appear to be complex when computing the manifold, they turn out to be real eventually. Therefore, absolute values of the eigenvalues instead of absolute values of the real part of the eigenvalues can be considered. The absolute values of the eigenvalues along the manifold are given in the Figures 3.4, 3.5 and 3.6 for schemes I, II and III, respectively.

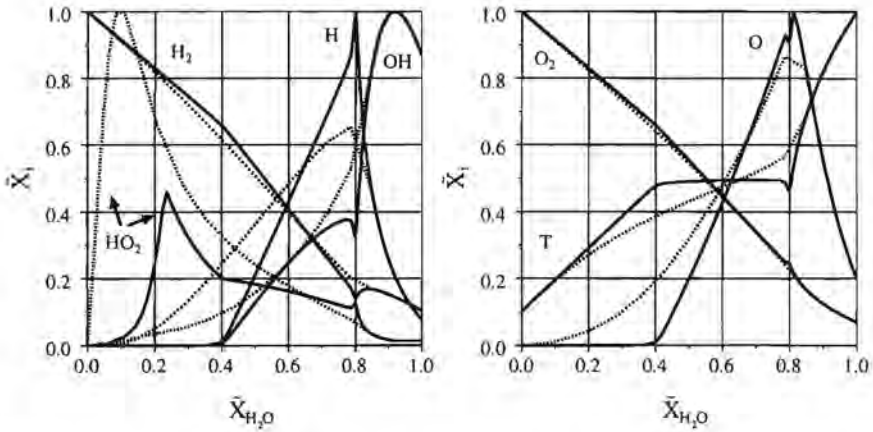


Figure 3.2: Scaled mole fractions and temperature as function of the control variable \bar{X}_{H_2O} ; comparison of reduced (continuous lines) and full flat-flame calculations (dashed lines), for system II. The maximum values are: O_2 : $1.5 \cdot 10^{-1}$, H : $8.9 \cdot 10^{-2}$, OH : $2.7 \cdot 10^{-2}$, O : $1.7 \cdot 10^{-2}$, H_2 : $3.0 \cdot 10^{-1}$, H_2O : $2.7 \cdot 10^{-1}$, HO_2 : $2.4 \cdot 10^{-4}$ and T : 2740K

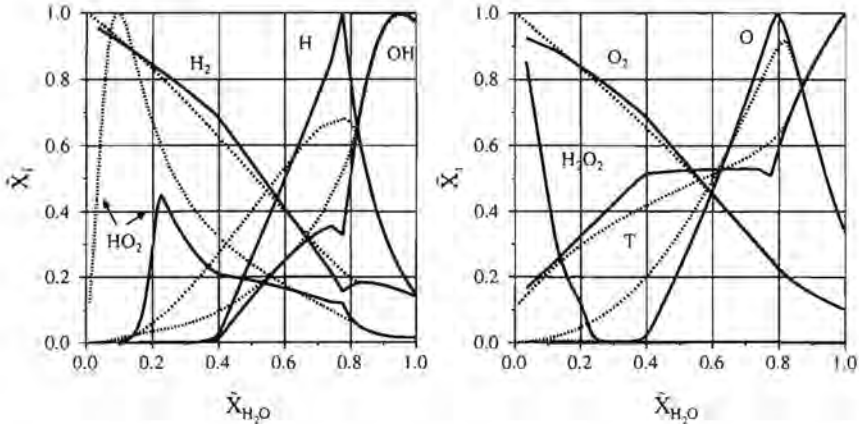


Figure 3.3: Scaled mole fractions and temperature as function of the control variable \bar{X}_{H_2O} ; comparison of reduced (continuous lines) and full flat-flame calculations (dashed lines), for system III. The maximum mole fractions are: O_2 : $1.5 \cdot 10^{-1}$, H : $9.8 \cdot 10^{-2}$, OH : $2.7 \cdot 10^{-2}$, O : $1.7 \cdot 10^{-2}$, H_2 : $2.9 \cdot 10^{-1}$, H_2O : $2.7 \cdot 10^{-1}$, HO_2 : $2.4 \cdot 10^{-4}$, H_2O_2 : $9.8 \cdot 10^{-3}$ and T : 2750K. Note that the mole fraction of H_2O_2 for the full scheme is not visible in the figure because it is much smaller than for the reduced scheme.

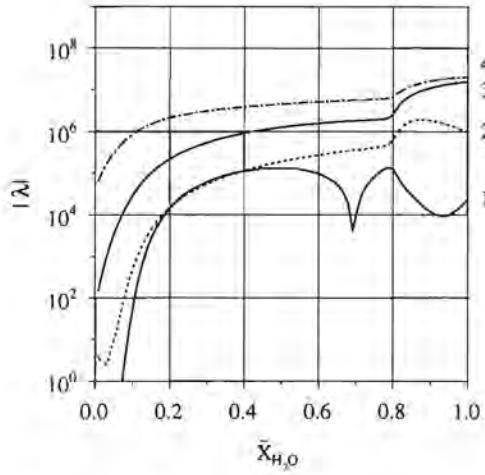


Figure 3.4: Eigenvalues of the reduced hydrogen/air reaction system I

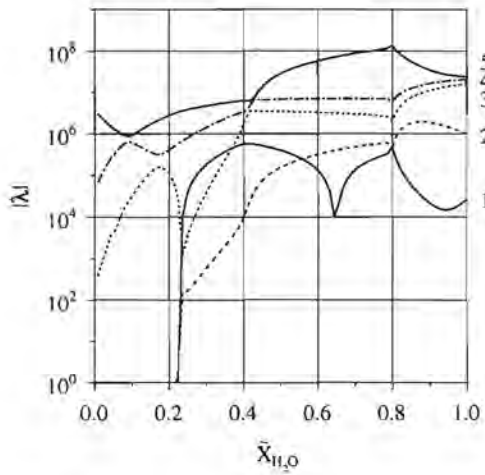


Figure 3.5: Eigenvalues of the reduced hydrogen/air reaction system II. Note that eigenvalues 1 and 2 approach zero for $\bar{X}_{H_2O} \lesssim 0.22$.

Since reaction system I contains six active species, it contains six time scales, systems II and

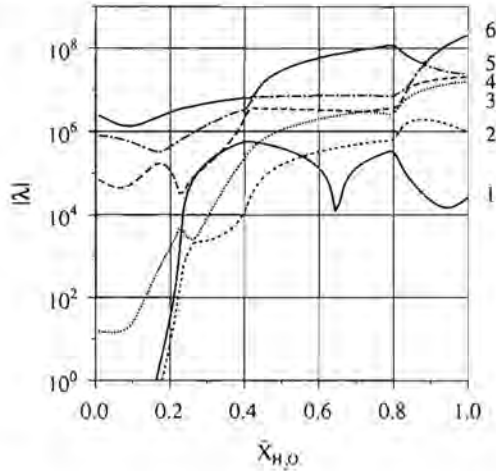


Figure 3.6: Eigenvalues of the reduced hydrogen/air reaction system III. Note that eigenvalues 1 and 2 approach zero for $\bar{X}_{H_2O} \lesssim 0.18$.

III contain seven and eight time scales, respectively. Due to conservation of elements (O and H) two of the eigenvalues are equal to zero. The other eigenvalues are ordered in descending order of real part, i.e. eigenvalue 1 has the largest real part. Most eigenvalues are negative, only eigenvalue 1 is positive for $\bar{X}_{H_2O} \lesssim 0.7$ for system I. This also holds for $\bar{X}_{H_2O} \lesssim 0.65$ for systems II and III. As the first eigenvalue changes sign, it goes to zero at $\bar{X}_{H_2O} \approx 0.7$ (or $\bar{X}_{H_2O} \approx 0.65$) so that $\text{Log}(|\text{Re}(\lambda_1)|) \rightarrow -\infty$. Note that the species profiles are smooth here because the transition of the first eigenvalue from positive values to negative values is smooth. Considering the full system (see next section) it can be seen that the chemical source term of H_2O reaches a maximum at this position ($\frac{\partial w_{H_2O}}{\partial \phi_{H_2O}} = 0$). Note that at $\bar{X}_{H_2O} \approx 0.55$ eigenvalues 1 and 2 are not equal in Figures 3.5 and 3.6; eigenvalue 1 is positive and eigenvalue 2 is negative.

Comparing the mole fractions and eigenvalues of systems I and II we see that, except for the fact that system II has one more eigenvalue, the mole fractions and the eigenvalues are not changed much for values of $\bar{X}_{H_2O} \gtrsim 0.5$. One major difference is that the first eigenvalue is equal to the second one for system II near $\bar{X}_{H_2O} = 0.8$ and for $\bar{X}_{H_2O} \lesssim 0.22$. The reduction method is not accurate here and the profiles of the species are therefore not smooth at $\bar{X}_{H_2O} \approx 0.8$.

3.1.2 Flat Flame Calculations

Reduced and detailed flat-flame calculations are performed with the three aforementioned reaction schemes. The results of the complex calculations are also presented as a function of \bar{X}_{H_2O} in Figures 3.1, 3.2 and 3.3 by the dotted lines. Furthermore, the profiles of the species

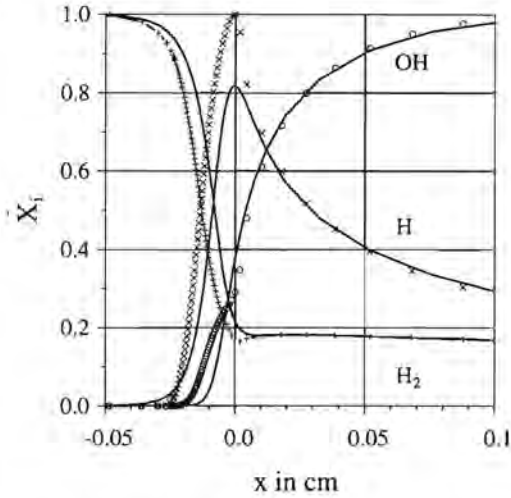


Figure 3.7: Scaled mole fractions as function of distance x ; comparison of reduced (markers) and full flat-flame calculations (lines), for system I.

are shown in Figures 3.7, 3.8, 3.9 and 3.10 as function of x for systems I and II. It appears that only the H -radical mole fraction is over-estimated for system I. The mole fractions of the other species are predicted quite well. (Figure 3.7 and 3.8). For system II and III it is seen in Figures 3.2 and 3.3 that the difference between the reduced and full scheme is large for HO_2 (and H_2O_2). Differences between other radical profiles are large around $\bar{X}_{H_2O} \approx 0.8$, where the first two eigenvalues are equal (see Figure 3.5). Note that over-estimates of radicals are sometimes also observed in conventional reduced schemes. Comparing the mass burning rates of the complex and the reduced calculations of system I and II (Table 1), we see that the influence of adding species HO_2 to the reaction system on the mass burning rate is large. Reduced scheme

Scheme	$\dot{M}_{detailed}$	\dot{M}_{red}
I	0.115	0.116
II	0.195	0.155
III	0.193	0.160

Table 3.1: Mass burning rates in $g/(cm^2s)$ for adiabatic flames using detailed and reduced reaction schemes.

calculations with schemes II and III predict too low HO_2 concentrations and, therefore, underestimate the mass burning rates considerably. The influence of variations in ϕ_{HO_2} on the burning velocity is studied in more detail by considering the sensitivity of the net chemical source term

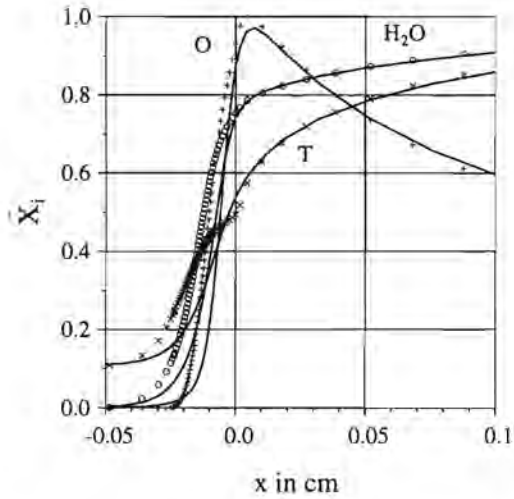


Figure 3.8: Scaled mole fractions as function of distance x ; comparison of reduced (markers) and full flat-flame calculations (lines), for system I.

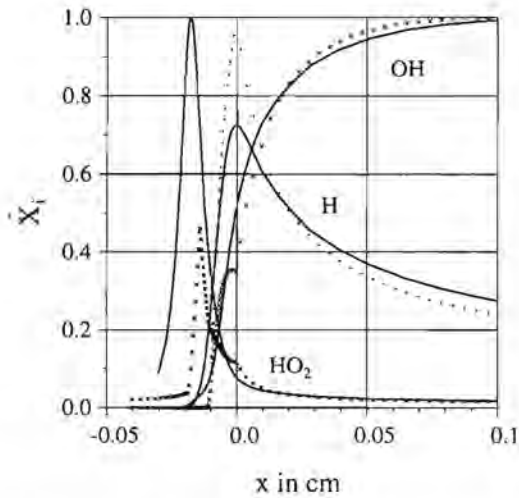


Figure 3.9: Scaled mole fractions as function of distance x ; comparison of reduced (markers) and full flat-flame calculations (lines), for system II.

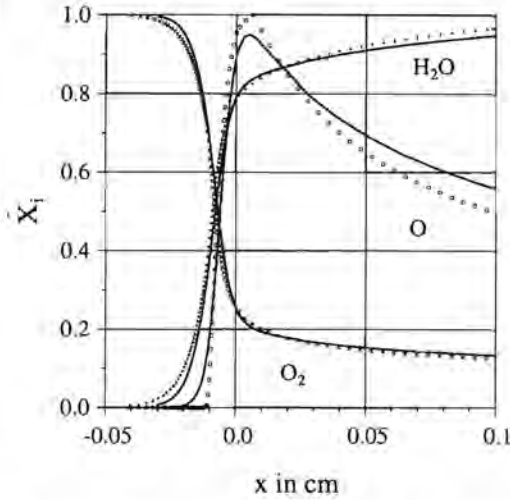


Figure 3.10: Scaled mole fractions as function of distance x ; comparison of reduced (markers) and full flat-flame calculations (lines), for system II.

($w_{red} = (w, \frac{d\phi}{d\alpha}) / |\frac{d\phi}{d\alpha}|^2$) of the reduced scheme to variations in the specific mole numbers of HO_2 . The sensitivity is defined as the relative variation in the source term divided by the relative variation in ϕ_{HO_2} : $\frac{\partial w_{red}}{\partial \phi_{HO_2}} \frac{\phi_{HO_2}}{w_{red}}$. This sensitivity is shown in Figure 3.11 for systems II and III as function of \bar{X}_{H_2O} . It is seen that the sensitivity becomes large for low values of \bar{X}_{H_2O} . If the sensitivity is equal 10, a variation of 1% in the specific mole number of HO_2 causes a change of 10% in the source term. The net source term of the one-step reduced scheme therefore depends strongly on the specific mole number of HO_2 . This explains the deviations between profiles and mass burning rates of reduced and full scheme calculations with system II and III.

3.1.3 Time Scale Analysis of the Full system

The Mathematical Reduction Technique is based on the assumption that the fastest reactions groups are in steady-state. It will be clear that the accuracy of the reduced scheme depends on the difference in the time scale of the slowest reaction group assumed to be in steady-state and the fastest reaction group not in steady-state. Moreover, the time scales of the reaction groups assumed to be in steady-state should be smaller than the convective and diffusive time scales of the system. If all chemical, convective and diffusive time scales are known, it can be examined whether the reduced scheme is accurate.

On the other hand, the chemical source term needs to be predicted accurately only if the largest time scale of the reaction system is smaller than the convective and diffusive time scales. If the magnitudes of convective and diffusive time scales are smaller than chemical time scales,

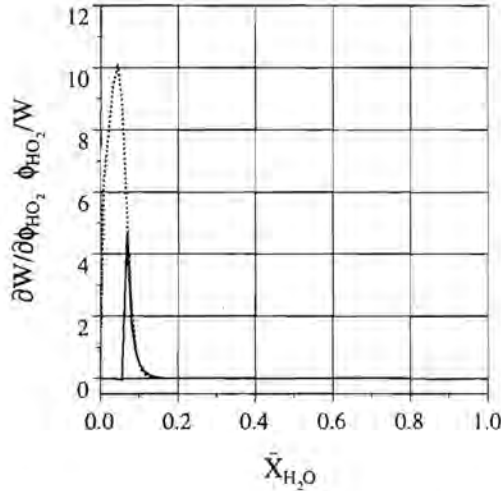


Figure 3.11: Sensitivity of the net source term of the one-step reduced scheme for variations in specific mole numbers of HO_2 . The continuous line denotes results for system II, the dashed line for system III.

the chemical source term will be smaller than convective and diffusive terms. Accurate prediction of the source term is then not required. In order to check whether the introduced assumptions are valid, the behaviour of the convective and diffusive time scales for all species of the full reaction scheme are studied. Therefore, the differential equation for species i of the complex system (eq. 2.40) is considered. This equation contains convective ($c_i = \rho u \frac{d\phi_i}{dx}$), diffusive ($f_i = -\frac{d}{dx} \rho D_i \frac{d\phi_i}{dx}$) and chemical reaction (ρw_i) contributions. To find the typical local time scales of these terms they are linearized as follows:

$$\begin{aligned}
 c_i &= c_i^0 + \left(\frac{dc_i}{d\phi_i} \right)^0 (\phi_i - \phi_i^0), \\
 f_i &= f_i^0 + \left(\frac{df_i}{d\phi_i} \right)^0 (\phi_i - \phi_i^0), \\
 w_i &= w_i^0 + \left(\frac{dw_i}{d\phi_i} \right)^0 (\phi_i - \phi_i^0).
 \end{aligned} \tag{3.1}$$

In analogy with the time scales defined by eq. (2.11), the typical convective, diffusive and re-

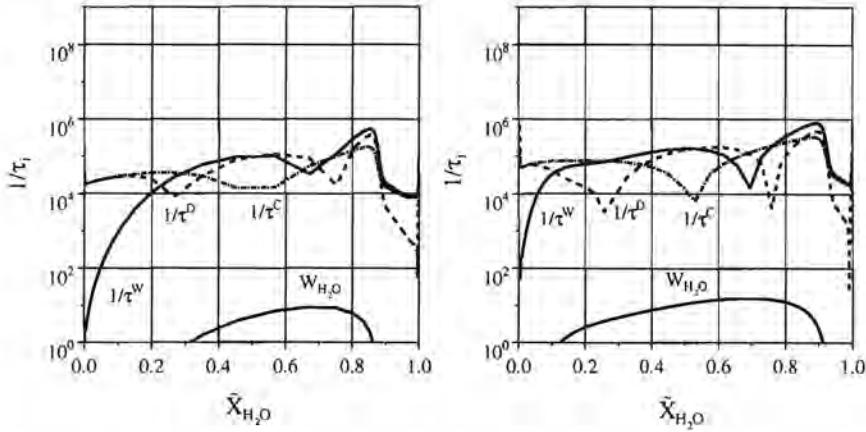


Figure 3.12: Time scales of H_2O as function of \tilde{X}_{H_2O} , systems I (left) and II (right)

action time scales τ_i^C , τ_i^D and τ_i^W are given by:

$$\begin{aligned}\tau_i^C &= \left| \rho \frac{1}{\frac{dc_i}{d\phi_i}} \right|, \\ \tau_i^D &= \left| \rho \frac{1}{\frac{dJ_i}{d\phi_i}} \right|, \\ \tau_i^W &= \left| \frac{1}{\frac{dw_i}{d\phi_i}} \right|.\end{aligned}\tag{3.2}$$

Note that this time scale analysis is not very accurate. However, it is useful to study the order of magnitude of the various terms in the differential equation. These time scales are calculated using the solution of the full system. The typical time scales of H_2O are shown in Figure 3.12 as function of \tilde{X}_{H_2O} for reaction system I and II. The order of magnitude of the time scales of the other species is comparable. The source term w_{H_2O} is also shown in Figure 3.12. Note that the time scale of the source term $\tau_{H_2O}^W$ is infinite at the position where the source term reaches its maximum value. Here $\frac{dw_i}{d\phi_i} = 0$, so that the time scale is infinite by definition. The time scales of convection and diffusion can also be infinite for similar reasons, e.g. the term $\frac{dC_{H_2O}^C}{d\phi_{H_2O}} = 0$ at the position where $\rho\mu\frac{d\phi_{H_2O}}{dx}$ reaches a maximum, so that $\tau^C \rightarrow \infty$ and $\log(1/\tau_{H_2O}) \rightarrow -\infty$. The diffusion time scale is infinite when $\frac{d}{dx} \left(\rho D_{H_2O} \frac{d\phi_{H_2O}}{dx} \right)$ has a maximum or a minimum. These points are visible in Figure 3.12 by the dips in the time-scale profiles. Considering system I in Figure 3.12 we see that for $\tilde{X}_{H_2O} \lesssim 0.1$ convective and diffusive terms (and time scales) are of the same order of magnitude while for $\tilde{X}_{H_2O} \gtrsim 0.9$ convective and source terms are of comparable magnitude. Note that at least two time scales must be of the same order of magnitude, in

order to obey eq. (2.40). Also note that the behaviour of the time scale of the source term in Figure 3.12 resembles that of the slowest time scales of the chemical source terms of the reduced scheme (Figures 3.4 and 3.5). This is an indication of the accuracy of the reduction technique.

If Figures 3.5 and 3.12 are compared it can be seen that the time scale of the slowest reaction group which is supposed to be in steady-state is larger than convective and diffusive time scales for $\bar{X}_{H_2O} \lesssim 0.22$. For $\bar{X}_{H_2O} \lesssim 0.1$ the source term is small (the time scale of the source term is larger than convective and diffusive time scales) and accurate prediction of the source term is not necessary. There is, however, a region ($0.1 \lesssim \bar{X}_{H_2O} \lesssim 0.22$) where the source term may not be neglected and where the reduction method is not appropriate. This causes that the HO_2 profile, which reaches its maximum within this region, is not predicted accurately. We have already seen that variations in ϕ_{HO_2} have a large influence on the reaction rate and adiabatic mass burning rate. This brings us to the conclusion that system II and III cannot be reduced to an accurate one-step reduced scheme, within this region. The main reason for the failure of the one-step reduced scheme of system II and III is that the second eigenvalue approaches zero at $\bar{X}_{H_2O} \lesssim 0.22$. It is likely that a two-step reduced scheme would give better results.

Now we have seen the reason for the failure of the one-step reduced schemes for systems II and III, it is interesting to investigate why the one-step reduced scheme of system I gives accurate results. For this scheme the time scale of the slowest reaction group that is supposed to be in steady-state is larger than convective and diffusive time scales for $\bar{X}_{H_2O} \lesssim 0.2$. Here, however, the source term is already small and does not need to be predicted accurately. Although the assumptions for the reduction are not valid for this region where the source term is much smaller than convective and diffusive terms, manifold composition may still be used: radical specific mole numbers are very low at these low temperatures and the manifold compositions satisfy the conservation equations for the elements so that $2\phi_{H_2} + \phi_{O_2} - 2\phi_{H_2O} \approx 0$ within this region. As we use unit Lewis numbers this is also valid for the full reaction scheme, as long as the radical specific mole numbers are small enough.

About the results of the one-step reduced schemes when applied to adiabatic flames we may draw the following conclusions.

The one-step reduced schemes give only appropriate results for the most simple reaction system I, without species HO_2 and H_2O_2 . For the other reaction systems most species are still approximated well. But the mole fraction of HO_2 is under-estimated considerably and it appears that this species has a large influence on the source term of the control variable. As it is expected that a two-step reduced scheme will be more accurate, a two step reduced scheme will be considered in the next subsection.

3.1.4 Two-Step Reduced Mechanism

In the previous subsection one-step reduced schemes for several hydrogen/air reaction mechanisms are considered. It is observed that the reaction mechanisms including HO_2 cannot be described accurately by a one-step reduced mechanism. In this section we consider a two-step reduced scheme. We apply the Mathematical Reduction Technique on the reaction mechanism II (see Appendix B). As control variables we use ϕ_{H_2O} and ϕ_H . Although species H does not increase monotonously as we assumed for rewriting derivatives of x to derivatives of α_j (i.e.

$\frac{\partial \phi_j}{\partial x} = \frac{\partial \phi_j}{\partial \alpha_j} \frac{\partial \alpha_j}{\partial x}$, this did not give numerical problems ($\frac{\partial \alpha_j}{\partial x}$ does not become zero). The grid used for the manifold is locally refined and has already been presented in chapter 2 (see Figure 2.10). As in the previous sections unit Lewis numbers are used. In contrast to previously presented results we here use temperature dependent specific heats of the species (1.37). This gives more realistic results. The adiabatic mass burning rate will therefore be different from the adiabatic mass burning rate presented in the previous subsection. The computations are performed with the code which solves all variables simultaneously by use of a damped Newton method. This code is developed to model flat flames using detailed reaction mechanisms [Som94] and has been modified for the use of reduced mechanisms. Results for adiabatic flat flames are presented in Figures 3.13 and 3.14 for system II, where also results of computations using detailed reaction mechanisms are shown. It can be seen that the reduced scheme calculations agree very

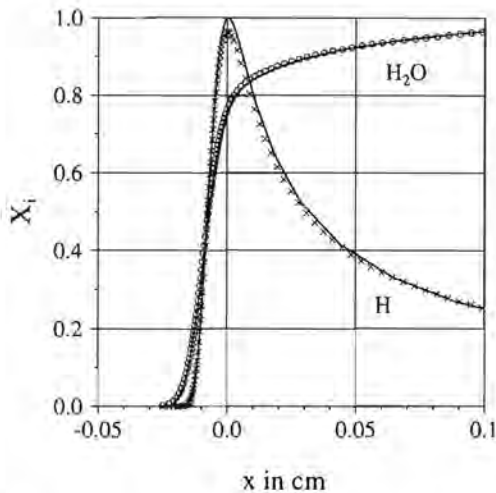


Figure 3.13: Comparison of results of a two-step reduced hydrogen/air reaction mechanism (markers) and detailed computations (lines) for reaction system II. The mole fractions of the species are scaled with the maximum mole fractions. These are given by H: $5.16 \cdot 10^{-2}$, H_2O : $3.0 \cdot 10^{-1}$.

well with the detailed computations. This is also true for the adiabatic mass flow rate which is $0.127 \text{ g}/(\text{cm}^2 \text{ s})$ for the complex mechanism and $0.1285 \text{ g}/(\text{cm}^2 \text{ s})$ for the reduced mechanism.

So far we considered Lewis numbers equal to one. A unity Lewis number assumption is not realistic for the species H and H_2 , for which the Lewis numbers are 0.18 and 0.3, respectively. The Lewis numbers of the other species, however, are close to 1. For a methane flame [Som94], it has been observed that if a non-unity Lewis number is used for H only, the results agree well with computations with non-unity Lewis numbers for all species. If this is also true for hydrogen/air flames, this would imply a large simplification if reduced reaction mechanisms are used. If only non-unit Lewis numbers are used for H and H_2 , the element mole numbers for O and N

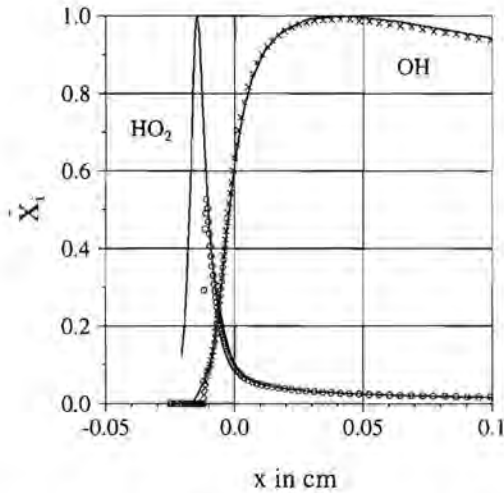


Figure 3.14: Comparison of results of a two-step reduced hydrogen/air reaction mechanism (markers) and detailed computations (lines) for reaction system II. The mole fractions of the species are scaled with the maximum mole fractions. These are given by OH: $1.5 \cdot 10^{-2}$, HO_2 : $2.38 \cdot 10^{-4}$.

do not change in the flame. Even the mole fraction of H remains constant, because the element mass fractions of O and N and therefore also for H are conserved (see eq. (1.43)). This means that no variations in specific element mole numbers have to be taken into account, which reduces the number of independent variables for the reduced mechanism. Results of computations with non-unit Lewis numbers for H and H_2 are compared with results using non-unit Lewis numbers for all species (see Figures 3.15 and 3.16). It can be seen that the differences are small. The importance of preferential diffusion of H and H_2 becomes apparent if the adiabatic mass burning rates are compared. The adiabatic mass burning rate is $0.127 \text{ g}/(\text{cm}^2 \text{ s})$ if unit Lewis numbers are used, $0.205 \text{ g}/(\text{cm}^2 \text{ s})$ if non-unit Lewis numbers are applied for H and H_2 and $0.206 \text{ g}/(\text{cm}^2 \text{ s})$ if non-unit Lewis numbers are applied for all species. Finally, we performed reduced scheme computations using non-unit Lewis numbers for H and H_2 . It should be noted that the enthalpy will not be constant anymore and a differential equation for the enthalpy should be taken into account. However, we expect relatively small variations in the enthalpy through the flame as the energy flux by preferential diffusion is relatively small. At first, we neglect these enthalpy variations, so that the same manifold can be used as for computation with unit Lewis numbers. Some results are presented in Figures 3.17 and 3.18. The profiles of the major species agree well with the detailed computations. Some radicals show more deviations. This is probably caused by differences in enthalpy between detailed and reduced computations. The adiabatic mass burning rate for the reduced mechanism is found to be $0.172 \text{ g}/(\text{cm}^2 \text{ s})$, which agrees reasonably well with the mass burning rate found with the detailed computations ($0.205 \text{ g}/(\text{cm}^2 \text{ s})$). This

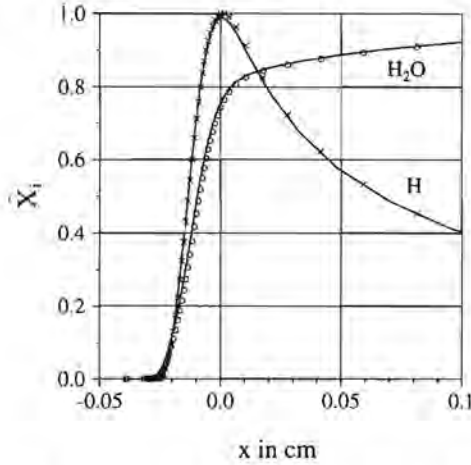


Figure 3.15: *Complex hydrogen/air computations using various transport models. The lines correspond to computations using non-unit Lewis numbers for all species, the markers with computations with unit Lewis numbers, except for H and H₂. The mole fractions of the species are scaled with the maximum mole fractions. These are given by H: $4.28 \cdot 10^{-2}$, H₂O: $3.04 \cdot 10^{-1}$, $\Phi = 1.0$.*

might be caused by the differences in HO₂ profiles of reduced and detailed computations. We have already seen that this species has a large influence on the mass burning rate of hydrogen/air reaction mechanisms.

3.2 Burner-Stabilized Flames

In this section, results of calculations with the Mathematical Reduction Technique, applied to burner-stabilized flames are presented. We use unit Lewis numbers and constant and for all species equal specific heat c_p , as in subsection 3.1. As the flame is cooled at the burner edge, the enthalpy is not conserved now. Therefore, the enthalpy appears as an additional variable. As we use unit Lewis numbers the enthalpy will be constant in the region above the burner, and can be obtained easily by computing the enthalpy at the burner edge. As a result we have to use two- and three-dimensional manifolds for one- and two-step reduced schemes. For the manifolds we use an equidistant grid. The refinement procedure was not implemented yet at the time these computations were performed.

Again ϕ_{H_2O} is taken as control variable for the one-step reduced scheme. For the two-step reduced scheme the specific mole numbers of H₂O and H₂ are used. These control variables increase or decrease monotonously with x , as is required when eq. (2.52) is derived. The same reaction mechanisms I and II (see Appendix B) as for the adiabatic flames are used here.

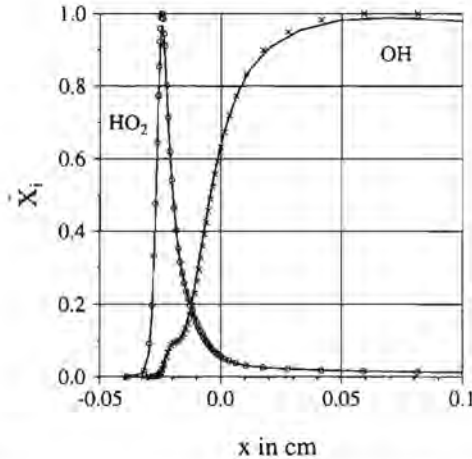


Figure 3.16: *Complex hydrogen/air computations, using various transport models. The lines correspond to computations using non-unit Lewis numbers for all species, the markers with computations with unit Lewis numbers, except for H and H₂. The mole fractions of the species are scaled with the maximum mole fractions. These are given by OH: $1.55 \cdot 10^{-2}$, HO₂: $4.14 \cdot 10^{-4}$, $\Phi = 1.0$.*

For the reaction mechanism I, a one-step reduced scheme is applied. This one-step reduced scheme will be used to model burner-stabilized flames for several values of the equivalence ratio and mass flow rate. The results will be compared with complex computations in the next subsection.

A one-step reduced scheme is also used for the reaction scheme including HO₂. For this scheme, however, only low mass flow rates can be applied, otherwise the flame will blow off. This is caused by the fact that the one-step scheme underestimates the adiabatic burning velocity considerably as we have seen before (section 3.1).

For larger mass flow rates, close to the adiabatic mass burning rate, a two-step reduced scheme is used instead. It is expected that this two-step scheme gives a significant improvement of the H₂/air flame structure. This is shown in the next subsection.

3.2.1 Results

The one-step reduced mechanism of system I is applied to burner-stabilized flame calculations with several equivalence ratios Φ and mass flow rates \dot{M} . In Fig. (3.19) we show one example of the differences between results of the full scheme and the reduced mechanism. The temperature at a distance of 1.0cm down-stream of the burner is shown in Fig. (3.20) for all full scheme and reduced scheme calculations. Considering these two figures, we may conclude that the difference between results of the one-step reduced scheme of system I and the full scheme calcula-

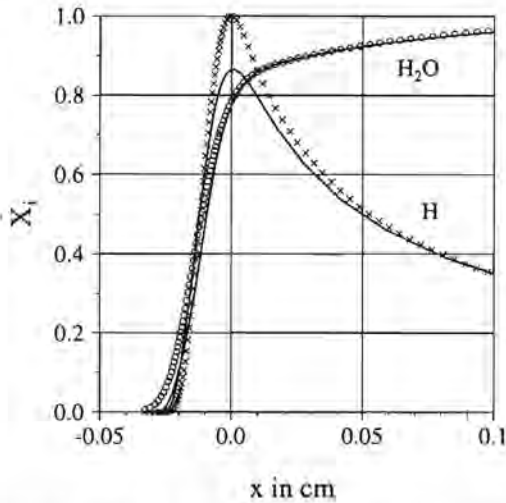


Figure 3.17: Comparison of results of a two-step reduced hydrogen/air reaction mechanism (markers) and detailed computations (lines) for reaction system II. Only the Lewis numbers for H and H_2 are not equal to 1. The mole fractions of the species are scaled with the maximum mole fractions. These are given by H: $4.95 \cdot 10^{-2}$, H_2O : $2.91 \cdot 10^{-1}$.

tions is quite small. Furthermore, it can be seen that the differences between the computations increase for increasing Φ values.

To apply the one-step reduced scheme of system II to burner-stabilized flame calculations, the flow velocity must be considerably lower than the adiabatic burning velocity, otherwise the flame will blow off as already mentioned. Results of the one-step reduced scheme calculations using a mass flow rate of $0.14 \text{ g}/(\text{cm}^2 \text{ s})$ are presented in Figures 3.21 and 3.22. The adiabatic mass burning rate for system II is equal to $0.193 \text{ g}/(\text{cm}^2 \text{ s})$. It should be noted that the profiles of the main species such as H_2 and H_2O are predicted quite well. The results of the temperature and radicals OH , H and HO_2 show larger differences. The temperature of the reduced computations is almost constant in the flame front, in contrast to detailed computations for which the temperature increases continuously. This is probably caused by the fast increase of radical concentrations for the reduced mechanism induced by the steady-state assumptions. Note that the total enthalpy has to be constant so that an rapid increase of radical concentrations limits the temperature increase. The flame structure is still predicted reasonably well. This is related to the fact that the composition is predicted well in the high temperature region.

As the one-step reduced scheme of system II cannot be used for flow velocities close to the adiabatic burning mass burning rate, a two-step reduced scheme is applied, to study whether this gives improvements.

The calculation using the two-dimensional scheme is performed for a mass flow rate of $\dot{M} = 0.19 \text{ g}/(\text{cm}^2 \text{ s})$, which is close to the adiabatic mass burning rate found with the detailed

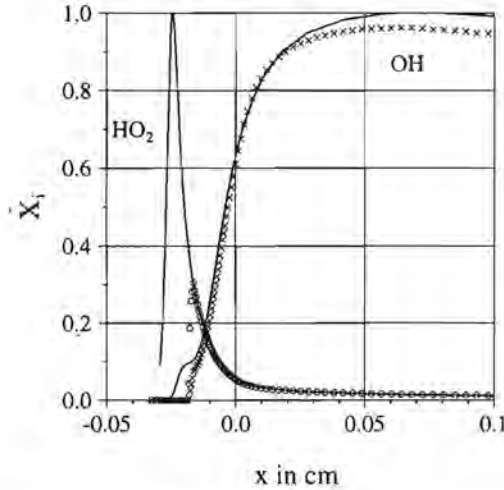


Figure 3.18: Comparison of results of a two-step reduced hydrogen/air reaction mechanism (markers) and detailed computations (lines) for reaction system II. Only the Lewis numbers for H and H_2 are not equal to 1. The mole fractions of the species are scaled with the maximum mole fractions. These are given by OH: $1.55 \cdot 10^{-2}$, HO_2 : $4.14 \cdot 10^{-4}$.

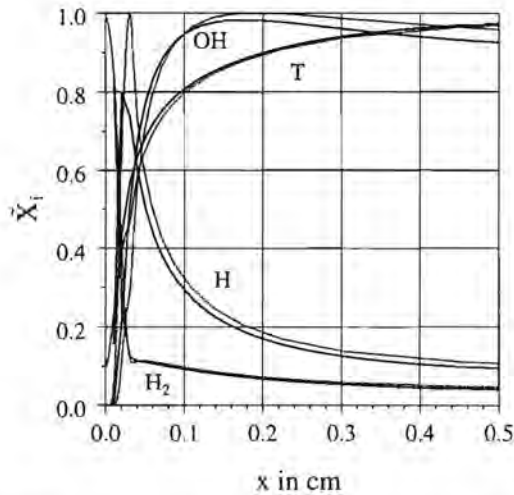


Figure 3.19: Profiles of several species using the full (continuous lines) and one-step reduced mechanism (dashed lines) applied to burner-stabilized flames with an equivalence ratio $\Phi = 0.9$ and mass flow rate $M = 0.10 \text{ g}/(\text{cm}^2 \text{ s})$, using reaction system I.

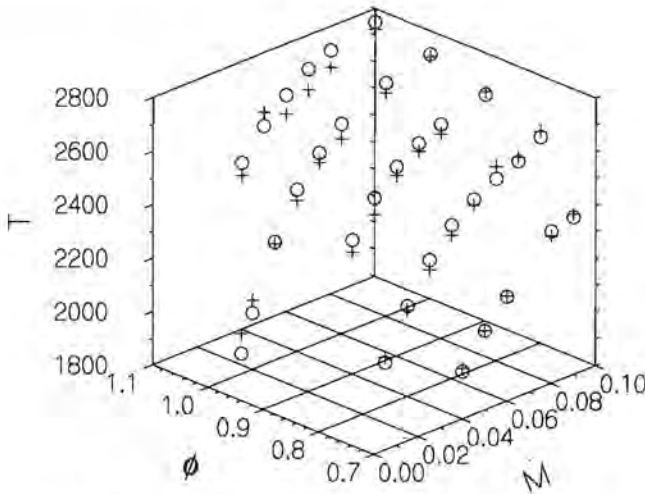


Figure 3.20: Comparison of the flame temperature at a height of 1.0cm down-stream of the burner between one-step reduced (+) and full scheme (o) calculations, as function of equivalence ratio Φ and mass flow rate \dot{M} .

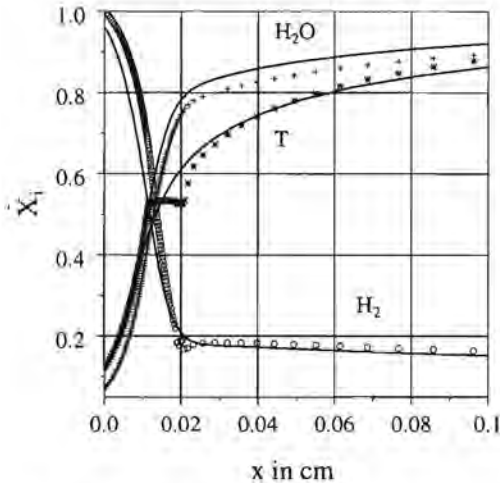


Figure 3.21: Profiles of species using full (lines) and one-step reduced mechanism (markers) applied to burner-stabilized flames with an equivalence ratio $\Phi = 1.0$ and mass flow rate $\dot{M} = 0.14 \text{g}/(\text{cm}^2\text{s})$, for reaction system II.

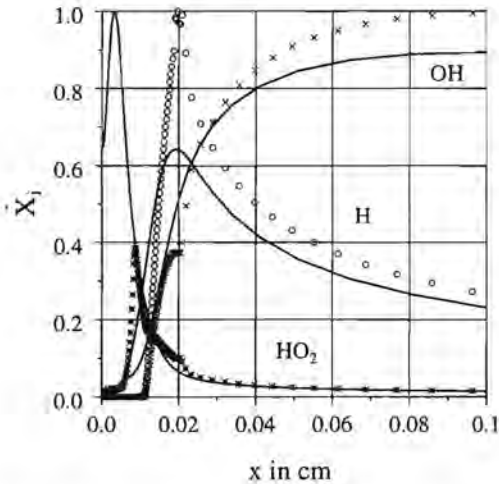


Figure 3.22: Profiles of species using full (lines) and one-step reduced mechanism (markers) applied to burner-stabilized flames with an equivalence ratio $\Phi = 1.0$ and mass flow rate $\dot{M} = 0.14 \text{ g}/(\text{cm}^2 \text{ s})$, for reaction system II.

computation. The results are shown in Figs. (3.23) and (3.24). Note that flames using the one-step reduced scheme will blow off at this flow rate. The two-step reduced scheme, however, gives stable flames. The results show that the mole fractions of the species are predicted well. The main difference between reduced and full scheme calculations is that the stand-off distance of the computation with the reduced scheme is larger, observed in Figures 3.23 and 3.24 by the shift in the x direction. The mole fractions show more deviations in the down-stream part of the flame. This is mainly caused by the relatively large grid spacing on the manifold there. Furthermore, it appears that an explicit solution method (solving the differential equations for the control variables subsequently in an uncoupled way) can be used here, due to the fact that the degree of stiffness is reduced by using the reduction method. The implicit method (solving all variables simultaneously), however, is much faster.

Finally, computations with the implicit method are performed. Now also temperature dependent specific heats of the species are applied. The manifold is locally refined in the direction of the control variables H and H_2O , but equidistant in the enthalpy. We used a mass flow rate of $0.1 \text{ g}/(\text{cm}^2 \text{ s})$. The results are presented in Figure 3.25 and 3.26. The reduced computations agree well with the detailed computations for most species. The OH -profiles show the larger differences. The temperature profiles agree very well.

Considering the results of the burner-stabilized flame computations we may conclude that the one-step reduced scheme applied to a reaction scheme without HO_2 gives quite accurate results. If HO_2 is taken into consideration the one-step reduced scheme can only be used for low mass flow rates. The flame will blow off otherwise. For small mass flow rates, the one-step

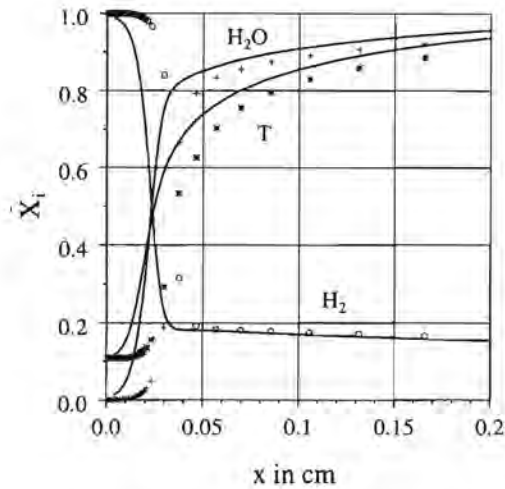


Figure 3.23: Comparison of some major species profiles in a burner-stabilized flat flame using the full (lines) and a two-step reduced mechanism (markers), $\Phi = 1.0$, $\dot{M} = 0.19\text{g}/(\text{cm}^2\text{s})$, system II.

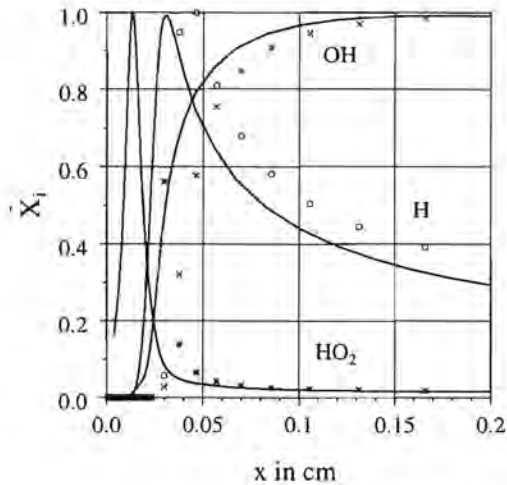


Figure 3.24: Comparison of some minor species profiles in a burner-stabilized flat flame using the full (lines) and a two-step reduced mechanism (markers), $\Phi = 1.0$, $\dot{M} = 0.19\text{g}/(\text{cm}^2\text{s})$, system II.

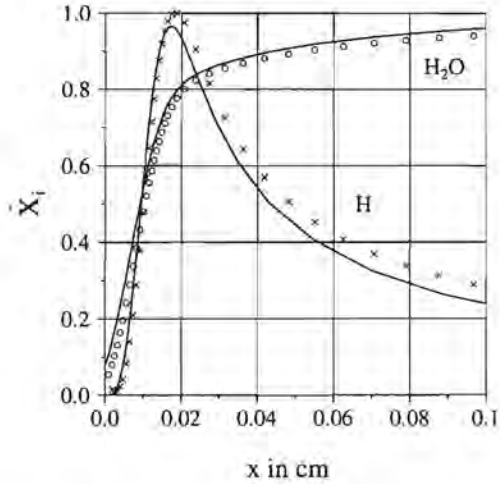


Figure 3.25: Comparison of H and H_2O profiles in a burner-stabilized flat flame using the full (lines) and a two-step reduced mechanism (markers), $\Phi = 1.0$, $M = 0.1 \text{ g}/(\text{cm}^2 \text{ s})$, temperature dependent specific heats, system II.

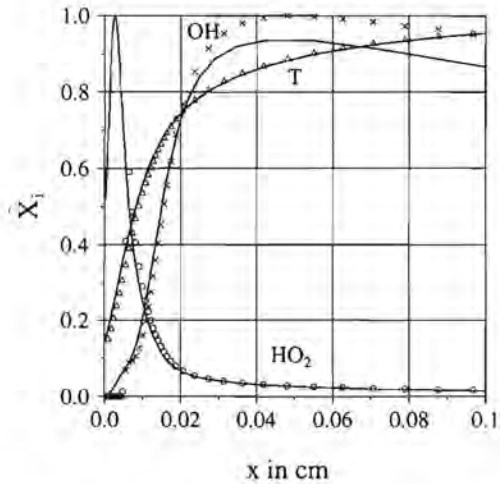


Figure 3.26: Comparison of OH , HO_2 and temperature profiles in a burner-stabilized flat flame using the full (lines) and a two-step reduced mechanism (markers), $\Phi = 1.0$, $M = 0.1 \text{ g}/(\text{cm}^2 \text{ s})$, temperature dependent specific heats, system II.

reduced scheme still gives quite accurate results for the flame structure. For a large mass flow rate a two-step reduced scheme should be used.

3.3 Reduced Schemes for Carbon Monoxide- Hydrogen/Air Mechanisms

3.3.1 Introduction

In this section, we will compare results of the Mathematical Reduction Technique with those of Conventional Reduction Methods. The conventional reduced reaction mechanisms are based on partial-equilibrium assumptions or steady-state assumptions as explained in sections 1.5 and 2.4.1. The reduction methods are applied to hydrogen/air and carbon monoxide-hydrogen/air reaction mechanisms. These mechanisms are presented in Appendix B, indicated by IV and V, respectively.

In contrast to the previous two sections we now fix the temperature for the manifold computations. In principle it is a matter of choice whether the temperature or the enthalpy is taken as independent variable. An advantage of taking the enthalpy as variable is that the energy equation in terms of the enthalpy has a simpler form. However, the reduced reaction mechanisms presented in this section are meant for application in turbulent flames¹ where a constant temperature was assumed, initially. To compare how the reduced models perform, computations are performed out at temperatures of 1200K and 2000K. As turbulent combustion modelling is very complicated, one-step reduced schemes are considered in first instance only. Furthermore, temperature dependent specific heats of the species are used.

As explained before, the Mathematical Reduction Technique determines the fast and slow reaction groups automatically. For applications of conventional reduction methods, however, we have to decide which assumptions should be used. First, we will decide which reactions are assumed to be in partial-equilibrium. Then, we will decide which species are considered to be in steady-state.

Considering the H_2 reaction scheme IV (see Appendix B), the two-body reactions (1), (2), (3), (17) and (18) are classified as fast and assumed to be in partial-equilibrium. Note that reactions (1), (2), (3) and (4) are dependent. If steady-state assumptions are introduced for reaction (1), (2), (3), reaction (4) is also in partial-equilibrium. The three-body reactions (5), (6), (7), (8) and (15) are slow and are assumed not to be in equilibrium [Dix75], [Jan82], [Cor85]. Instead of applying partial-equilibrium assumptions for reactions (17) and (18), also computations with reaction (9) and (16) in partial-equilibrium are performed. This leads, however, to the same results. This is caused by the fact that the reactions are dependent: $(9) = (17) - (18) - (4)$ and $(16) = (18) - (2)$. For the CO/H_2 -air reaction system V an additional partial-equilibrium assumption for reaction (20) is applied. This reaction is assumed to be faster than the three-body reaction (21).

¹The turbulent flame modelling is not considered here. At the Twente University of Technology, however, these reduced modelled are used for modelling turbulent combustion processes.

If the mechanism is reduced by use of steady-state assumptions, we apply steady-state assumptions for the O , H , OH , HO_2 and H_2O_2 species in the hydrogen-air reaction system. Furthermore, for the reaction system which includes CO and CO_2 , an additional steady-state assumption is introduced for CO at $2000K$. At $1200K$, however, H_2 is assumed to be in steady-state. It is found that this gives the most accurate approximation.

3.3.2 Results

The species mass fraction databases obtained from using various reduction methods are compared in this subsection. As the data-bases are meant for use in turbulent combustion processes, we used $\phi_{H_2}^*$ defined by eq. (2.99) as a control variable. Since all other variables are given in mass fractions we define the combined mass fraction $Y_{H_2}^* = \phi_{H_2}^* * M_{H_2}$. This control variable has the quality that the source term does not include contributions of fast reactions. Furthermore, it decreases continuously during the combustion process. The equilibrium value is therefore found at very low $Y_{H_2}^*$ value. Figure 3.27 shows the dependence of H , OH and O on the $Y_{H_2}^*$

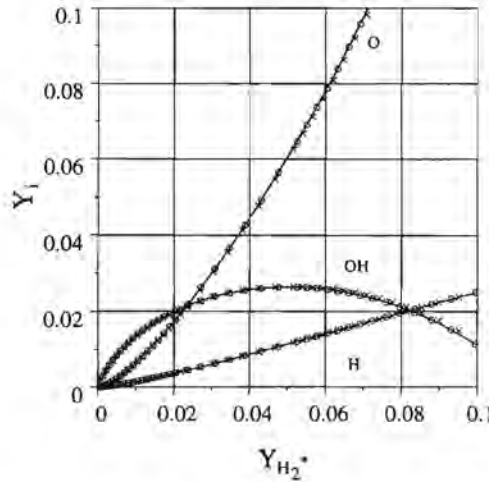


Figure 3.27: Mass fractions of H , OH and O radicals as a function of $Y_{H_2}^*$, at a temperature of $2000K$ and stoichiometric condition (H_2 -air), Line: ILDM-method, Cross: Steady-State approximations, Circle: Partial-equilibrium approximations.

variable at a temperature of $2000K$, for a stoichiometric H_2 -air mixture. Comparing the results of the various reduction methods it can be concluded that at the high temperature ($T = 2000K$) the partial-equilibrium and steady-state assumptions perform very well. Figure 3.28 shows the results of HO_2 and H_2O_2 mass fractions at $2000K$. The results of the steady-state assumptions agree within 5% with the results of the Mathematical Reduction Technique (ILDM-method). The reduction method based on partial-equilibrium assumptions, however, gives much lower

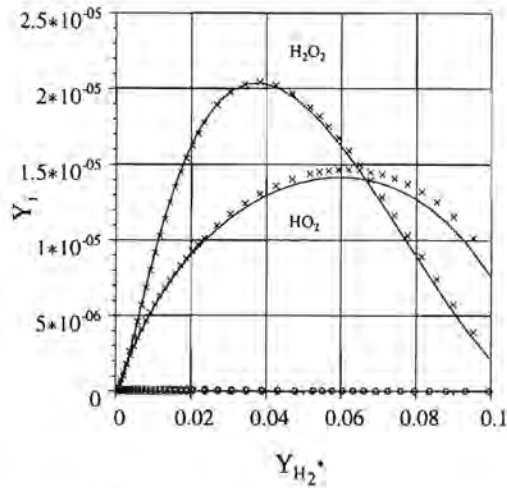


Figure 3.28: Mass fraction of HO_2 and H_2O_2 radicals as a function of $Y_{H_2}^*$, at a temperature of 2000K and stoichiometric condition (H_2 -air). Line: ILDM-method, Cross: Steady-State approximations, Circle: Partial-equilibrium approximations.

HO_2 and H_2O_2 mass fractions. This indicates that there are no appropriate partial-equilibrium assumptions possible for reactions which include the HO_2 or H_2O_2 species. Figure 3.29 shows the H , OH , O mass fractions as a function of $Y_{H_2}^*$ in the H_2 /air mixture at 1200K. Now, significant differences can be observed between the reduction methods. The differences between the results of the reduction method based on partial-equilibrium assumptions and the Mathematical Reduction Technique are smaller than the differences between the method based on steady-state assumptions and the Mathematical Reduction Technique. This indicates that the partial-equilibrium assumptions for reactions containing O , H and OH radicals are more accurate approximations than steady-state approximations for these radicals. Apparently, these reactions are also much faster than other reactions at low temperatures. In general, however, the reactions which are important in the initial phase of the combustion processes differ from the reactions which are most important close to the equilibrium composition. The choice of steady-state species, however, is somewhat easier as it may be expected that radicals are associated with fast reaction throughout the entire combustion processes. If, however, stable species such as H_2 or CO have to be applied in steady-state, the choice is much more complicated. In general, the most accurate steady-state assumption may depend on the temperature.

For HO_2 and H_2O_2 the partial-equilibrium assumptions are again not accurate (see Figure 3.30). Also the steady-state assumptions for HO_2 and H_2O_2 are less accurate than at 2000K. Turning to the stoichiometric CO/H_2 -air reaction system (the fuel composition is 60% CO , 30% H_2 and 10% N_2) the following conclusions can be drawn. As for the H_2 -air reaction system, the partial-equilibrium and steady-state assumptions give accurate results for O , H and OH at

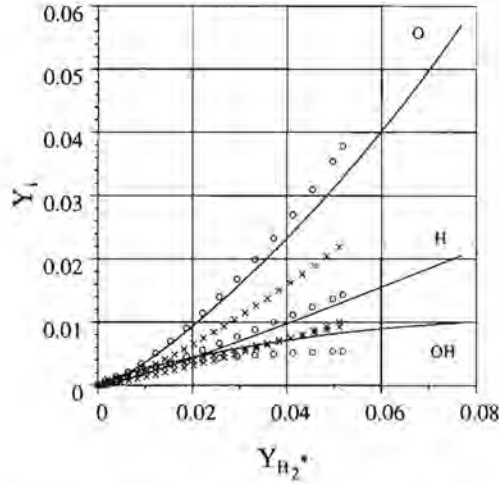


Figure 3.29: Mass fractions of H , OH and O radicals as a function of $Y_{H_2}^*$, at a temperature of $1200K$ and stoichiometric condition (H_2 -air), Line: ILDM-method, Cross: Steady-State approximations, Circle: Partial-equilibrium approximations.

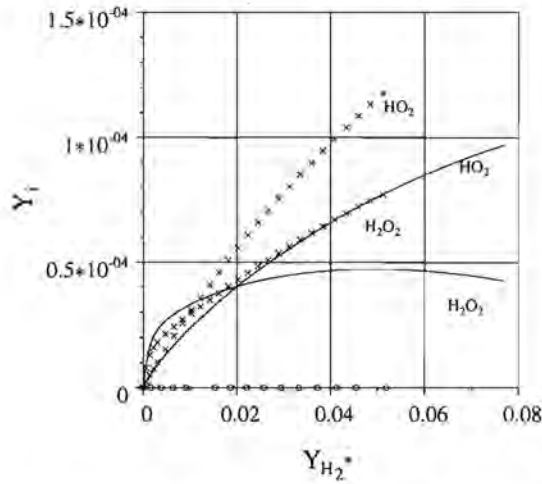


Figure 3.30: Mass fraction of HO_2 and H_2O_2 radicals as a function of $Y_{H_2}^*$, at a temperature of $1200K$ and stoichiometric condition (H_2 -air), Line: ILDM-method, Cross: Steady-State approximations, Circle: Partial-equilibrium approximations.

$T = 2000K$. The O , H and OH mass fractions profiles are similar to those of the H_2 -air reaction system (Figure 3.27). The maximum mass fractions of OH and H are, however, lower (0.02 and 0.01, respectively). Also the partial-equilibrium assumptions fail to predict accurate results for HO_2 and H_2O_2 (Figure 3.31). The results of the method which makes use of steady-

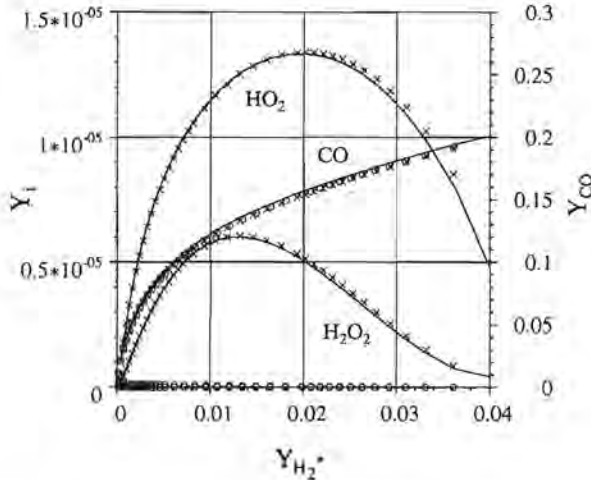


Figure 3.31: Mass fraction of HO_2 , H_2O_2 radicals and CO as a function of $Y_{H_2}^*$, at a temperature of $2000K$ and stoichiometric condition (60% CO and 30% H_2), Line: ILDM-method, Cross: Steady-State approximations, Circle: Partial-equilibrium approximations.

state assumptions agree very well with the results of the Mathematical Reduction Technique; the differences are less than 5% at $2000K$.

Computations are also performed at $1200K$. Mass fractions of HO_2 , H_2O_2 and CO are shown in Figure 3.32. The differences between the reduction method based on steady-state assumptions and the Mathematical Reduction Technique increase at this temperature, while the results of the method which uses partial-equilibrium assumptions gives large deviations compared to the other methods. At this temperature also the predicted CO mass fraction shows large differences.

The results indicate that the conventional methods give satisfactory results at high temperature. At low temperature the inaccuracies increase. The mass fractions of HO_2 and H_2O_2 , however, cannot be predicted accurately by applying partial-equilibrium assumptions.

3.3.3 Influence on NO Formation

Finally, to study the effect of the differences in thermal NO formation the databases for the H_2 -air reaction system are used to compute thermal NO formation rates in a post-processing step.

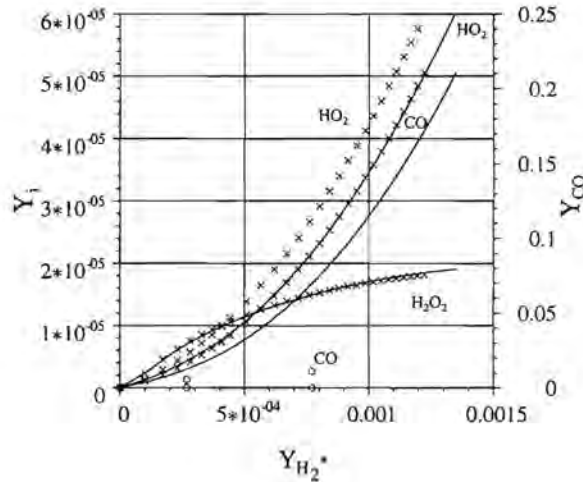


Figure 3.32: Mass fraction of HO_2 , H_2O_2 radicals and CO as a function of $Y_{H_2}^*$, at a temperature of 1200K and stoichiometric condition (60% CO and 30% H_2), Line: ILDM-method, Cross: Steady-State approximations, Circle: Partial-equilibrium approximations.

The formation of NO is explained in chapter 4, where an expression for the thermal NO formation rate is derived (see eq. (4.5)).

At a temperature of 2000K the differences between the various methods are very small. At this temperature the NO formation rate increases from 0 to $0.6 \text{ kg}/(\text{m}^3 \text{ s})$ when $Y_{H_2}^*$ varies from 0 to 0.1. At a temperature of 1200K, the differences in the NO source term using the various reduction methods are of the same order of magnitude as the differences in O radical mass fractions (15%). More important, however, is that the NO source term remains much smaller than at 2000K, due to the low temperature and low O mass fraction. It increases as a function of $Y_{H_2}^*$ to a value as low as $5.010^{-7} \text{ kg}/(\text{m}^3 \text{ s})$ at $Y_{H_2}^* = 0.08$. Hence, in the region where the difference in NO source term is significant, the NO production rate is irrelevantly small.

3.4 Mathematically Reduced Methane-Air Reaction Schemes.

In many industrial and household applications methane is used as fuel. Therefore, it is desirable to develop reduced models for methane-air reaction systems. In this section the Mathematical Reduction Technique is applied to a methane-air reaction mechanism. The reaction mechanism used, is the skeletal scheme of Smooke [Smo91], which is the most simple reaction mechanism for the combustion of methane. It consists of 16 species and 26 reactions. Furthermore, temperature dependent specific heats of the species are used. The methane-air reaction system is reduced to a two-step reduced scheme. As control variables we use the specific mole numbers

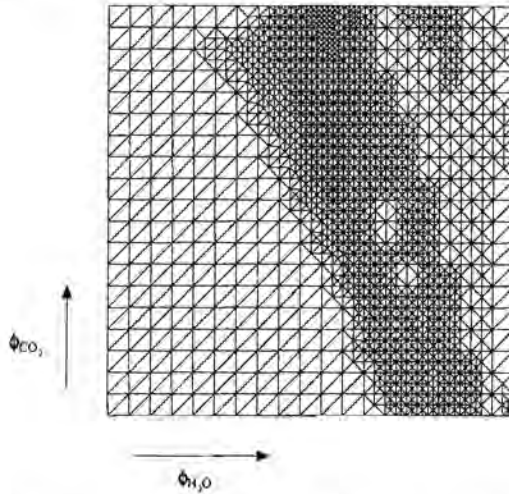


Figure 3.33: *Locally refined grid for a two-step reduced methane-air reaction mechanism (skeletal scheme). In the horizontal direction the specific mole number of H_2O is used as control variable. In the vertical direction the specific mole number of CO_2 is used as control variable.*

of H_2O and CO_2 . The mesh for the manifold data-base is locally refined and presented in Figure 3.33. In Figures 3.34 and 3.35 contour lines of the temperature and the OH mole fraction the manifold are presented. Below a temperature of $1200K$ no manifold solutions are found. This is caused by the fact that the reaction rates are very low there. However, in order to use the manifold it is necessary that mixture composition are available for all values of the control variables. Therefore, compositions in the low temperature region are obtained by assuming that only stable species have non-zero specific mole numbers. Since the radical concentrations are already low between temperatures of $1200K$ and $1300K$ (where solutions for the manifold composition are found) the temperature profiles are smooth on the manifold. Only near the region where the transition takes place between computed manifold compositions and the area with stable species, the temperature and radical contour lines are slightly curved (Figure 3.34).

The reduced mechanism is applied to an adiabatic flat flame. Again unit Lewis numbers are used, so that the specific element mole numbers and enthalpy remain constant. Results are presented in Figures 3.36 and 3.37, where also results of the full system are given. Significant deviations between reduced and full scheme results are observed. Also a large difference of roughly a factor two in adiabatic mass burning rate is found. The adiabatic mass burning rate is $2.79 \cdot 10^{-2} g/(cm^2 s)$ for the detailed mechanism and $5.8 \cdot 10^{-2} g/(cm^2 s)$ for the reduced mechanism. The results are comparable with results obtained by Riedel et al. [Rie94]. The differences in the post-flame zone are mainly caused by the differences in mass flow rate. This becomes apparent if Figures 3.38 and 3.39 are considered. In these figures profiles of the full system are

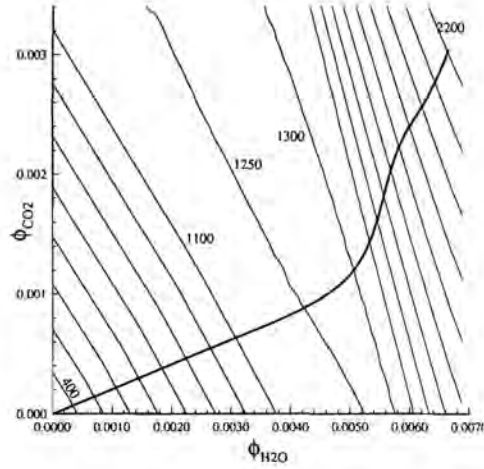


Figure 3.34: Contour lines of the temperature on a two-dimensional manifold for methane. In the x -direction the specific mole number of H_2O is used as control variable. In the y -direction the specific mole number of CO_2 is used as control variable. The reaction path of the adiabatic flat flame is sketched by the thick line ($\Phi = 1.0$).

compared with interpolations on the manifold. The profiles of ϕ_{CO_2} and ϕ_{H_2O} of the full system are used for the interpolation to obtain the profiles of the other species from the manifold data-base. This indicates that the manifold is much more accurate behind the flame front than in the flame front. Further, it is observed that the mole fractions of CH_3 , CH_3O , CH_2O and HCO predicted by the reduced scheme are much lower than those predicted by the detailed computations. The maximum mole fractions predicted by the reduced scheme are of order of magnitude of 10^{-14} , 10^{-14} , 10^{-8} and 10^{-5} , whereas these are given by: $3 \cdot 10^{-3}$, $5 \cdot 10^{-6}$, $2 \cdot 10^{-3}$ and $8 \cdot 10^{-5}$, respectively for the detailed computations. The results indicate that for an accurate modelling of premixed laminar methane/air flames more than two degrees of freedom should be taken into account.

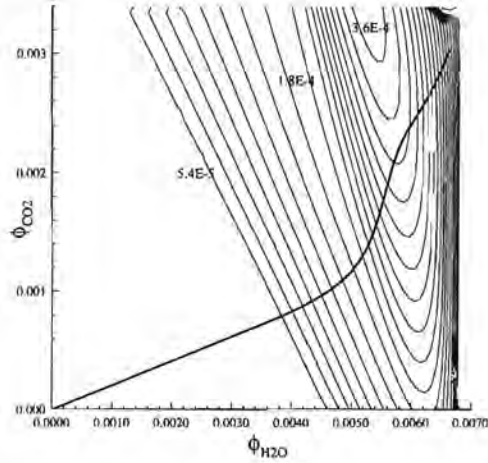


Figure 3.35: Contour lines of the OH specific mole number on the two-dimensional manifold for methane. In the horizontal direction the specific mole number of H_2O is used as control variable. In the vertical direction the specific mole number of CO_2 is used as control variable. The reaction path of the adiabatic flat flame is sketched by the thick line ($\Phi = 1.0$).

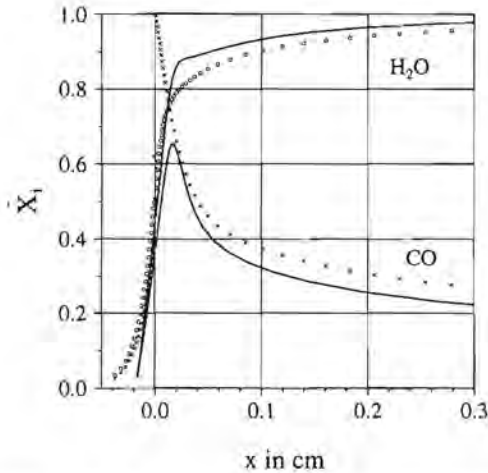


Figure 3.36: Comparison of a two-step reduced scheme and a detailed computation applied on an adiabatic flat methane-air flame. The mole fractions are scaled with: $CO: 6.78 \cdot 10^{-2}$, $H_2O: 1.82 \cdot 10^{-1}$, $\Phi = 1.0$

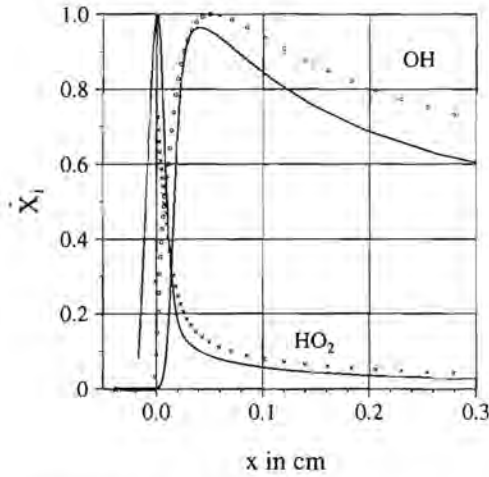


Figure 3.37: Comparison of a two-step reduced scheme and a detailed computation applied on an adiabatic flat methane-air flame. The mole fractions are scaled with: $OH: 8.78 \cdot 10^{-3}$, $HO_2: 6.97 \cdot 10^{-5}$, $\Phi = 1.0$

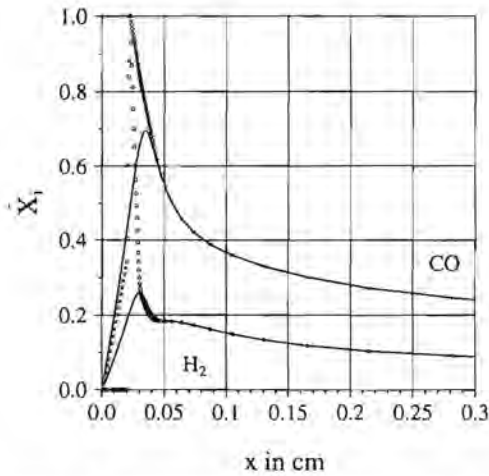


Figure 3.38: Comparison of interpolation on the manifold and detailed profiles for an adiabatic flat methane-air flame. The lines denote the detailed results, the symbols correspond to interpolation on the manifold. The mole fractions are scaled with: $CO: 6.37 \cdot 10^{-2}$, $H_2: 7.51 \cdot 10^{-2}$, $\Phi = 1.0$

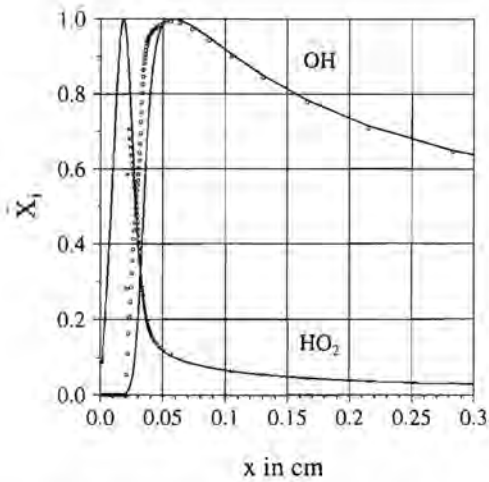


Figure 3.39: Comparison of interpolation on the manifold and detailed profiles for an adiabatic flat methane-air flame. The lines denote the detailed results, the symbols correspond to interpolation on the manifold. The mole fractions are scaled with: OH: $8.47 \cdot 10^{-3}$, HO₂: $6.97 \cdot 10^{-5}$, $\Phi = 1.0$

Chapter 4

Post-Processing Method for Modelling NO Formation

To reduce environmental pollution, regulations concerning *NO* emission have become more stringent recently. To decrease the emission of *NO*, increasing knowledge of *NO* formation in combustion processes is required. From a chemical point of view the formation of *NO* in methane/air flames is reasonably well understood [Bow92]. This has led to the development of detailed reaction mechanisms, in which a large number of species and reactions is involved. An example of a complex reaction mechanism is that of Miller and Bowman [Mil89], which consists of 51 species and over 200 reactions. Apart from the fact that this reaction mechanism is suitable to model the formation of *NO*, also information about the formation of *N₂O* and *NO₂* is obtained. In literature it is often referred to *NO_x* being the sum of *NO* and *NO₂*. However, for most applications presented in this chapter the temperature of the exhaust gases at the end of the computational domain is very high, so that the concentration of *NO₂* is much lower (almost two orders of magnitude) than the concentration of *NO*. Therefore, most results concern the formation of *NO*. In the atmosphere, however, *NO* will be converted into *NO₂*. Although the reaction mechanisms are well known, there are relatively large uncertainties in the reaction rate data. If more recently published reaction rate data are used [Gla92], significant differences in predicted *NO* concentrations are observed (this will be shown in this chapter).

The use of such complex reaction mechanisms for modelling *NO* formation leads to extravagant computational effort. Reduced models to predict the *NO* formation are therefore required. In chapter 1 several methods to reduce the computational effort of modelling flames with detailed reaction mechanisms are presented. One of the methods presented is based on the decoupling of a group of species from the reaction mechanism. This is possible if these species have low mass fractions and are of minor influence on the flame structure. The decoupling results in the possibility to treat part of the chemistry in a post-processing step. In this chapter we will show that the production of *NO* can be modelled successfully by use of this method.

The objective of the research presented in this chapter is to investigate how the formation of *NO* in laminar methane/air flames can be modelled numerically, with a minimum of computational effort. This implies that we start with the most detailed reaction mechanism including the entire nitrogen chemistry. We investigate which reactions and species are of minor importance

and may be omitted. Furthermore, the consequences of the assumptions introduced in the post-processor are studied. It is, however, not easy to extend the results of this chapter to the *NO* formation in practical burners. This is related to the fact that we focus on simple burner geometries such as flat flames and slit burners only. The main difference between flat flames and practical burners is that the flat flames are not cooled and in this chapter it will be shown that the *NO* formation depends strongly on the temperature. Although the effect of the cooling by the environment is taken into account for the slit burner computations, only few results are presented as the computational effort is still large (several days on a modern super computer). Furthermore, the burner configuration is still simple and the computational domain is small compared to practical situations (the combustion chamber is not modelled here). The present work and the numerical tools developed, however, can be used to estimate the *NO* production in a small region of a few centimeters above the burner using simplified models for the burner such as multiple slit or perforated plate burners. The *NO* produced in the down stream zone further away from the burner can be modelled in a separate computational step. For this step it is not necessary to account for the complete kinetics as most combustion reactions are in equilibrium. The equilibrium composition can be computed relatively easy. Having determined the equilibrium composition, the formation of *NO* can be obtained.

An introduction into the mechanisms which describe the formation of *NO* is given in section 4.1. Several mechanisms will be used for modelling the *NO* formation in laminar flat flames. The results are presented in section 4.2. The post-processing method and the implementation will be presented in section 4.3. First, the post-processor is applied to one-dimensional flames (section 4.4). Since it is possible to perform detailed computations for these flames within a reasonable amount of computing time, the accuracy of the post-processing method can be examined by comparing the post-processor results with detailed computations. Furthermore, the results of detailed computations are used to study which reactions are most important. Since the temperature has a large influence on the formation rate of *NO*, adiabatic flames are also considered using various reaction mechanisms (the adiabatic flame temperature is not determined by the reaction mechanism but by the thermo-dynamic properties of the species). Since there are relatively large uncertainties in reaction rate data, it is necessary to compare results of computations with measurements. In section 4.4 results of computations of the *NO* formation of a ceramic foam burner are compared with measurements. Furthermore, the formation of *NO* in two-dimensional flames will be considered in detail in section 4.5. Two geometries are used: a micro-slit burner with nearly flat flames and a single-slit burner in a confined environment with cooled walls. For the single slit burner we compare the formation of prompt *NO* using detailed reaction mechanisms with an empirical model for prompt *NO* formation. Most results presented in this chapter are also published in [Egg94], [Egg95c] and [Egg95d].

4.1 Thermal and Prompt *NO* Mechanisms

Often a distinction between thermal and prompt *NO* is made. The thermal mechanism is described by the well known Zeldovich reactions:





These reactions give the following thermal production rate:

$$\dot{\rho}_{NO}^{th} = M_{NO}(r_1 + r_2 + r_3), \quad (4.4)$$

where the indices 1, 2, 3 refer to the first, second and third Zeldovich reactions (4.1), (4.2) and (4.3), respectively. This mechanism is referred to as thermal mechanism because of the strong temperature dependence of the NO production rate. This becomes clear if the thermal production rate is considered in more detail.

When the N -radicals are assumed to be in steady-state and the fast reaction $H + O_2 \rightleftharpoons OH + O$ is supposed to be in partial-equilibrium, the following well known expression for the thermal NO formation rate [Ive73] may be derived:

$$\dot{\rho}_{NO}^{th} = 2M_{NO}k_1[O][N_2] \frac{1 - \frac{[NO]^2}{K_1 K_2 [N_2][O_2]}}{1 + \frac{k_{-1}[NO]}{k_2[O_2] + k_3[OH]}}. \quad (4.5)$$

Since the concentration of NO is generally very low, this reaction rate is approximately equal to:

$$\dot{\rho}_{NO}^{th} \approx 2M_{NO}k_1[O][N_2]. \quad (4.6)$$

The strong temperature dependence is found in the large activation energy of the reaction rate k_1 . The reaction rate of this reaction is given by:

$$k_1 = A_1 \exp(-E_1/RT), \quad (4.7)$$

with $E_1/R = 38370K$. Equation (4.7) indicates that:

$$\frac{dk_1}{k_1} = \frac{E_1}{R} \frac{dT}{T}. \quad (4.8)$$

This implies that at a temperature of $1500K$, an increase in temperature of 1% induces an increase of the reaction rate of about 25%. Although the thermal mechanism is relatively simple to model, it requires knowledge of the O -radical concentration profile. If this concentration is not known it is often approximated by assuming the O -radicals in chemical equilibrium with O_2 . This implies that the following reaction is assumed to be in partial-equilibrium.



leading to:

$$[O] = \sqrt{K_4[O_2]}, \quad (4.10)$$

with K_4 the equilibrium constant of (4.9). The equilibrium O concentration can now be determined by use of the concentration of O_2 and the temperature. We refer to NO_{eq} as being that part of the thermal NO which would be formed if O radicals would be in equilibrium with O_2 . In the next section we will show that the equilibrium assumption for O -radicals leads to a considerable

under-estimate of the thermal NO concentration. Note that in contrast to the O -radical concentration, the concentration of NO is far below the equilibrium concentration. This is caused by the fact that most reactions that produce NO are slow, compared to the residence times in the flame.

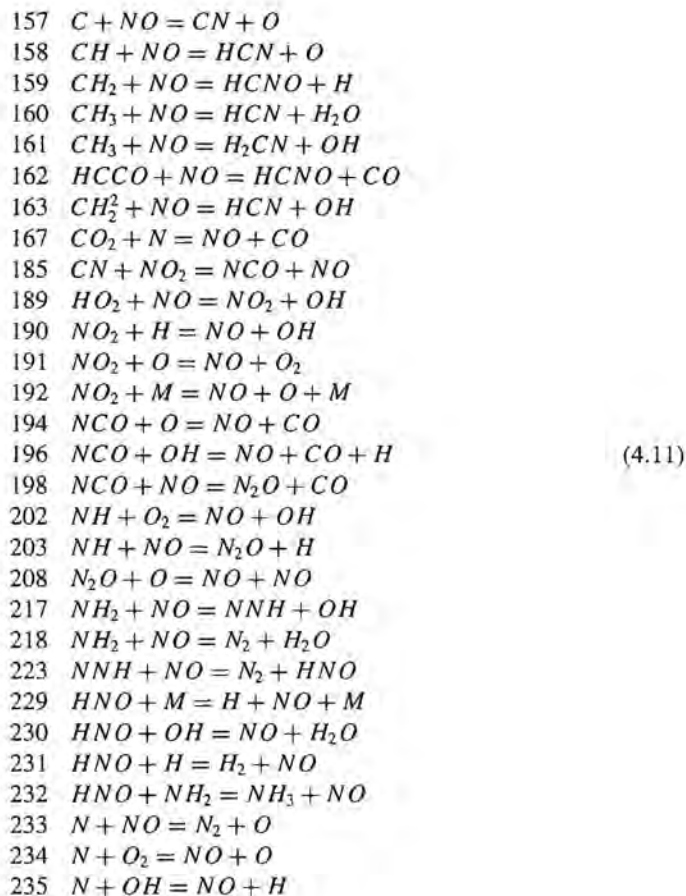
Besides the thermal mechanism, the prompt mechanism is responsible for a part of the totally formed NO . In this thesis we will refer to prompt NO , as NO which is formed by reactions that are not part of the thermal mechanism. Originally, the expression "prompt NO " was introduced to account for the apparently instantaneous formation of NO observed by researchers [Fen71]. When the measured profile of NO in a flat flame burner is extrapolated to the surface, the intercept obtained was referred to as "prompt NO ". This definition of "prompt NO " implies that a part of the "prompt NO " is due to the thermal mechanism enhanced by super-equilibrium O radical concentrations. Furthermore, often the reactions in which N_2O is involved are considered separately as a third mechanism (besides the thermal and prompt mechanism) which is important for the formation of NO . As already mentioned before, here we will only make distinction between thermal and prompt NO and assume reactions with N_2O to be part of the prompt mechanism.

The prompt mechanism is much more complicated than the Zeldovich mechanism and has been fully understood only recently. The mechanism developed by Miller and Bowman [Mil89] is widely accepted and used. This mechanism contains 29 reactions which may produce NO as given by (4.11), where the last three reactions are part of the thermal mechanism. However, this mechanism (which will be referred to as MB) is modified frequently, because new measurements provide new data for the reaction rates which is expected to be more reliable and measurements often indicate that other reactions play a significant role. Disturbing for the researcher is the fact that published reaction rate data show variations, leading to quite large differences in results of calculations.

Recently, Glarborg and co-workers [Gla92] developed a simplified reaction mechanism including prompt NO formation. This reaction mechanism is based on that of Miller and Bowman. It is a subset of this mechanism, but also some reactions are added and data are changed according to new measurements. This reduced set of reactions contains 77 reactions of the initial set of 234. Here we study whether this reaction mechanism of Glarborg et al. is valid for flat flame calculations, and how large differences are with the reaction mechanism of Miller and Bowman.

To determine how large the influence is of the neglected reactions and of the changes in reaction rate data, we modified the reaction mechanism Miller and Bowman. Reaction rate data are changed according to the data of Glarborg et al. and reactions, not present in the initial mechanism of Miller and Bowman, are added. As a result the Glarborg et al.'s mechanism is a subset of the modified Miller and Bowman mechanism.

Since the data used by Glarborg et al. are the most recent ones, we use this modified Miller and Bowman reaction mechanism (denoted as MB_{mod}) as reference and compare all other results to calculations with this. Flame calculations using the original reaction mechanism of Glarborg et al. gave unacceptable results for the burning velocity and are therefore considered to be not sufficient to be used for flat flame calculations. In literature, it has been shown [Smo91] that a skeletal mechanism for lean methane/air flames, which consists of a minimum number of



reactions and species, is able to predict the burning velocity quite well. Therefore, we extended this skeletal mechanism with the nitrogen chemistry part of the Glarborg et al.'s mechanism (this mechanism will be denoted as Skel_G). For the three above mentioned mechanisms MB, MB_{mod} and Skel_G we performed full flat flame calculations to estimate the consequences of neglecting a number of reactions and the effect of changes in the data. The results are presented in the next section.

4.2 Flat Flame Computations using Various Reaction Mechanisms

Various reaction mechanisms, as presented in the previous section, are used to model flat flames. These computations are performed using the PREMIX code of the Sandia Package [Kee85]. The results of the various mechanisms are presented in Table 4.1 for a stoichiometric methane/air

<i>scheme</i>	NO_{eq}	NO_{th}	NO	T
MB _{mod}	$0.36 \cdot 10^{-5}$	$2.31 \cdot 10^{-5}$	$3.91 \cdot 10^{-5}$	2072
MB	$0.37 \cdot 10^{-5}$	$2.36 \cdot 10^{-5}$	$2.90 \cdot 10^{-5}$	2073
Skel _G	$0.67 \cdot 10^{-5}$	$2.91 \cdot 10^{-5}$	$4.80 \cdot 10^{-5}$	2118

Table 4.1: Equilibrium, thermal and total NO mole fractions and temperature, at a distance of 1cm above the burner, calculated with the various mentioned reaction mechanisms. ($\Phi = 1.0$, $M = 3.2610^{-2} \text{g}/(\text{cm}^2\text{s})$).

flame with a mass flow rate of $3.26 \cdot 10^{-2} \text{g}/(\text{cm}^2\text{s})$. Apart from the mole fractions of NO we also give the flame temperature T at a distance of 1cm above the burner. In Table 4.2 we have shown the dependence of the MB_{mod} and MB results on the stoichiometry Φ . By performing additional computations we estimated the part formed by the thermal mechanism (NO_{th}) using eq. (4.5) and the equilibrium part (NO_{eq}) of the thermal NO_{th} , formed by O equilibrium concentrations, given by eq.(4.10). The remaining part of the thermal NO is formed by the super equilibrium O- radical concentration. The results are presented in Tables 4.1 and 4.2 and are also shown in Tables 4.3 and 4.4, where the various contributions are given as fraction of the total formed NO. Comparing the results of the MB_{mod} and MB mechanism, we see that the differences in temperature, equilibrium NO and thermal NO are very small. The amount of prompt NO estimated by the mechanisms MB_{mod} and MB, however, differ considerably, due to the changed reaction rate data and added reactions. The reaction mechanism Skel_G predicts even higher prompt NO concentrations (note that the temperature predicted by the skeletal mechanism is higher). These differences are of the same order of magnitude as the variations that arise from the changed reaction rate data. The question arises whether the differences are

<i>scheme</i>	Φ	NO_{eq}	NO_{th}	NO_{pr}	NO	T
MB _{mod}	0.90	$4.18 \cdot 10^{-6}$	$2.21 \cdot 10^{-5}$	$1.40 \cdot 10^{-5}$	$3.61 \cdot 10^{-5}$	2038
MB _{mod}	0.95	$4.44 \cdot 10^{-6}$	$2.50 \cdot 10^{-5}$	$1.55 \cdot 10^{-5}$	$4.05 \cdot 10^{-5}$	2061
MB _{mod}	1.00	$3.59 \cdot 10^{-6}$	$2.31 \cdot 10^{-5}$	$1.60 \cdot 10^{-5}$	$3.91 \cdot 10^{-5}$	2072
MB _{mod}	1.05	$1.96 \cdot 10^{-6}$	$1.58 \cdot 10^{-5}$	$1.51 \cdot 10^{-5}$	$3.09 \cdot 10^{-5}$	2061
MB _{mod}	1.10	$0.79 \cdot 10^{-6}$	$0.85 \cdot 10^{-5}$	$1.41 \cdot 10^{-5}$	$2.26 \cdot 10^{-5}$	2032
MB	0.85	$3.53 \cdot 10^{-6}$	$1.84 \cdot 10^{-5}$	$0.37 \cdot 10^{-5}$	$2.21 \cdot 10^{-5}$	2014
MB	0.90	$4.32 \cdot 10^{-6}$	$2.27 \cdot 10^{-5}$	$0.44 \cdot 10^{-5}$	$2.71 \cdot 10^{-5}$	2041
MB	0.95	$4.63 \cdot 10^{-6}$	$2.57 \cdot 10^{-5}$	$0.51 \cdot 10^{-5}$	$3.08 \cdot 10^{-5}$	2065
MB	1.00	$3.69 \cdot 10^{-6}$	$2.36 \cdot 10^{-5}$	$0.54 \cdot 10^{-5}$	$2.90 \cdot 10^{-5}$	2073
MB	1.05	$2.02 \cdot 10^{-6}$	$1.62 \cdot 10^{-5}$	$0.64 \cdot 10^{-5}$	$2.26 \cdot 10^{-5}$	2062
MB	1.10	$0.79 \cdot 10^{-6}$	$0.85 \cdot 10^{-5}$	$0.78 \cdot 10^{-5}$	$1.63 \cdot 10^{-5}$	2032

Table 4.2: The dependence of NO mole fraction and temperature on the stoichiometry Φ at a distance of 1cm above the burner ($\dot{M} = 3.2610^{-2} \text{g}/(\text{cm}^2\text{s})$).

<i>scheme</i>	$\frac{NO_{eq}}{NO}$	$\frac{NO_{th}}{NO}$	$\frac{NO_{pr}}{NO}$
MB _{mod}	9.2	59.1	40.9
MB	12.7	81.4	18.6
SkelG	13.9	60.6	39.4

Table 4.3: Contributions of the various mechanisms that produce NO, given in fractions (%) of the total formed NO, at a distance of 1cm above the burner, $\Phi = 1.0$, $\dot{M} = 3.2610^{-2} \text{g}/(\text{cm}^2\text{s})$.

<i>scheme</i>	Φ	$\frac{NO_{th}}{NO}$	$\frac{NO_{th}}{NO}$	$\frac{NO_{pr}}{NO}$
MB _{mod}	0.90	11.6	61.2	38.8
MB _{mod}	0.95	11.0	61.7	38.3
MB _{mod}	1.00	9.2	59.1	40.9
MB _{mod}	1.05	6.3	51.1	48.9
MB _{mod}	1.10	3.5	37.6	62.4
MB	0.85	16.0	83.3	16.7
MB	0.90	15.9	83.8	16.2
MB	0.95	15.0	83.4	16.6
MB	1.00	12.7	81.4	16.5
MB	1.05	8.9	71.7	28.3
MB	1.10	4.8	52.1	47.8

Table 4.4: Contributions of the various NO mechanisms given in fractions (%) of the total formed NO, at a distance of 1cm above the burner, $\dot{M} = 3.2610^{-2} \text{ g}/(\text{cm}^2 \text{ s})$.

<i>scheme</i>	Φ	NO_{th}^c	NO_{pr}^c	NO^c
MB _{mod}	0.90	$2.43 \cdot 10^{-5}$	$1.54 \cdot 10^{-5}$	$3.97 \cdot 10^{-5}$
MB _{mod}	0.95	$2.62 \cdot 10^{-5}$	$1.62 \cdot 10^{-5}$	$4.24 \cdot 10^{-5}$
MB _{mod}	1.00	$2.31 \cdot 10^{-5}$	$1.60 \cdot 10^{-5}$	$3.91 \cdot 10^{-5}$
MB _{mod}	1.05	$1.51 \cdot 10^{-5}$	$1.44 \cdot 10^{-5}$	$2.96 \cdot 10^{-5}$
MB _{mod}	1.10	$0.78 \cdot 10^{-5}$	$1.29 \cdot 10^{-5}$	$2.07 \cdot 10^{-5}$
MB	0.85	$2.13 \cdot 10^{-5}$	$0.43 \cdot 10^{-5}$	$2.56 \cdot 10^{-5}$
MB	0.90	$2.50 \cdot 10^{-5}$	$0.48 \cdot 10^{-5}$	$2.98 \cdot 10^{-5}$
MB	0.95	$2.69 \cdot 10^{-5}$	$0.56 \cdot 10^{-5}$	$3.39 \cdot 10^{-5}$
MB	1.00	$2.36 \cdot 10^{-5}$	$0.54 \cdot 10^{-5}$	$2.90 \cdot 10^{-5}$
MB	1.05	$1.55 \cdot 10^{-5}$	$0.61 \cdot 10^{-5}$	$2.16 \cdot 10^{-5}$
MB	1.10	$0.78 \cdot 10^{-5}$	$0.72 \cdot 10^{-5}$	$1.49 \cdot 10^{-5}$

Table 4.5: The dependence of corrected NO mole fractions on the stoichiometry Φ , at a distance of 1cm above the burner ($\dot{M} = 3.2610^{-2} \text{ g}/(\text{cm}^2 \text{ s})$).

caused by the omission of reactions in the prompt *NO* mechanism or are a result of the omission of reactions that describe the flame structure (the skeletal mechanism is a subset of the complex reaction mechanism). We will return to this later. If we consider the dependence of *NO* formation on the stoichiometry we see the same tendency for the MB_{mod} and MB mechanisms; the *NO* mole fraction decreases from stoichiometric to lean as well as from stoichiometric to rich mixtures. We further see that for rich mixtures a larger fraction of the total amount of *NO* is prompt *NO*. However, that part of the total formed *NO* by the prompt mechanism does not depend strongly on the stoichiometry. To make a fair comparison between the results of the various stoichiometries, the *NO* mole fractions are also corrected to $\Phi = 1.0$. The *NO* mole fraction are corrected by: $X_{NO^c} = (X_{NO}/X_{CH_4})X_{CH_4}^{\Phi=1.0}$. The corrected values are presented in Table (4.5). These results show how prompt *NO* depends on the stoichiometry. Most prompt *NO* is formed at $\Phi = 1.0$ and decreases for leaner and richer mixtures. Assuming that the results of the MB_{mod} mechanism are the most reliable we may conclude that, even for lean mixtures, prompt *NO* formation in flat laminar flames may not be neglected. Because the prompt *NO* mechanism is quite complex it would be desirable to have method to predict prompt *NO* production with less computational effort (typical computation times using the mechanism of Miller and Bowman are about 6 to 8 hours on a workstation). In the next section we will show that this can be achieved by use of a post-processing method.

4.3 Post-Processing Method

The post-processing method is based on the assumption that the species involved in the *NO* chemistry have very low mass fractions and a minor influence on the main combustion species. Following the approach of Glarborg and co-workers [Gla92], the reaction mechanism is split into two groups of species. The set of differential equations of one part, which includes the most important species and reactions in methane/air flames, is solved first. The remaining species equations are solved in a post-processing step. A further reduction of the computational effort is achieved by adapting steady-state assumptions for intermediates. The computational effort of the first step is much smaller than for the complex computation with the full mechanism, because the number of main species is relatively small (e.g. 16 instead of 51). As the species are solved simultaneously in this step, the computational effort depends quadratically on the number of species [Kee85],[Som95]. The computational effort for the second post-processing step is also relatively small due to the fact that the main species, flow and temperature are fixed. Therefore, the set of equations is less stiff.

For the computation of the main combustion species we use the skeletal mechanism for methane oxidation [Smo91]. This reaction mechanism involves the following species: CH_4 , CH_3 , CH_3O , CH_2O , HCO , CO , CO_2 , O , H , OH , O_2 , H_2 , H_2O , HO_2 , H_2O_2 and N_2 . In the post-processing step, the species of this reaction mechanism are compared with the species involved in the reaction mechanism which includes the nitrogen chemistry. All species (except *NO* and *HCN*) which are part of the complementary part of the two reaction mechanisms are considered to be steady-state species. For the reaction mechanism of Glarborg et al. this means that

the species: 3CH_2 , 1CH_2 , CH , C , NH , NCO , N_2O , CN and N are assumed to be in steady-state¹.

For all post-processor computations, differential equations are solved for NO and HCN . These are given by:

$$\rho v \nabla Y_i - \nabla (\rho D_i \nabla Y_i) = \dot{\rho}_i. \quad (4.12)$$

Here, we assume that the diffusion coefficients of NO and HCN are equal. For both species we apply unit Lewis number approximations ($Le_i = \lambda / (\rho D_i c_p) = 1$). Computations with other values for the diffusion coefficients indicate that the sensitivity of the results on the Lewis numbers is extremely small (less than 0.5% if the diffusion coefficient is varied with a factor of 2). This validates the choice of unit Lewis numbers.

4.3.1 Steady-State Equations

For the remaining species (not in the initial reaction mechanism) steady-state assumptions are applied, given by:

$$\dot{\rho}_i = M_i \sum_{j=1}^{N_r} \nu_{ij} r_j = 0. \quad (4.13)$$

In order to formulate an algebraic expression for the steady-state species, we consider the chemical reaction rates in more detail. In general, a chemical reaction j can be written as (eq. (1.31))

$$\sum_{i=1}^N \nu'_{ij} A_i = \sum_{i=1}^N \nu''_{ij} A_i, \quad (4.14)$$

with A_i the symbols of the species. The reaction rate r_j of the j^{th} reaction is given by eq. (1.32):

$$r_j = k_j^f \prod_{i=1}^N ([A_i])^{\nu'_{ij}} - k_j^b \prod_{i=1}^N ([A_i])^{\nu''_{ij}}. \quad (4.15)$$

The chemical source term of a steady-state species i is split into a 'production' and 'destruction' part: $\dot{\rho}_i = \dot{\rho}_i^{(+)} - \dot{\rho}_i^{(-)}$. As the reaction rate of the j^{th} reaction depends on the concentrations of the reacting species as indicated by eq. (4.15), the destruction part of the source term of this reaction $r_j^{(-)}$ depends explicitly on the concentration $[A_i]$ of species A_i and may be written as $r_j^{(-)} = [A_i] * \gamma_{ij}$, where γ_{ij} is given by:

$$\gamma_{ij} = k_j^{(-)} ([A_i])^{\nu''_{ij}-1} \prod_{m=1, m \neq i}^N ([A_m])^{\nu''_{mj}}. \quad (4.16)$$

Note that most reactions are two-body reactions, so that $\nu''_{ij} = 1$. Then, γ_{ij} does not depend on the concentration of the steady-state species i anymore. In eq. (4.16) we introduced a reaction

¹Note that Glarborg et al. assumes the species O , CH_3 , CH_2OH , HCO , H_2O_2 and HO_2 also to be in steady-state. Furthermore, OH is obtained from a partial-equilibrium assumption and H_2O_2 is not taken into account. We did not use these assumptions because the concentration profiles of these species are known through the skeletal mechanism.

rate $k_j^{(-)}$ as being the reaction rate of reactions in which the steady-state species i reacts with other species. This reaction rate is equal to the backward reaction rate k_j^b if the j^{th} reaction produces species i , thus if ν_{ij} is positive. Furthermore, $\nu_{ij}^{(-)}$ will be equal to ν_{ij}'' . Otherwise $k_j^{(-)}$ is equal to the forward reaction rate k_j^f and $\nu_{ij}^{(-)}$ equals ν_{ij}' . The decoupling into reactions which form or destruct the steady-state species makes it possible to formulate an explicit expression for the steady-state species from eq. (4.13):

$$[A_i] = \frac{\sum_{j=1}^{N_r} \nu_{ij} r_j^{(+)}}{\sum_{j=1}^{N_r} \nu_{ij} \gamma_{ij}}, \quad (4.17)$$

The number of steady-state equations equals $(n - n_s - 2)$, where n is the number of species in the reaction mechanism used in the post-processing step and n_s is the number of main species² of the first computational step.

4.3.2 Discretization

The differential equations (4.12) for flat flames become (see also eq. (2.40)):

$$M \frac{d\phi_i}{dx} - \frac{d}{dx} \left(\rho D_i \frac{d\phi_i}{dx} \right) = \rho w_i \quad \text{for } i = NO, HCN, \quad (4.18)$$

which can be written as:

$$c'_1 \frac{d\phi_i}{dx} + \frac{d}{dx} \left(c'_2 \frac{d\phi_i}{dx} \right) + c'_3 = 0, \quad (4.19)$$

with

$$c'_1 = \dot{M}, \quad c'_2 = -\rho D_i, \quad c'_3 = -\rho w_i,$$

for $i = NO, HCN$. Now the differential equations are written in the same form as eq. (2.84) and for the subsequent discretization, the finite-volume technique as presented by Thiart [Thi90] is used. The discretization method is already treated in section 2.3.4, leading to:

$$a_i^W \phi_{i,W} + a_i^P \phi_{i,P} + a_i^E \phi_{i,E} = b_i, \quad (4.20)$$

Also a modification of this discretization will be used, where all coefficients are the same except b_i which is modified to:

$$b_i = -c_{A,i} \Delta x, \quad (4.21)$$

with $\Delta x = (x_{i+1} - x_{i-1})/2$. In this equation the source terms are not weighted with the function $W(P)$, with $W(P) = \frac{1}{P} - \frac{1}{e^{P-1}}$ (see also section 2.3.4). The effect of the difference in the discretization of the source term will be considered later.

²Here, $n_s = 16$, the number of species in the skeletal mechanism.

For the two-dimensional flames the discretization is similar to that for the one-dimensional situation. The source term for the two-dimensional computations is not weighted. The equations for the two-dimensional geometries are given by:

$$c'_1 \frac{d\phi_i}{dx} + \frac{d}{dx} \left(c'_2 \frac{d\phi_i}{dx} \right) + c'_3 \frac{d\phi_i}{dy} + \frac{d}{dy} \left(c'_2 \frac{d\phi_i}{dy} \right) + c'_4 = 0, \quad (4.22)$$

with

$$\begin{aligned} c'_1 &= \rho u, \\ c'_2 &= -\rho D_i, \\ c'_3 &= \rho v, \\ c'_4 &= -\rho w_i, \end{aligned}$$

which after discretization results into:

$$a_i^W \phi_{i,W} + a_i^P \phi_{i,P} + a_i^E \phi_{i,E} + a_i^N \phi_{i,N} + a_i^S \phi_{i,S} = b_i, \quad (4.23)$$

with

$$a_i^E = \frac{c'_{2,i-1} \Delta y}{\Delta x_E} A(-P_i^w),$$

$$a_i^W = \frac{c'_{2,i+1} \Delta y}{\Delta x_W} A(P_i^e),$$

$$a_i^N = \frac{c'_{2,i-1} \Delta x}{\Delta y_N} A(P_i^n),$$

$$a_i^S = \frac{c'_{2,i+1} \Delta x}{\Delta y_S} A(-P_i^s),$$

$$a_i^P = -(a_i^E + a_i^W + a_i^N + a_i^S),$$

$$b_i = -c_{4,i-1} \Delta y \Delta x.$$

Note that additional terms for the north and south points appear. The distances Δx_E , Δx_W , Δy_N , Δy_S , Δx and Δy are presented in Figure 4.1. Further, the local Peclet numbers are given by:

$$P_i^w = \frac{-c'_{1,i}}{c'_{2,i}} \Delta x_W,$$

$$P_i^e = \frac{-c'_{1,i}}{c'_{2,i}} \Delta x_E,$$

$$P_i^n = \frac{-c'_{3,i}}{c'_{2,i}} \Delta y_N,$$

$$P_i^s = \frac{-c'_{3,i}}{c'_{2,i}} \Delta y_S.$$

The discretization coefficients depend on the temperature, the density, the diffusion coefficients, the flow velocity and the grid-spacing only, which do not change during the post-processing

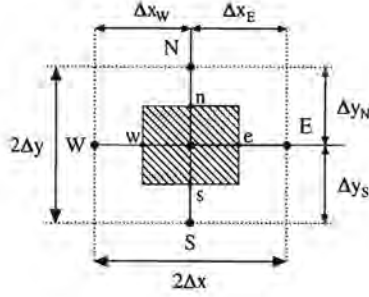


Figure 4.1: Discretization molecule for two-dimensional computations.

step. Therefore, the discretization coefficients a_w , a_e , a_n , a_s and a_p may be considered as constant, so that the equations have to be discretized only once.

The steady-state equations and the differential equations, treated in the post-processing step are coupled. Due to the reduced stiffness, the differential equations are solved sequentially by a tridiagonal matrix equation solver, in contrast to the complex computations where all equations are solved simultaneously using Newton's method [Som94], [Kee85]. The discretized differential equations for the two-dimensional flame are solved by the ADI method. Before the differential equations are updated, the steady-state species are solved in an inner iteration loop, in which the chemical source terms of *NO* and *HCN* are also computed. This inner iteration procedure solves the equations (4.17) sequentially for all steady-state species until the relative variations in the source terms of *NO* and *HCN* in successive iterations is small enough (generally 10^{-6}). Thus, the inner-iteration loop is repeated until the average relative change in source terms q_1 is small enough, with q_1 defined by:

$$q_1 = \frac{1}{2N_p} \sum_{k=1}^{N_p} \sum_{i=NO}^{HCN} \frac{|\dot{\rho}_{i,k}^{j_1} - \dot{\rho}_{i,k}^{j_1-1}|}{|\dot{\rho}_{i,k}^{j_1} + \dot{\rho}_{i,k}^{j_1-1}|}, \quad (4.24)$$

with species index i , position index k , iteration index of the inner-iteration loop j_1 and N_p the number of grid points. The solution of the tridiagonal matrix equation solver $Y_{i,k}^{j_1+1}$, is damped according to:

$$\bar{\phi}_{i,k}^j = R * \phi_{i,k}^j + (1 - R) \phi_{i,k}^{j-1} \quad k = 1, \dots, N_p \quad i = NO, HCN. \quad (4.25)$$

The variations in the steady-state species mass fractions are also damped in the inner iteration loop. The procedure is repeated until the average relative variation q_2 in the specific mole numbers of *NO* and *HCN* is small enough, where q_2 is defined by:

$$q_2 = \frac{1}{2N_p} \sum_{k=1}^{N_p} \sum_{i=NO}^{HCN} \frac{|\phi_{i,k}^{j_2} - \phi_{i,k}^{j_2-1}|}{|\phi_{i,k}^{j_2} + \phi_{i,k}^{j_2-1}|}. \quad (4.26)$$

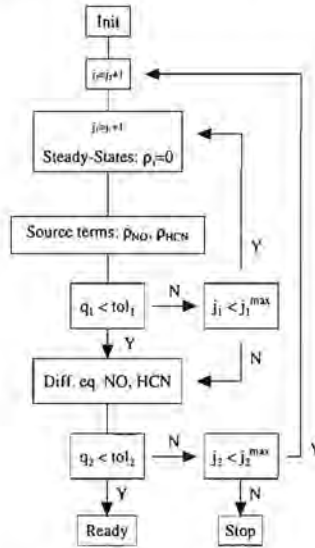


Figure 4.2: Flow diagram of the post-processor

Here, j_2 is the iteration index of the main iteration loop. The solution procedure is sketched in Figure 4.2. Typical relaxation factors R for NO , HCN and the steady-state species are 0.2, 0.1 and 0.8 for the Glarborg et al.'s reaction mechanism and 0.06, 0.04 and 0.8 for the modified Miller and Bowman mechanism.

For the two-dimensional flame, relaxation factors of 0.8, 0.5 and 0.8 are used for NO , HCN and the steady-state species (using the reaction mechanism Glarborg et al.). Moreover, to speed up the 2-D computations the source terms (and steady-state species) are not updated every iteration but only after every 20 iterations.

4.4 One-Dimensional Flames

The post-processing method is applied to one-dimensional flames first. For these flames it is also possible to perform detailed computations. This makes it possible to compare post-processor results with detailed computations. This is done in subsection 4.4.1. In subsection 4.4.2 the differences between the discretization methods (2.89) and (4.21) are considered. Results of detailed computations are presented in subsection 4.4.3. They are used to investigate which reactions of the reaction mechanism are most important. In subsection 4.4.4 results of adiabatic flames are presented. The advantage of considering adiabatic flames is that no differences in flame temperature occur when various reaction mechanisms are used. Finally, computations are compared with measurement in section 4.4.5.

4.4.1 Comparison of Post-Processor Results with Detailed Computations

To test the post-processing method, results of the post-processor are compared with detailed computations. The results of the detailed computations are presented in section 4.2. To investigate the effect of introducing steady-state assumptions for intermediate species, we did the following. We first performed detailed computations with the full mechanisms. The results are used as input for the post-processor. The profiles of the main species (part of the skeletal mechanism) are fixed in post-processor. The remaining species, which are part of Glarborg et al.'s mechanism and not part of the skeletal mechanism, are computed again. For *NO* and *HCN* differential equations are solved and steady-state equations are introduced for the other species. The results are subsequently compared with the results of the detailed computations. Differences between post-processor results and detailed computations may not only be caused by the introduction of steady-state assumptions for intermediate species but also by the reduced numbers of species and reactions in the post-processing step. The latter effect is studied by using various reaction mechanisms in the full computations, while in the post-processing step the reaction mechanism of Glarborg et al. is applied only.

Furthermore, the skeletal mechanism is also used in combination with detailed as well as simplified thermodynamic and transport properties (SkelSTTP).

The results of the various reaction mechanisms are presented in Table 4.6 for a stoichiometric flame. In Table 4.7 we compare the results of the post-calculations performed with the MB_{mod} and MB mechanisms with the results of the complex calculations, as function of the stoichiometry Φ . The columns *NO* and *NO_{post}* represent results of full calculations and post-flame calculations, respectively. The results of Table 4.6 are also shown in the Table 4.8,

<i>scheme</i>	<i>NO_{eq}</i>	<i>NO_{th}</i>	<i>NO</i>	<i>NO_{post}</i>	<i>T</i>
MB _{mod}	$0.36 \cdot 10^{-5}$	$2.31 \cdot 10^{-5}$	$3.91 \cdot 10^{-5}$	$3.88 \cdot 10^{-5}$	2072
MB	$0.37 \cdot 10^{-5}$	$2.36 \cdot 10^{-5}$	$2.90 \cdot 10^{-5}$	$3.95 \cdot 10^{-5}$	2073
Skel _G	$0.67 \cdot 10^{-5}$	$2.91 \cdot 10^{-5}$	$4.80 \cdot 10^{-5}$	$4.95 \cdot 10^{-5}$	2118
Skel	$0.57 \cdot 10^{-5}$	$2.60 \cdot 10^{-5}$	—	$4.49 \cdot 10^{-5}$	2103
SkelSTTP	$0.62 \cdot 10^{-5}$	$2.66 \cdot 10^{-5}$	—	$4.65 \cdot 10^{-5}$	2105

Table 4.6: Comparison of equilibrium, thermal and total *NO* mole fractions at a distance of 1 cm above the burner with post-calculations using various reaction mechanisms, $\Phi = 1.0$, $M = 3.26 \cdot 10^{-2} \text{ g}/(\text{cm}^2 \text{ s})$.

where the contributions of the thermal and prompt *NO* formation are given as fraction of total formed *NO*. We used both the total formed *NO*, determined with the full reaction mechanism calculations³ as well as the result of post-calculations (*NO_{post}*) as reference here. A very im-

³This is only possible for the reaction mechanism that include nitrogen chemistry.

<i>scheme</i>	Φ	<i>NO</i>	<i>NO_{post}</i>
MB _{mod}	0.90	$3.61 \cdot 10^{-5}$	$3.54 \cdot 10^{-5}$
MB _{mod}	0.95	$4.05 \cdot 10^{-5}$	$4.00 \cdot 10^{-5}$
MB _{mod}	1.00	$3.91 \cdot 10^{-5}$	$3.88 \cdot 10^{-5}$
MB _{mod}	1.05	$3.09 \cdot 10^{-5}$	$3.05 \cdot 10^{-5}$
MB _{mod}	1.10	$2.26 \cdot 10^{-5}$	$2.18 \cdot 10^{-5}$
MB	0.85	$2.21 \cdot 10^{-5}$	$3.01 \cdot 10^{-5}$
MB	0.90	$2.71 \cdot 10^{-5}$	$3.63 \cdot 10^{-5}$
MB	0.95	$3.08 \cdot 10^{-5}$	$4.11 \cdot 10^{-5}$
MB	1.00	$2.90 \cdot 10^{-5}$	$3.95 \cdot 10^{-5}$
MB	1.05	$2.26 \cdot 10^{-5}$	$3.11 \cdot 10^{-5}$
MB	1.10	$1.63 \cdot 10^{-5}$	$2.19 \cdot 10^{-5}$

Table 4.7: Comparison of NO with complex and post-calculations as function of the stoichiometry.

<i>scheme</i>	$\frac{NO_{th}}{NO}$	$\frac{NO_{th}}{NO_{post}}$	$\frac{NO_{pr}}{NO}$	$\frac{NO_{pr,post}}{NO_{post}}$
MB _{mod}	59.1	59.6	40.9	40.4
MB	81.4	59.7	18.6	40.3
Skel _G	60.6	58.8	39.4	41.2
Skel	-	57.9	-	42.1
Skel _{STTP}	-	57.2	-	42.8

Table 4.8: Thermal and prompt contributions of the complex and post calculations.

portant result is that the computed *NO* mole fractions obtained from the post-processor using the profiles of the major species of the detailed computation obtained from MB and MB_{mod} as input are only slightly different from the results of the complex calculations with the modified Miller and Bowman reaction mechanisms, for all Φ values. This implies that the differences in profiles of major species are not influenced by the changed reaction rate data (only the reaction rate data of species involved in the nitrogen reactions are modified). Furthermore, we may conclude that the reaction mechanism of Glarborg et al. (used in the post-processing step), which is a reduced set of the modified Miller and Bowman reaction mechanism, gives accurate results compared with the detailed computations (using MB_{mod}). This indicates that the species and reactions which are omitted in the reaction mechanism of Glarborg et al. are of minor importance. We also may conclude that the inaccuracy introduced by the steady-state assumptions in the post-calculations is small and acceptable, especially when we keep in mind that variations of at least the same order of magnitude arise from uncertainties in reaction rate data in the full reaction mechanisms.

The differences in *NO* post-calculations using the Skel_G, Skel, Skel_{STTP} mechanisms are small and almost the same as the *NO* mole fraction estimated by the full calculations with the Skel_G mechanism. This indicates that the differences of the post-calculations between the MB_{mod} mechanism and the Skel_G mechanism are mainly caused by the difference in description of flame structure and not by the reduced set of reactions that describe the nitrogen chemistry. Especially the difference in flame temperature predicted by the skeletal mechanism and the Miller and Bowman mechanism has a large influence on the *NO* formation.

4.4.2 Comparison of the Discretization Methods

The differences between the discretization methods (2.89) and (4.21) are considered in this subsection. We have used a fine and a coarse grid (see Figure 4.3). One grid is coarse at the end of the domain, the second grid has more points at the end of the domain, while the total number of grid points is equal. The relative difference in the mass fractions of the main species (of the skeletal mechanism) found with the two grids is less than a few percent. The *NO* profiles, obtained in the post-processing step (using the reaction mechanism of Glarborg et al.), however, deviate up to 15%. There are also considerable deviations between computations using the discretization methods (2.89) and (4.21) for the grid which is rough at the end of the domain. The distinction between the discretization methods is less noticeable for the other grid. The results indicate that special attention has to be paid to the grid for accurate *NO* predictions. A (non-equidistant) grid which is suitable to predict the main species may be too rough for accurate prediction of *NO* in the post-processing step. This is caused by the fact that the *NO* concentration still increases in the post-flame zone, whereas most other species are in chemical equilibrium. The *NO* concentration is far below the equilibrium value.

4.4.3 Reaction Paths of NO

To get more insight in the prompt *NO* formation, it is studied which reactions are important for the formation of *NO*. Therefore, we consider the contributions of the various reactions that may

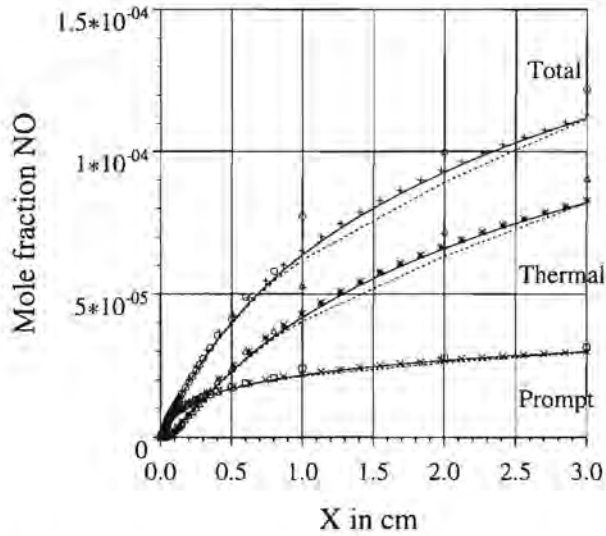


Figure 4.3: Profiles of NO mole fractions on various grids and using different source term discretizations. The lines denote the computations with eq. (2.89), markers correspond to eq. (4.21). Continuous lines correspond to a fine grid and dashed lines with a course grid in the post-flame zone. The position of the markers corresponds to the position of grid points. The \circ , Δ and \square markers correspond to the dashed lines. The $+$, $*$ and \times markers correspond to the continuous lines. The mass flow rate used for the computations is $0.0395 \text{ g}/(\text{cm}^2 \text{ s})$ and the equivalence ratio $\Phi = 1.0$.

produce NO . We consider a burner-stabilized flat flame with a flow velocity of 29.2cm/s and a corresponding mass flow rate of $3.26\text{g}/(\text{cm}^{-2}\text{s})$. The Miller and Bowman mechanism as well as the modified Miller and Bowman mechanism are applied in the post-processing step. We use complex computations to investigate which reactions are most important. However, since the complex computations are performed with the Sandia Package [Kee85], the source terms of the various reactions cannot be obtained easily (they are not part of the output of the code). Therefore, the source terms are computed in the post-processor code. As all profiles of radicals are available, no steady-state assumptions are introduced in the post-processor. Only the profiles of NO and HCN are computed again. The computed NO mole fraction at the end of the domain is compared with the original detailed computations in Table (4.9). It can be seen that the differences are small. It is therefore expected that the sources terms obtained in the post-processor are accurate. Furthermore, also the results of the post-processing method using the modified Miller and Bowman reaction mechanism and the input of the skeletal mechanism are examined.

Scheme	NO_{th}	NO	NO_p
MB	104.4	113.0	113.3
MB _{mod}	102.2	135.3	135.8
Skel	91.2	-	113.6

Table 4.9: Comparison of post-calculations of the NO mole fraction (in ppm) using the original and the modified Miller and Bowman mechanism, at a distance of 8cm above the burner. The post-processing results of the skeletal mechanism are also presented.

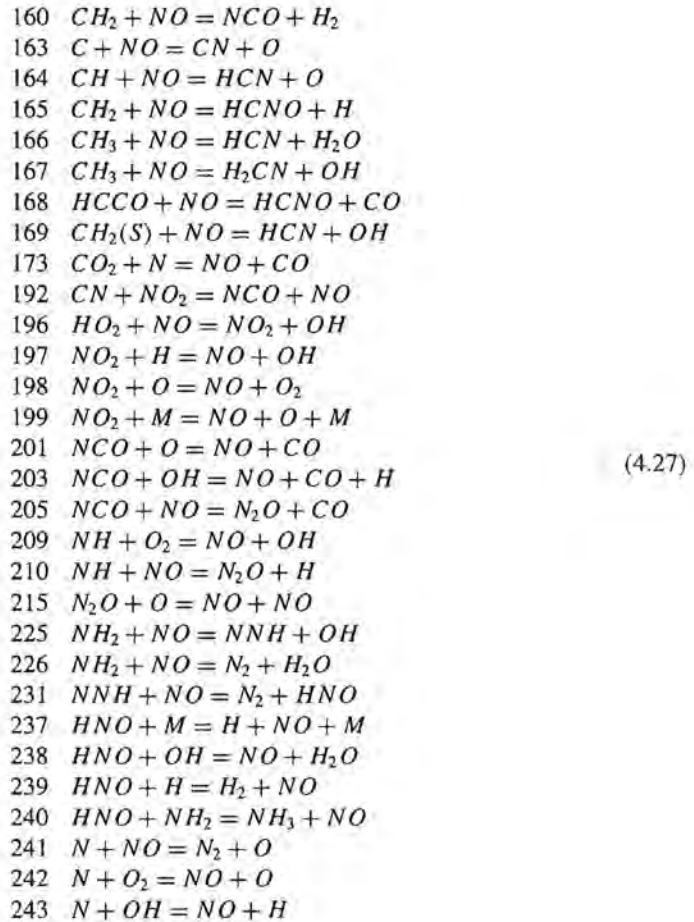
The reactions which produce NO_x in the original Miller and Bowman mechanism are already given in (4.11). The reactions included in the modified Miller and Bowman mechanism are given in (4.27).

To study which reactions are most important, we computed which reactions have the largest contribution to the totally formed NO . Therefore we introduce the following quantity:

$$C_j = \int_{x=0}^{x_e} r_j v_{NO,j} dx, \quad (4.28)$$

with x_e the end of the domain which will be either 1cm or 8cm . Thus, if C_j is positive, the j^{th} reaction produces NO . The 10 reactions which have the largest contribution C_j over a distance of 1cm and 8cm above the burner are presented in Figures 4.4 and 4.5.

The reactions 233, 234 and 235 are the thermal NO reactions. For the Miller and Bowman mechanism 92.0% of the total NO is formed by the thermal mechanism at a height of 1cm above the burner and 92.2% at a height of 8cm above the burner. If the thermal NO formation is calculated with the simplified formula for thermal NO formation (4.5), the estimated contribution of the thermal mechanism is 79.6% at 1cm and 92.4% at 8cm . This indicates that more NO is formed by the reactions of the thermal mechanism than predicted by eq. (4.5). This is caused by



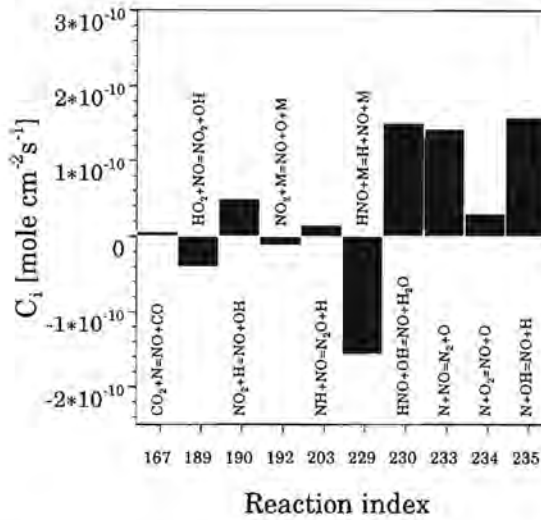


Figure 4.4: The 10 reactions with the largest contribution in the total NO formation, 1cm above the burner (original Miller and Bowman mechanism).

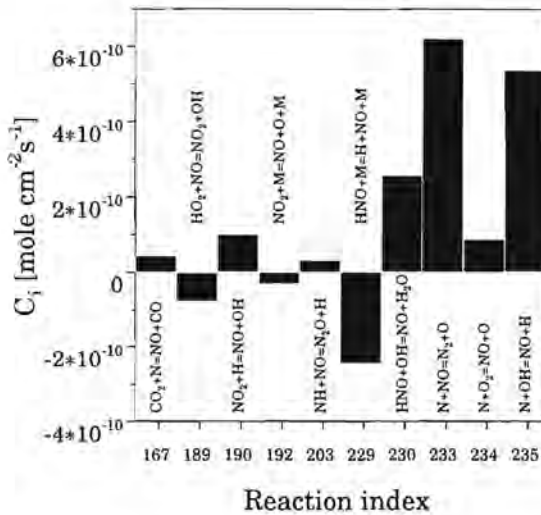


Figure 4.5: The 10 reactions with the largest contribution in the total NO formation, 8cm above the burner (original Miller and Bowman mechanism).

the fact that N radicals are not only produced by the first Zeldovich reaction, but also by other reactions. The N -radicals may subsequently react with O_2 or OH as indicated by the second and third Zeldovich reactions. This can also be seen in Figure 4.4, where it can be seen that the sum of the integrated reaction rates of reaction 234 and 235 is larger than the integrated reaction rate of 233. If the N -radicals would be formed by the Zeldovich mechanism only, these should be equal.

The same is done for the modified Miller and Bowman mechanism. The results are shown in Figures 4.6 and 4.7. The reactions 241, 242, 243 of the thermal mechanism form 71.74% of the total NO at a height of 1 cm above the burner and 73.1% at a height of 8 cm . Equation (4.5) gives a contributions of 58.5 and 75.5% for the thermal mechanism at a height of 1 cm and 8 cm , respectively. Comparing the results of both mechanisms it is obvious that the modification of the reaction rates has quite a large influence.

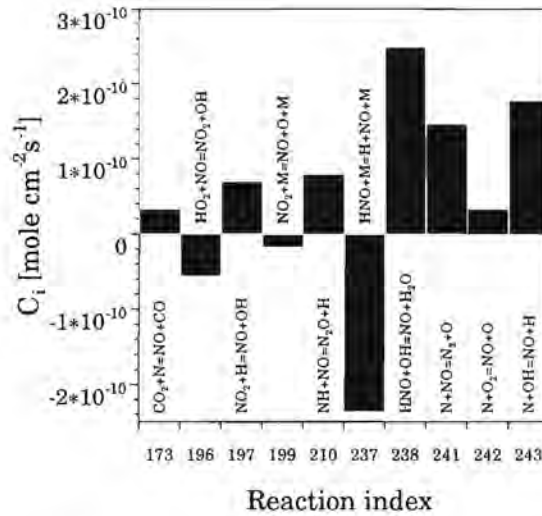


Figure 4.6: The 10 reactions with the largest contribution in the total NO formation, 1 cm above the burner (modified Miller and Bowman mechanism).

The results of Figures 4.4-4.7 indicate that some reactions which include NO_2 are important for the NO formation. However, it should be noted that these reactions do not give a net contribution to the NO formation. This is caused by the fact that NO_2 is only formed by consuming NO in all reactions. If the original reaction mechanism of Miller and Bowman is considered, it

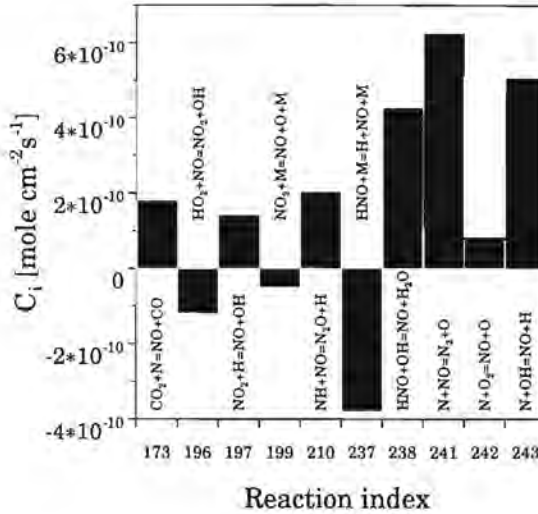
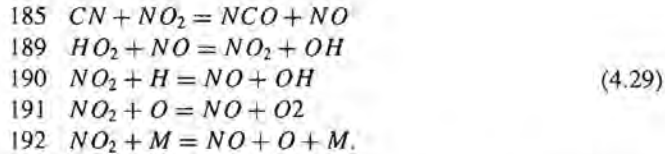


Figure 4.7: The 10 reactions with the largest contribution in the total NO formation, 8cm above the burner (modified Miller and Bowman mechanism).

can be seen that NO_2 is formed by the following reactions:



Note that NO is involved in all reactions with NO_2 , so that the sum $\text{NO}_x = \text{NO} + \text{NO}_2$ is conserved. For the flames considered here, the temperature remains high, so that the concentration of NO_2 is very low. The maximum mole fraction is of order of magnitude of NO_2 is 0.1 ppm, whereas the mole fraction at a distance of 8cm above the burner is $1.8 \cdot 10^{-2}$ ppm for the original Miller and Bowman mechanism and $2.2 \cdot 10^{-2}$ ppm for the modified mechanism. NO will be converted into NO_2 at low temperatures only.

Additionally, some reactions including HNO appear to be important in Figures 4.4-4.7. However, the total contribution to the NO formation of all reactions which include HNO is small for the original Miller and Bowman mechanism, whereas it is much larger for the modified Miller and Bowman mechanism. Further, the results show that the following reactions give a considerable contribution to the total NO formation:



where the first reaction indicates the importance of N_2O . Furthermore, CO_2 can be converted into NO and CO .

We also determined the reactions with the largest contributions to the totally formed NO for a computation with the skeletal mechanism. The NO formation is subsequently computed in a post-processing step with the modified Miller and Bowman mechanism. The results are presented in Figures 4.8 and 4.9. For the computation using the skeletal mechanism 78.6% of the NO is formed by the reactions of the thermal mechanism at a height of 1cm above the burner and 75.4% at 8cm (68.7% and 80.3% at 1cm and 8cm using (4.5)). The main difference be-

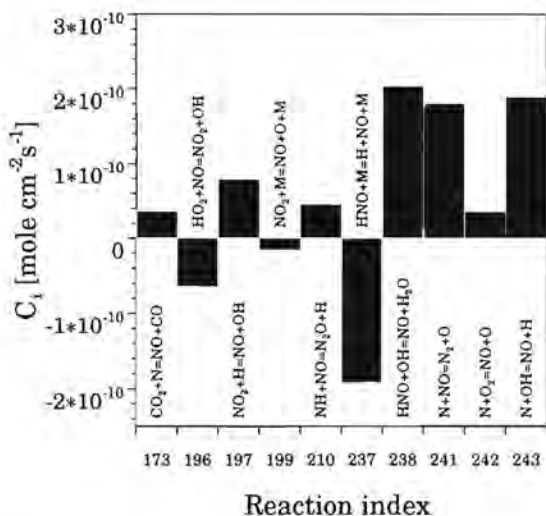


Figure 4.8: The 10 reactions with the largest contribution in the total NO formation at 1cm above the burner (skeletal reaction mechanism, post-processing with modified Miller and Bowman mechanism).

tween the results of the post-processing with the modified Miller and Bowman mechanism using the skeletal mechanism for computing the major species and the detailed computation using the modified Miller and Bowman mechanism is that the reaction rates of the reactions which include NO_2 and the contribution of reactions which include HNO are much smaller. This is probably caused by the steady-state assumptions which are introduced for NO_2 and HNO . Furthermore, the predicted NO concentrations show deviations caused by distinctions in the flame temperature due to the different adiabatic mass burning rates of the various mechanisms. Finally, the results indicate that the reactions of the prompt mechanism give a significant contribution to the total formed NO not only in the flame front but also at a higher distance above the burner, although the contribution decreases with increasing height.

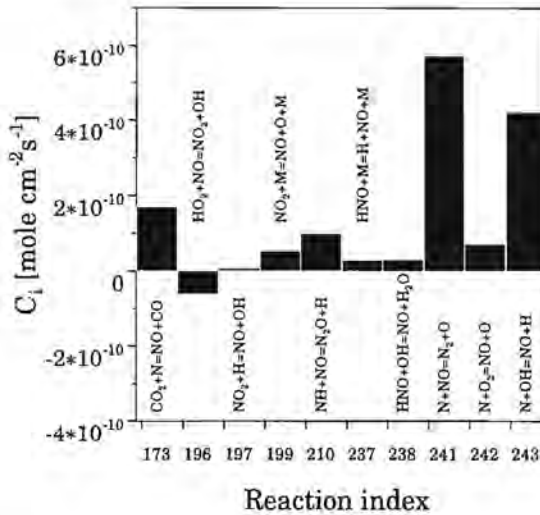


Figure 4.9: The 10 reactions with the largest contribution in the total NO formation at 8cm above the burner (skeletal reaction mechanism, post-processing with modified Miller and Bowman mechanism).

4.4.4 Adiabatic Flames

From the detailed results and post-processing results we concluded in the final part of subsection 4.4.1 that significant differences in predicted NO profiles can be observed, which are mainly caused by variations in flames structure. The effect of omitting nitrogen reactions is expected to be smaller. In this subsection we will verify whether this is true. One major difference between the results of the various reaction mechanisms is that the predicted flame temperature deviates. This is caused by distinction in adiabatic burning velocity of the various reaction mechanisms⁴. We have already seen before that even small changes in temperature may cause significant deviations in the NO production term. A possibility to eliminate temperature effects in computations using various reaction mechanisms is to consider adiabatic flames. The flame temperature of adiabatic flames is determined by the equilibrium composition of the mixture and is therefore independent of the reaction mechanism. The chemical equilibrium composition is determined by thermo-dynamic properties of the species in the mixture. However, the chemical equilibrium composition is only predicted accurately if all reactions are assumed to be reversible and if all reverse reaction rates are obtained from the equilibrium constants. Therefore, all reactions are assumed to be reversible and reverse reaction rates are obtained from the equilibrium constants.

To test the errors introduced by the approximations in the post-processing method, we compare results of the post-processing method with complex computations with the full mechanism.

⁴The adiabatic burning velocities found with the modified Miller and Bowman and skeletal schema are 41.4cm/s and 44.8cm/s, respectively.

For the post-processor we used the reaction mechanism of Glarborg et al. and the modified Miller and Bowman mechanism. For the complex computations we used the modified Miller and Bowman reaction mechanism. The results of the post-processing method and the complex

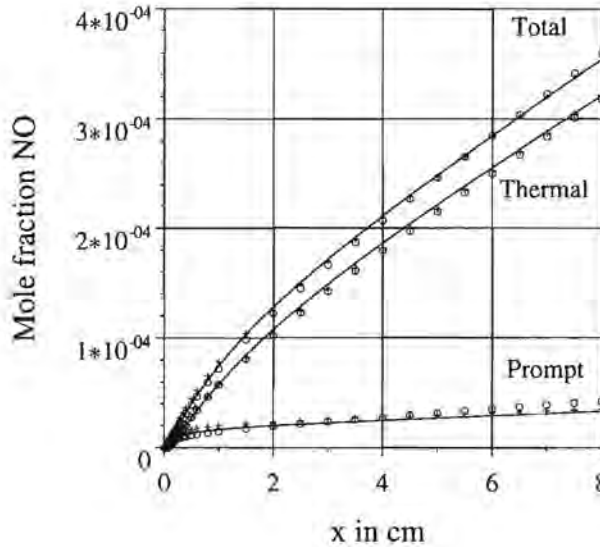


Figure 4.10: Results of the post-processing method (markers) and complex computations (lines) for an adiabatic stoichiometric methane/air flame. (\circ): Skeletal mechanism for the main species and modified Miller and Bowman mechanism for the post-processing. ($+$): Skeletal mechanism for the main species and Glarborg et al.'s mechanism for the post-processing. Complex computations are performed with the modified Miller and Bowman mechanism.

computations are presented in Figure 4.10. The results of the post-processing method agree well with the detailed results. This indicates that the decoupling of the main species and the application of steady-state assumptions have a negligible influence on the results. Furthermore, the differences between the results of post-calculations with the modified Miller and Bowman mechanism and the Glarborg et al.'s mechanism are also small. This means that the species and reactions omitted in the reduced mechanism of Glarborg et al. are of minor interest. We like to stress the importance of the assumptions that all reactions are reversible and that all reverse reaction rates are obtained from the equilibrium constants are of major importance. It has appeared that these modifications may result in differences up to 10% in final NO mole fractions. The computational effort of the post-processing method (using the reaction mechanism Glarborg et al.) is roughly a factor of 20 lower than the computational effort of the complex computations. If the modified reaction mechanism of Miller and Bowman mechanism is used in the post-processing step, the computational effort is roughly twice as large as for the Glar-

borg et al.'s mechanism. Note, that the mole-fraction of NO is relatively high at the end of the computational domain because adiabatic flames are considered here. For these flames the temperature is maximal giving a large NO production. Furthermore, we consider a flat flame which means that the exhaust gases downstream of the burner are not cooled by surrounding air as in practical situations.

4.4.5 Comparison of Computations and Measurements

To validate the post-processing method and the accuracy of the reaction mechanisms, the results are compared with measurements of NO above a ceramic foam surface burner. The measurements are performed by use of a water cooled suction probe, while the gas samples are analyzed by chemoluminescence. The burner is positioned in a combustion chamber which is constructed in such a way that the energy loss of the gas is minimal. This justifies the use of a one-dimensional flat flame burner model (without energy losses to the environment) to compute the NO formation, so that numerical results can be compared with measurements. The post-processor code was extended to model flames on this burner. The ceramic burner and the measurements are described in more detail by Bouma et al. [Bou93], [Bou95a] and [Bou95b]. To model flames on this burner, again the skeletal mechanism is used to predict main species concentrations and the reaction mechanism of Glarborg et al. is used for the post-processing step. Some results for $\Phi = 0.77$ and $\Phi = 0.91$ are shown in Figures 4.11, 4.12 and 4.13 which

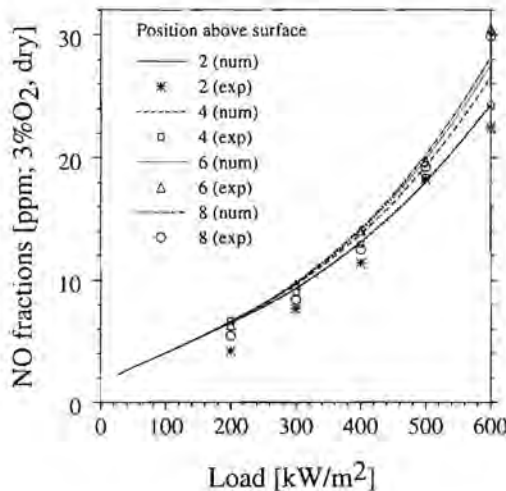


Figure 4.11: Comparison of measurements and computations of NO , formed in methane/air flames ($\Phi = 0.77$) stabilized on a radiant ceramic foam burner.

agree well with the measurements. The differences are smaller than 20%. This is within the accuracy range of the measurements. This indicates that the reaction mechanism gives accurate

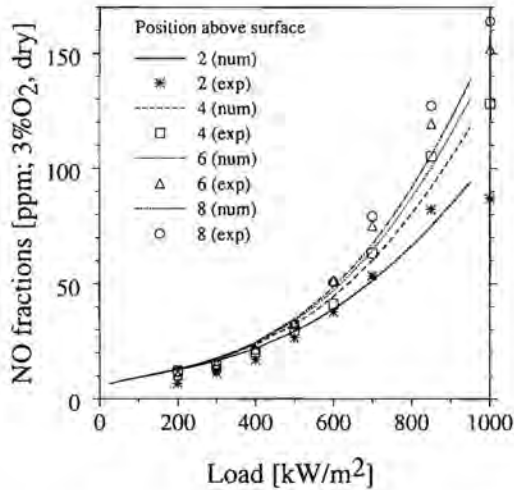


Figure 4.12: Comparison of measurements and computations of NO, formed in methane/air flames ($\Phi = 0.91$) stabilized on a radiant ceramic foam burner.

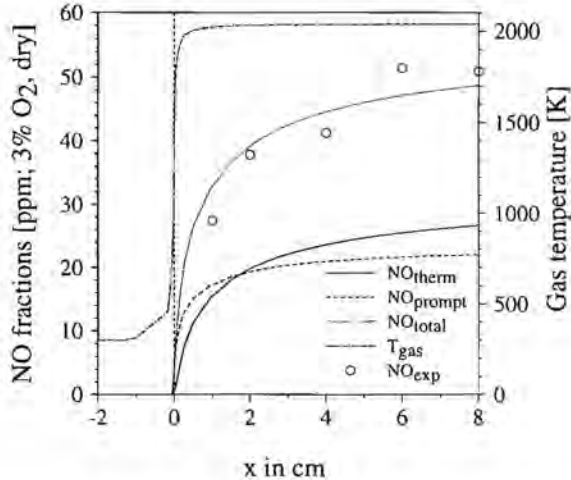


Figure 4.13: Comparison of measurements and computations of NO as function of the distance above the burner surface, formed in methane/air flames ($\Phi = 0.91$, and thermal load of 600 kW/m^2) stabilized on a radiant ceramic foam burner. The burner surface is positioned at $x = 0$ and the burner plate is 1cm thick.

results. The accuracy of the computations is of the same order of magnitude, due to uncertainties in the reaction rate data. Note that the *NO* emission of this burner is low compared with the emission of the adiabatic flames. However, the *NO* emission of this burner in a more practical situation will be even lower, because the exhaust gases will be cooled more rapidly.

4.5 Two-Dimensional Flames

The post-processing method has been tested extensively for one-dimensional flames in the previous section. The results indicate that it is possible to model the formation of *NO* by use of a post-processing method efficiently and accurately. The next step is to extend the method to two-dimensional flames. As it is not possible yet to perform detailed *NO* computations for these flames, only post-processor results are presented. However, considering the results of the one-dimensional flames it is to be expected that the results for the two-dimensional flames are accurate. There are two geometries considered: a multiple micro-slit burner and a single-slit burner. The flames on the burner mentioned first are nearly flat, which allows for comparing the results with those of one-dimensional flames. For the two-dimensional flames, all flame computations are performed with the skeletal mechanism. These computations are performed by Somers et al. [Som94], [Som95]. For the post-calculations the reaction mechanism of Glarborg et al. [Gla92] is used.

The grid used for the two-dimensional flame computations is locally refined during the first computation step. A static refinement procedure is used [Lan92], [Som94]. The method starts with a coarse grid and points are added in the active zone with large gradients. If a rectangular control volume has to be refined, it is divided into four equal rectangles. An example of a refined grid is shown in Figure 4.16.

There are points on the edge of the refinement areas which do not have four surrounding points. Variables in these points are obtained by linear interpolation. If, for example, there is no north or south point on the same interpolation level available, linear interpolation of the data at the west and east point is carried out.

To test the two-dimensional post-processing code we first consider a multiple-slit burner with a small slit width (0.4mm) and a small pitch (0.6mm). The computational domain, shown in Figure 4.14, has a width of only one half pitch with symmetry boundary conditions at the sides. The domain is 0.3mm wide and 4mm high. The burner wall (in the computational domain) is 0.1mm wide and 0.8mm thick. As the slits and the spacing between the slits are very small, distortions from one-dimensional behaviour are damped out very fast at the burner outlet, so that the flame may be considered as a flat flame [Goe94]. The results of this burner are compared with results of a perfectly flat flame burner. The differences between the one- and two-dimensional computations are small (see Figure 4.15). The only visible differences are close to the burner where the flow is different. The maximum velocity in the inlet is 78.8cm/s for the micro-slit burner (the velocity profile in the burner inlet slit is parabolic), whereas the inlet velocity is 35.3cm/s for the flat flame burner. The total mass flow rates at the outlet of the burners, however, are equal.

A single slit burner in a confined environment with cooled walls is considered, finally. The

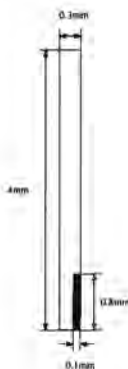


Figure 4.14: Computational domain of the multiple-slit burner.

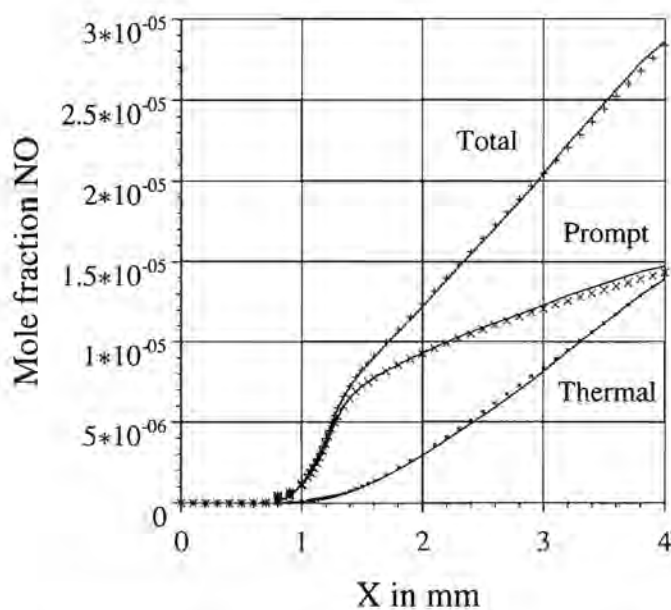


Figure 4.15: Comparison of results for a two-dimensional micro-slit burner (symbols) ($v_{max} = 78.75 \text{ cm/s}$, $\Phi = 1.0$) and a one-dimensional flame (lines) ($\dot{M} = 0.0395 \text{ g/(cm}^2 \text{ s)}$, $v = 35.3 \text{ cm/s}$, $\Phi = 1.0$).

burner geometry and the locally refined mesh used for the computations are shown in Figure 4.16. The computational domain is 8mm high and 6mm wide. In the computations only one

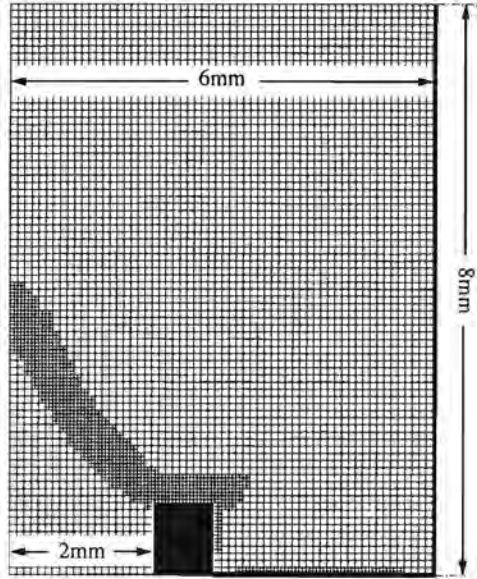


Figure 4.16: Computational domain and locally refined mesh of the single slit-burner. The thick lines indicate walls.

half slit (which is 2mm wide) is modelled with symmetry boundary conditions at the center line. The burner edge is 1mm high and 0.8mm wide. The complex computation of the major combustion species is described in more detail by Somers and de Goey [Som95]. Post-processing is performed using the reaction mechanism of Glarborg et al.. The chemical source terms of the thermal and prompt NO formation are presented in Figure 4.17 and 4.18, respectively. Temperature contour lines are given in Figure 4.19. The prompt NO source term reaches its maximum between 1700K and 1800K , where the flame front is positioned. The thermal source term reaches its maximum at a higher temperature. This can be seen more clearly in Figure 4.20, where the source terms on the center line ($x = 0.0$) are presented.

The prompt NO production rate reaches its maximum on the center line in the flame-front at $y = 4.2\text{mm}$, whereas the largest thermal NO production rate is located at $y = 5.5\text{mm}$, in the post-flame zone. Moreover, it can be observed that the prompt NO source term is also quite large in the post-flame area. Contour lines of NO mole fraction are shown in Figure 4.21. Maximum NO concentrations are observed on the center line above the flame. In Figure 4.22, thermal prompt and total NO mole fractions on the center line are presented. Although the maximum value of the prompt NO source term is much larger than the maximum thermal source term, most NO is formed by the thermal mechanism on the center line at the end of the domain (about 60

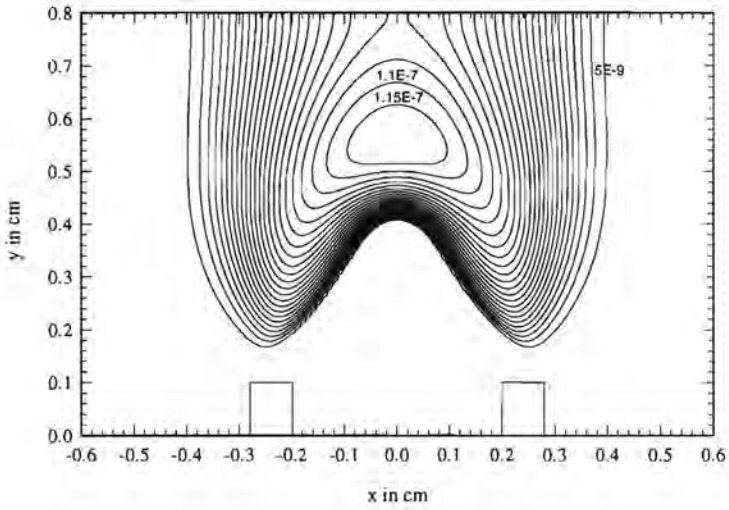


Figure 4.17: Thermal NO source term of the flame on the slit-burner, given in $\text{cm}^{-3}\text{s}^{-1}$.

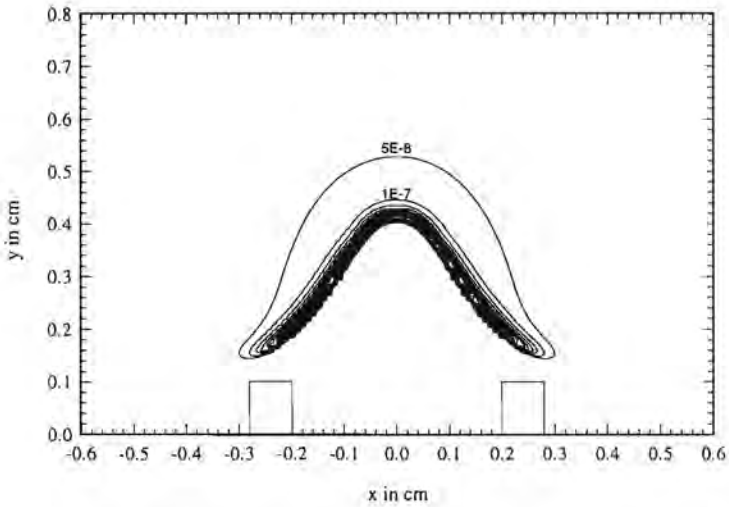


Figure 4.18: Prompt NO source term, given in $\text{cm}^{-3}\text{s}^{-1}$.

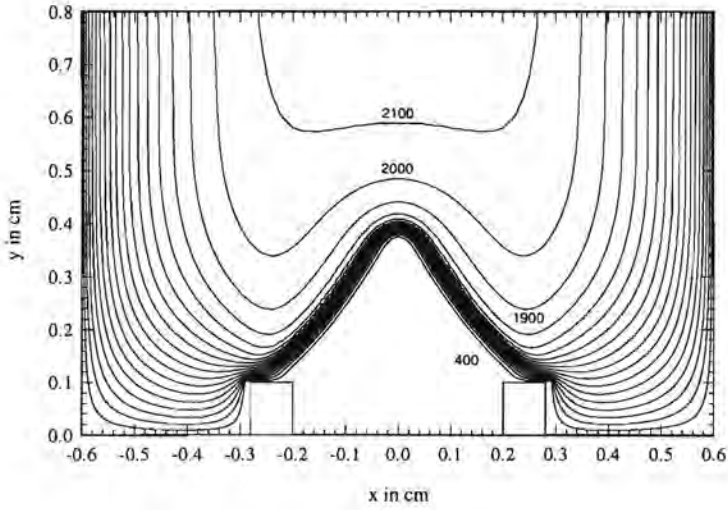


Figure 4.19: *Temperature contour lines.*

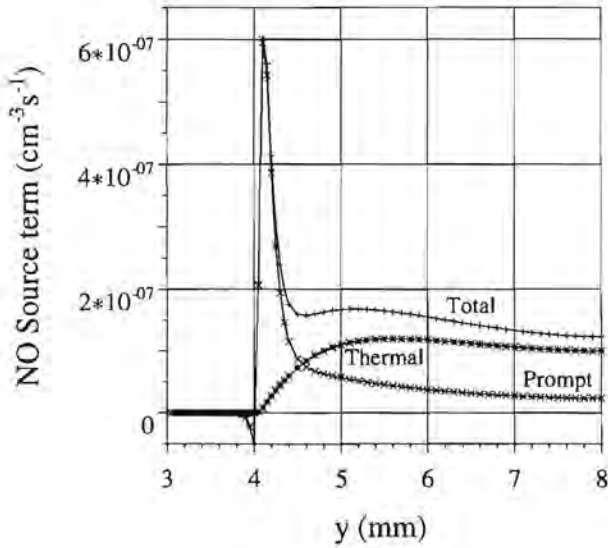


Figure 4.20: *Source terms of thermal, prompt and total NO formation on the center line of the single slit burner.*

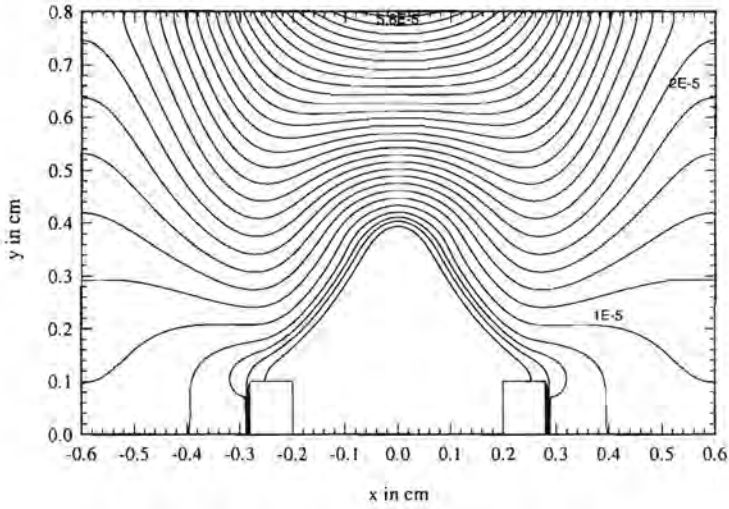


Figure 4.21: Contour-lines of total NO mole fraction.

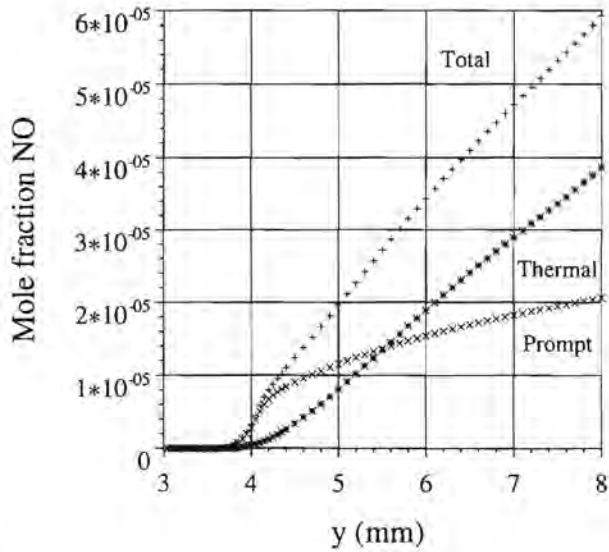


Figure 4.22: Thermal, prompt and total NO mole fractions on the center line of the single slit burner.

%). Considering the results of the one- and two-dimensional computations and measurements, we may conclude that the prompt *NO* mechanisms may have a significant contribution to the total *NO* formation. The ratio of thermal and prompt *NO*, however, depends strongly on the temperature of the flame and the position above the burner. Most of the *NO* in the adiabatic flames is formed by the thermal *NO* mechanism. The flames which are stabilized on burners, show a significant contribution of the prompt mechanism.

4.6 Empirical Model for Prompt NO Formation.

Since the application of complex reaction mechanisms to model realistic flame configurations is quite complicated, much attention has been given to developing simplified models for prompt *NO* formation. An empirical expression has been presented by Soete et al. [Soe74] first, which has been modified by Williams et al. [Wil92] for natural gas:

$$w_{NO}^{emp} = A \left(\frac{RT}{P} \right)^{\alpha+1} f [O_2]^\alpha [N_2] [CH_4]^\beta \exp(-E_a/RT). \quad (4.31)$$

The activation energy E_a has a value of 178 kJ/mol for temperatures below 1920 K and a value of 303 kJ/mol for higher temperatures. The factor f is a function of the equivalence ratio Φ as given by Dupont (1993):

$$f = 4.75 + C_1 n_c - C_2 \Phi + C_3 \Phi^2 - C_4 \Phi^3, \quad (4.32)$$

where n_c denotes the number of carbon atoms in the fuel and C_1, \dots, C_4 are known constants. In principle, the reaction orders α and β may depend on the position in the flame and vary between 0 and 1. Here, however, constant values $\alpha = 0.5$ and $\beta = 1$ are used. The two-dimensional computations are used to compare this empirical approximation with detailed results. The prompt *NO* source term as given by eq. (4.31) is presented in Figure 4.18. It can be observed that the prompt source term of the empirical model reaches its maximum in the flame front almost at the same position as the detailed prompt source term. The maximum value, however, is much higher. This can be seen more clearly in Figure 4.24. Furthermore, it can be seen that the prompt *NO* source term is negative, ahead of the flame front. A negative prompt source term cannot be predicted by the empirical model. Behind the flame front, the empirical source term is negligible, whereas the detailed computation shows that more reactions than just the Zeldovich reactions are important there. This is caused by the fact that the empirical model for prompt *NO* is linear with the CH_4 concentration which is almost zero after the flame front. Contour lines of prompt *NO* for the detailed computations and the empirical model are presented in Figures 4.25 and 4.26. These prompt *NO* mole-fractions are obtained by subtracting the thermal *NO* mole-fraction from the total *NO* mole-fractions. Considering these figures it can be concluded that the empirical model does not predict the prompt *NO* formation appropriately. The value of the formed prompt *NO* is approximated within a factor of 2.

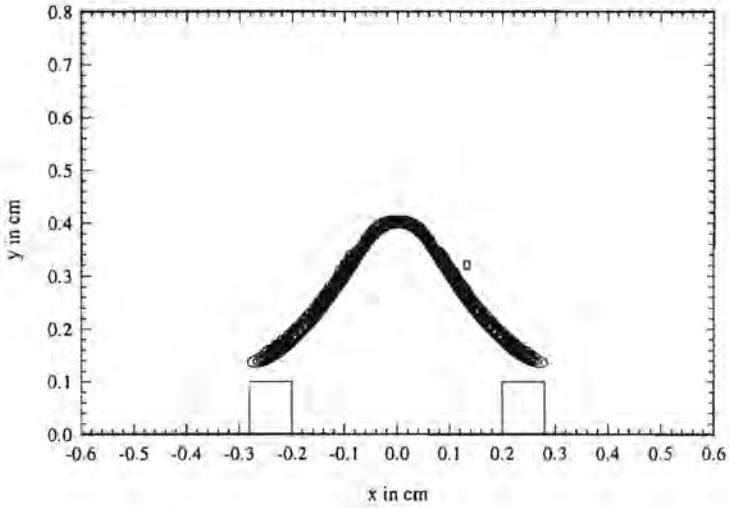


Figure 4.23: Empirical Prompt NO source term, given in $\text{cm}^{-3}\text{s}^{-1}$.

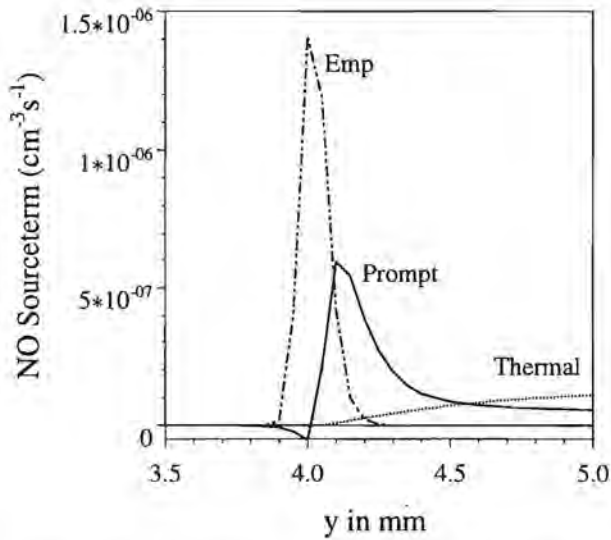


Figure 4.24: Thermal, prompt and empirical prompt NO source terms on the center line of the slit burner.

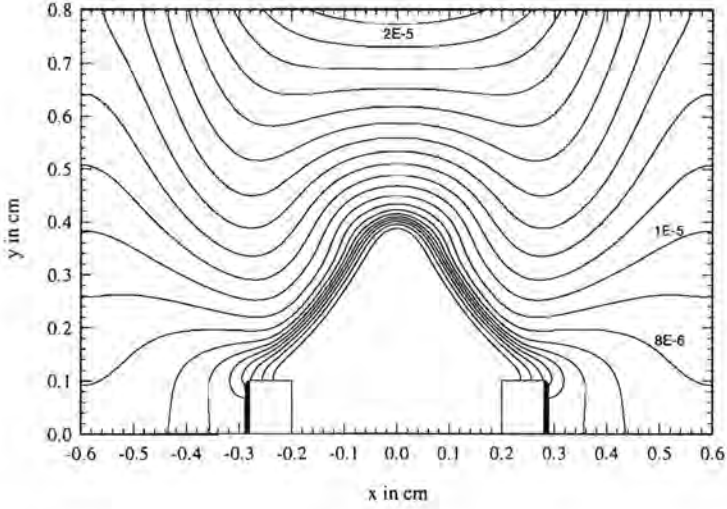


Figure 4.25: Contour-lines of prompt NO mole fraction according to the detailed reaction mechanism.

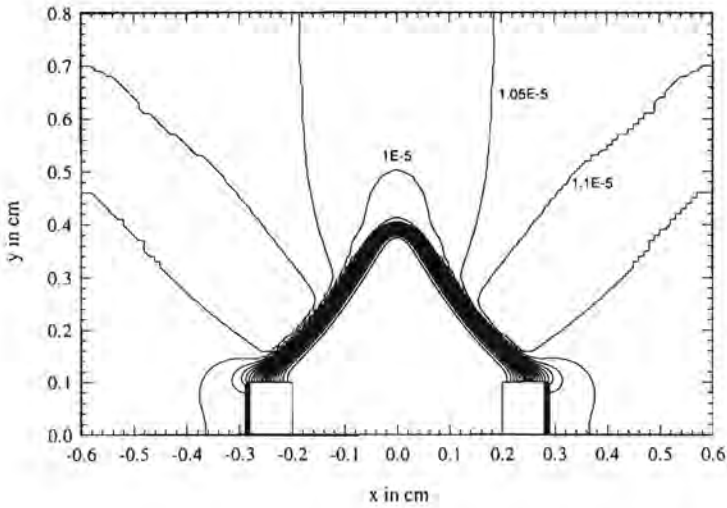


Figure 4.26: Contour-lines of prompt NO mole fraction using the empirical model.

Appendix A

Example Mathematical Reduction Technique

In this Appendix an example of the Mathematical Reduction Technique applied to a simple reaction system is presented. This example serves to better understanding the general procedure for simplifying chemical kinetics. The system considered is described first. Then the eigenvalues and eigenvectors of the system are obtained. These are used to solve the differential equations describing the system. From the solution the typical qualities of the system are derived. The system is reduced in a convenient way, but also the Mathematically Reduction Technique, as presented in chapter 2, is applied.

Reaction System

We consider a reaction system consisting of only three different components O , O^* and O^{**} . The mass fractions of these components are given by Y_1 , Y_2 en Y_3 . Further, we suppose that only the following three reactions are possible:



with reaction rates: w_1 , w_2 en w_3 (dimension $1/s$). The elementary reaction rates are given by:

$$\begin{aligned} w_1 &= Y_1 k_1, \\ w_2 &= Y_2 k_2, \\ w_3 &= Y_3 k_3, \end{aligned} \tag{A.2}$$

where k_i is the specific reaction rate coefficient of reaction i .

Homogeneous System at Constant Temperature

We make further simplifications by considering a homogeneous reactor at constant temperature. This implies that there are no spatial variations and that the reaction coefficients k_1 , k_2 and k_3

(which generally depend on the temperature) are constant. Therefore, we may write:

$$\begin{aligned} dY_1/dt &= -Y_1k_1, \\ dY_2/dt &= Y_1k_1 - Y_2k_2 + Y_3k_3, \\ dY_3/dt &= Y_2k_2 - Y_3k_3. \end{aligned} \quad (\text{A.3})$$

We write this set of equations in vector notation:

$$\frac{d}{dt} \begin{pmatrix} Y_1 \\ Y_2 \\ Y_3 \end{pmatrix} = \begin{pmatrix} -k_1 & 0 & 0 \\ k_1 & -k_2 & k_3 \\ 0 & k_2 & -k_3 \end{pmatrix} \begin{pmatrix} Y_1 \\ Y_2 \\ Y_3 \end{pmatrix}. \quad (\text{A.4})$$

This may also be written as:

$$\frac{d\mathbf{Y}}{dt} = \mathbf{A}\mathbf{Y}, \quad (\text{A.5})$$

with $\mathbf{Y} = (y_1, y_2, y_3)^T$ and

$$\mathbf{A} = \begin{pmatrix} -k_1 & 0 & 0 \\ k_1 & -k_2 & k_3 \\ 0 & k_2 & -k_3 \end{pmatrix}. \quad (\text{A.6})$$

We have chosen for a simple reaction system giving a linear set of equations. This enables us to solve this set analytically. There are many ways to solve these equations. This example serves to demonstrate the general procedure that will be applied to reduce chemical reaction schemes mathematically (determining Intrinsic Low-Dimensional Manifolds). Therefore, we apply the same procedure as used in chapter 2. This procedure consists of the following steps:

- Deduce eigenvalues and eigenvectors of the matrix \mathbf{A} and define a coordinate system in line of the basis of eigenvectors.
- Solve the set of equations in this basis.
- Transform the solution back to the original basis.

This procedure will be followed in the following sections.

Eigenvalues and Eigenvectors

The eigenvalues of the matrix are found from:

$$\text{Det}(\mathbf{A} - \lambda\mathbf{I}) = 0, \quad (\text{A.7})$$

with \mathbf{I} the identity matrix ($I_{ij} = \delta_{ij}$). Substitution of matrix \mathbf{A} , as defined in (A.6), gives:

$$\text{Det} \begin{pmatrix} -k_1 - \lambda & 0 & 0 \\ k_1 & -k_2 - \lambda & k_3 \\ 0 & k_2 & -k_3 - \lambda \end{pmatrix} = 0. \quad (\text{A.8})$$

So the characteristic equation is given by:

$$(k_1 + \lambda) (-k_2 - \lambda) (-k_3 - \lambda) - k_2 k_3 = \lambda(k_1 + \lambda)(k_2 + k_3 + \lambda) = 0. \quad (\text{A.9})$$

The eigenvalues of the system are clearly:

- $\lambda_1 = 0$
- $\lambda_2 = -k_1$
- $\lambda_3 = -(k_2 + k_3)$

The corresponding right eigenvectors are:

$$s_1 = \begin{pmatrix} 0 \\ k_3 \\ k_2 \end{pmatrix}, s_2 = \begin{pmatrix} k_1 - k_2 - k_3 \\ k_3 - k_1 \\ k_2 \end{pmatrix}, s_3 = \begin{pmatrix} 0 \\ -1 \\ 1 \end{pmatrix}. \quad (\text{A.10})$$

This gives us:

$$AS = SA, \quad (\text{A.11})$$

with Λ a diagonal matrix, given by:

$$\Lambda = \begin{pmatrix} 0 & 0 & 0 \\ 0 & -k_1 & 0 \\ 0 & 0 & -(k_2 + k_3) \end{pmatrix}. \quad (\text{A.12})$$

and

$$S = \begin{pmatrix} 0 & (k_1 - k_2 - k_3) & 0 \\ k_3 & (k_3 - k_1) & -1 \\ k_2 & k_2 & 1 \end{pmatrix}. \quad (\text{A.13})$$

Basis of Eigenvectors

Now, we transform the set of equations to the basis of eigenvectors. The transformation matrix S is defined by:

$$Y = S\hat{Y}, \quad (\text{A.14})$$

where $(\hat{Y}_1, \dots, \hat{Y}_3)$ denote the coordinates in the basis of eigenvectors. The differential equations (A.5) may be written in the new basis as:

$$S \frac{d\hat{Y}}{dt} = AS\hat{Y}, \quad (\text{A.15})$$

which gives us:

$$\frac{d\hat{Y}}{dt} = S^{-1}AS\hat{Y} = \Lambda\hat{Y}. \quad (\text{A.16})$$

The differential equations in this basis are:

$$\begin{aligned} d\hat{Y}_1/dt &= 0, \\ d\hat{Y}_2/dt &= -k_1\hat{Y}_2, \\ d\hat{Y}_3/dt &= -(k_2 + k_3)\hat{Y}_3. \end{aligned} \quad (\text{A.17})$$

The solution of this set of equations is simple because they are decoupled:

$$\hat{Y} = \begin{pmatrix} c_0 \\ c_1 e^{-k_1 t} \\ c_2 e^{-(k_2+k_3)t} \end{pmatrix} \quad (\text{A.18})$$

Transformation to the original basis gives (with A.14):

$$\begin{aligned} Y_1 &= c_1(k_1 - k_2 - k_3)e^{-k_1 t} \\ Y_2 &= c_0 k_3 + c_1(k_3 - k_1)e^{-k_1 t} - c_2 e^{-(k_2+k_3)t} \\ Y_3 &= c_0 k_2 + c_1 k_2 e^{-k_1 t} + c_2 e^{-(k_2+k_3)t}. \end{aligned} \quad (\text{A.19})$$

The coefficients c_0 , c_1 and c_2 can be obtained from the initial ($t = 0$) composition. As initial condition we choose the situation that only species O is present:

$$\begin{aligned} Y_1(t=0) &= 1, \\ Y_2(t=0) &= 0, \\ Y_3(t=0) &= 0. \end{aligned} \quad (\text{A.20})$$

This gives us:

$$\begin{aligned} c_0 &= \frac{1}{k_2+k_3} \\ c_1 &= \frac{1}{k_1-k_2-k_3} \\ c_2 &= \frac{k_3}{k_2+k_3} + \frac{k_3-k_1}{k_1-k_2-k_3} \end{aligned} \quad (\text{A.21})$$

This gives the equilibrium composition (at $t \rightarrow \infty$): $Y_1 = 0$, $Y_2 = \frac{k_3}{k_2+k_3}$ and $Y_3 = \frac{k_2}{k_2+k_3}$.

Conclusions

Considering the solution of this example we may conclude the following:

- The solution contains two time scales, namely $1/k_1$ and $1/(k_2 + k_3)$. Note that these time scales correspond to the reciprocal values of the (non -zero) eigenvalues.
- One of the eigenvalues is equal to zero; this implies that there is a conserved quantity ($s_1 e^0$, see (A.18)).

Reduction

Let us see what happens if one time scale is very small. Suppose that $(k_2 + k_3) \gg k_1$. Then, we may neglect $e^{-(k_2+k_3)t}$ for time t satisfying $|1/\lambda_3| \ll t \ll |1/\lambda_1|$. Within this approximation we may write:

$$\begin{aligned} Y_1 &= c_1(k_1 - k_2 - k_3)e^{-k_1 t} \\ Y_2 &= c_0 k_3 + c_1(k_3 - k_1)e^{-k_1 t} \\ Y_3 &= c_0 k_2 + c_1 k_2 e^{-k_1 t}. \end{aligned} \quad (\text{A.22})$$

Now, Y_2 en Y_3 may be written as function of Y_1 :

$$\begin{aligned} Y_2 &= \frac{k_3}{k_2+k_3} + \frac{k_3-k_1}{k_1-k_2-k_3} Y_1, \\ Y_3 &= \frac{k_2}{k_2+k_3} + \frac{k_2}{k_1-k_2-k_3} Y_1. \end{aligned} \quad (\text{A.23})$$

To reduce the reaction scheme we only made the assumption that $(k_2 + k_3) \gg k_1$. This assumption has a physical background since that time-scales in a reaction system may differ several orders of magnitude. Therefore, the fastest reactions will be in steady-state in a real system. To illustrate how good the approximation is we chose some values for the reaction coefficients. The solution (A.19) as well as the reduced trajectories (A.22) are shown in Figure A.1. In order

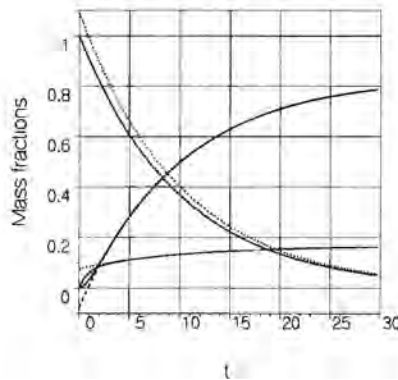


Figure A.1: *Example of Mathematical Reduction Technique. Lines: full scheme; dashed lines: reduced scheme. Values of reaction coefficients used are: $k_1 = 0.1$, $k_2 = 1.0$ and $k_3 = 0.2$.*

to show differences between exact and approximated solutions we have chosen values for the

reaction coefficients that satisfy $(k_2 + k_3) = 12k_1$. As we may expect, differences can be seen between the exact and approximated solution. However, for $t > \frac{1}{k_2 + k_3}$ the approximation is still good.

Mathematical Reduction Technique

In the previous section we obtained a reduction of the system by considering the analytical solution of the full system. For systems containing many species, however, analytical solutions do not always exist because these systems are mostly non-linear. Here, we will apply the Mathematical Reduction Technique as presented in chapter 2. Therefore we need the inverse matrix, which is given by:

$$\mathbf{S}^{-1} = \frac{1}{k_2 + k_3} \begin{pmatrix} 1 & 1 & 1 \\ \frac{k_2 + k_3}{k_1 - k_2 - k_3} & 0 & 0 \\ \frac{-k_1 k_2}{k_1 - k_2 - k_3} & -k_2 & k_3 \end{pmatrix} \quad (\text{A.24})$$

This matrix also may be written as:

$$\mathbf{S}^{-1} = \begin{pmatrix} \cdots & (s_1^L)^T & \cdots \\ \vdots & \vdots & \vdots \\ \cdots & (s_n^L)^T & \cdots \end{pmatrix}, \quad (\text{A.25})$$

where $(s_i^L)^T$ are the so-called left eigenvectors. Substitution of $\tilde{\mathbf{Y}} = \mathbf{S}^{-1} \mathbf{Y}$ in eq. (A.16) gives:

$$\frac{d}{dt} (\mathbf{S}^{-1} \mathbf{Y}) = \Lambda (\mathbf{S}^{-1} \mathbf{Y}) \quad (\text{A.26})$$

With use of (A.24) we may write:

$$\begin{aligned} \frac{dY_1}{dt} + \frac{dY_2}{dt} + \frac{dY_3}{dt} &= \lambda_1 (Y_1 + Y_2 + Y_3) = 0 \\ \frac{dY_1}{dt} &= \lambda_2 Y_1 \\ \frac{-k_1 k_2}{(k_1 - k_2 - k_3)} \frac{dY_1}{dt} - k_2 \frac{dY_2}{dt} + k_3 \frac{dY_3}{dt} &= \\ \lambda_3 \left(\frac{-k_1 k_2}{(k_1 - k_2 - k_3)} Y_1 - k_2 Y_2 + k_3 Y_3 \right) & \end{aligned} \quad (\text{A.27})$$

As $\lambda_1 = 0$, the first equation becomes:

$$\left(\begin{pmatrix} 1 \\ 1 \\ 1 \end{pmatrix}, \frac{d\mathbf{Y}}{dt} \right) = 0. \quad (\text{A.28})$$

This implies that $Y_1 + Y_2 + Y_3$ is constant. Since Y_i denotes a mass fraction, equation (A.28) states that the sum of the mass fractions is conserved, which agrees with $\sum_{i=1}^n Y_i = 1$ also following from the definition of the mass fractions. We already have seen that a zero valued eigenvalue corresponds to a conserved property. Now, we see that the conserved property is the conservation of the element O . The latter eq. of (A.27) gives us:

$$\frac{-k_1 k_2}{(k_1 - k_2 - k_3)} \frac{dY_1}{dt} - k_2 \frac{dY_2}{dt} + k_3 \frac{dY_3}{dt} = c_3 e^{\lambda_3 t}. \quad (\text{A.29})$$

For $t \gg 1/\lambda_3$ eq. (A.29) turns into:

$$\frac{-k_1 k_2}{(k_1 - k_2 - k_3)} \frac{dY_1}{dt} - k_2 \frac{dY_2}{dt} + k_3 \frac{dY_3}{dt} = 0. \quad (\text{A.30})$$

This algebraic equation for Y_1 , Y_2 and Y_3 agrees with eq. (A.23). Note that equation (A.30) follows from $(s_3^t, \mathbf{F}) = 0$. This is the definition of a steady-state relation for a fast reaction group if the mathematical reduction method is applied.

Principle of Reduction

The reduction strategy can also be applied to more general systems. The following steps are considered:

- Calculation of eigenvalues and eigenvectors.
- Reordering of reaction groups from large to small time scales.
- Introduction of steady-state relations for fast reaction groups. These are given by $(s_i^t, \mathbf{F}) = 0$ for i in $(n_c + n_e + 1, \dots, n)$. (n_e denotes the numbers of elements, n_c the dimension of the reduced scheme and n the number of species). Then calculate the mixture compositions from these equations as function of the (n_c) control variables (As control variable the mass fraction of one of the species may be used).

Appendix B

Reaction schemes

In this section the reaction mechanisms used for the applications of chapter 3 are presented. In chapter 1 it is explained how the reaction rate of a general reaction given by eq. (1.31) can be computed (with eq. (1.27)) if the reaction constants A_i , b_i and the specific activation energy E_i are known.

Sometimes, however, an additional species, which does not react ($\nu_{ij} = 0$), is involved in the reaction. This species is important for the reaction to proceed. Without it, it is impossible to obey momentum and energy conservation. As this species does not react itself it can be an inert species or any other species. The additional species will be denoted as M . An example of such a reaction is:



For this reaction, the reaction rate is proportional to $[M]$, which is given by:

$$[M] = \sum_{i=1}^n f_i X_i p / RT, \quad (\text{B.2})$$

where f_i are the so-called collision efficiencies, indicating the relative importance of species i in reaction (B.1). These are often equal to one, but may also have other values. In general they are specific for every reaction and species. Note that $[M] = n$ if $f_i = 1$, for $i = 1, \dots, n$.

Hydrogen Reaction Schemes

The reaction rates of reaction i are given by the Arrhenius expression (eq. (1.27)):

$A_i T^{\beta_i} \exp(-E_i/RT)$, where A_i and β_i are reaction constants, E_i the activation energy, R the universal gas constant and T the temperature. The coefficients A_i , β_i and E_i are successively given after the reactions in the following tables (A_i in $\text{cm}^3/\text{mol}\cdot\text{s}$; E_i in KJ/mol). Used collision efficiencies are: $f_{H_2} = 1.00$, $f_{O_2} = 0.35$, $f_{H_2O} = 6.50$, $f_{N_2} = 0.50$, $f_{CO} = 1.50$, $f_{CO_2} = 1.50$.

System I

This reaction scheme includes the following species:

O_2 , H , OH , O , H_2 , H_2O and N_2 .

The following reactions are used:

$H + O_2 \rightarrow OH + O$	$2.00 \cdot 10^{14}$	0.0	70.3
$OH + O \rightarrow H + O_2$	$1.46 \cdot 10^{13}$	0.0	2.08
$O + H_2 \rightarrow OH + H$	$5.06 \cdot 10^4$	2.67	26.3
$OH + H \rightarrow O + H_2$	$2.24 \cdot 10^4$	2.67	18.4
$H_2 + OH \rightarrow H_2O + H$	$1.00 \cdot 10^8$	1.6	13.8
$H_2O + H \rightarrow H_2 + OH$	$4.45 \cdot 10^8$	1.6	77.13
$OH + OH \rightarrow O + H_2O$	$1.50 \cdot 10^9$	1.14	0.42
$O + H_2O \rightarrow OH + OH$	$1.51 \cdot 10^{10}$	1.14	71.64
$H + H + M \rightarrow H_2 + M$	$1.80 \cdot 10^{18}$	-1.00	0.0
$H_2 + M \rightarrow H + H + M$	$6.99 \cdot 10^{18}$	-1.00	436.08
$OH + H + M \rightarrow H_2O + M$	$2.20 \cdot 10^{22}$	-2.00	0.0
$H_2O + M \rightarrow OH + H + M$	$3.80 \cdot 10^{23}$	-2.00	499.41
$O + O + M \rightarrow O_2 + M$	$2.90 \cdot 10^{17}$	-1.00	0.0
$O_2 + M \rightarrow O + O + M$	$6.81 \cdot 10^{18}$	-1.00	496.41

System II

Reactions and species of system I, extended with species HO_2 and the following reactions:

$H + O_2 + M \rightarrow HO_2 + M$	$2.30 \cdot 10^{18}$	-0.80	0.0
$HO_2 + M \rightarrow H + O_2 + M$	$2.26 \cdot 10^{18}$	-0.80	195.88
$HO_2 + H \rightarrow OH + OH$	$1.50 \cdot 10^{14}$	0.00	4.2
$OH + OH \rightarrow HO_2 + H$	$1.33 \cdot 10^{13}$	0.00	168.3
$HO_2 + H \rightarrow H_2 + O_2$	$2.50 \cdot 10^{13}$	0.00	2.9
$H_2 + O_2 \rightarrow HO_2 + H$	$6.84 \cdot 10^{13}$	0.00	243.10
$HO_2 + H \rightarrow H_2O + O$	$3.00 \cdot 10^{13}$	0.00	7.2
$H_2O + O \rightarrow HO_2 + H$	$2.67 \cdot 10^{13}$	0.00	242.52
$HO_2 + O \rightarrow OH + O_2$	$1.80 \cdot 10^{13}$	0.00	-1.7
$OH + O_2 \rightarrow HO_2 + O$	$2.18 \cdot 10^{13}$	0.00	230.61
$HO_2 + OH \rightarrow H_2O + O_2$	$6.00 \cdot 10^{13}$	0.00	0.0
$H_2O + O_2 \rightarrow HO_2 + OH$	$7.31 \cdot 10^{14}$	0.00	303.53

System III

This reaction mechanism consist of the species and reactions of system II, extended with species H_2O_2 and the following reactions:

$HO_2 + HO_2 \rightarrow H_2O_2 + O_2$	$2.50 \cdot 10^{11}$	0.00	-5.20
$OH + OH + M \rightarrow H_2O_2 + M$	$3.25 \cdot 10^{22}$	-2.00	0.00
$H_2O_2 + M \rightarrow OH + OH + M$	$2.10 \cdot 10^{24}$	-2.00	206.80
$H_2O_2 + H \rightarrow H_2 + HO_2$	$1.70 \cdot 10^{12}$	0.00	15.70
$H_2 + HO_2 \rightarrow H_2O_2 + H$	$1.15 \cdot 10^{12}$	0.00	80.88
$H_2O_2 + H \rightarrow H_2O + OH$	$1.00 \cdot 10^{13}$	0.00	15.00
$H_2O + OH \rightarrow H_2O_2 + H$	$2.67 \cdot 10^{12}$	0.00	307.51
$H_2O_2 + O \rightarrow OH + HO_2$	$2.80 \cdot 10^{13}$	0.00	26.80
$OH + HO_2 \rightarrow H_2O_2 + O$	$8.40 \cdot 10^{12}$	0.00	84.09
$H_2O_2 + OH \rightarrow H_2O + HO_2$	$5.40 \cdot 10^{12}$	0.00	4.2
$H_2O + HO_2 \rightarrow H_2O_2 + OH$	$1.63 \cdot 10^{13}$	0.00	132.71

System IV

This reaction scheme includes the following species:

O_2 , H , OH , O , H_2 , H_2O , HO_2 , H_2O_2 and N_2

The following reactions are used:

(1) $H + O_2 = OH + O$	$2.000 \cdot 10^{14}$	0.0	70.3
(2) $H_2 + O = OH + H$	$5.060 \cdot 10^4$	2.67	26.3
(3) $H_2 + OH = H_2O + H$	$1.000 \cdot 10^8$	1.60	13.8
(4) $OH + OH = H_2O + O$	$1.500 \cdot 10^9$	1.14	0.42
(5) $H + H + M = H_2 + M$	$1.800 \cdot 10^{18}$	-1.00	0.0
(6) $H + OH + M = H_2O + M$	$2.200 \cdot 10^{22}$	-2.00	0.0
(7) $H + O + M = OH + M$	$6.200 \cdot 10^{16}$	-0.60	0.0
(8) $H + O_2 + M = HO_2$	$2.30 \cdot 10^{18}$	-0.80	0.0
(9) $HO_2 + H = OH + OH$	$1.50 \cdot 10^{14}$	0.00	4.2
(10) $HO_2 + H = H_2 + O_2$	$2.50 \cdot 10^{13}$	0.00	2.9
(11) $HO_2 + H = H_2O + O$	$3.00 \cdot 10^{13}$	0.00	7.2
(12) $HO_2 + O = OH + O_2$	$1.80 \cdot 10^{13}$	0.00	-1.7
(13) $HO_2 + OH = H_2O + O_2$	$6.00 \cdot 10^{13}$	0.00	0.0
(14) $HO_2 + HO_2 = H_2O_2 + O_2$	$2.50 \cdot 10^{11}$	0.00	-5.2
(15) $OH + OH + M = H_2O_2 + M$	$3.25 \cdot 10^{22}$	-2.00	0.0
(16) $H_2O_2 + H = H_2 + HO_2$	$1.70 \cdot 10^{12}$	0.00	15.7
(17) $H_2O_2 + H = H_2O + OH$	$1.00 \cdot 10^{13}$	0.00	15.0
(18) $H_2O_2 + O = OH + HO_2$	$2.80 \cdot 10^{13}$	0.00	26.8
(19) $H_2O_2 + OH = H_2O + HO_2$	$5.4 \cdot 10^{12}$	0.00	4.2

System V

Reactions and species of system III, extended with species CO , CO_2 and the following reactions.

(20) $CO + OH = CO_2 + H$	$6.0 \cdot 10^6$	1.50	-3.1
(21) $CO + O + M = CO_2 + M$	$7.1 \cdot 10^{13}$	0.00	-19.0

Summary

The use of detailed reaction mechanisms for modelling combustion processes leads to excessive computational effort. Therefore, much attention has been given on developing reduced chemical models recently. The reduced mechanisms can be applied to laminar as well as turbulent flames. Several methods to reduce a reaction mechanism are presented in chapter 1 of this thesis. The Conventional Reduction Methods (CRM) are based on partial-equilibrium assumptions for elementary reactions and steady-state assumptions for intermediate species. A more recently developed Mathematical Reduction Technique, which determines Intrinsic Low dimensional Manifolds (ILDM) in composition space, is treated in detail in chapter 2. This Mathematical Reduction Method (MRT) applies steady-state assumptions to the fastest reaction groups of the chemical source term, so that the chemistry can be described by a reduced number of variables. The fastest reaction groups are found from an eigenvalues analysis of the Jacobian matrix of the chemical source term. In this work the reduction method is applied to hydrogen/air, $CO-H_2$ /air and methane/air reaction systems. Furthermore, one- and two-step reduced schemes are applied to stationary premixed flat flames and results are compared with detailed calculations. The results indicate that a hydrogen/air reaction mechanism without HO_2 and H_2O_2 can be reduced to an accurate one-step reduced mechanism. A two-step reduced mechanism is accurate for the hydrogen/air reaction mechanisms including HO_2 and H_2O_2 species. For the hydrogen/air and $CO-H_2$ /air reaction mechanisms Conventional Reduction Methods are compared with the Mathematical Reduction Technique. The results indicate that the Conventional Reduction Methods perform quite well at high temperature. The Conventional Reduction Methods are less accurate for lower temperatures and the accuracy strongly depends on the choice of species and reactions which are assumed to be in steady-state or in partial equilibrium. A two-step reduced methane/air reaction mechanism describes the flame structure for a flat flame quite well. The adiabatic burning velocity and some radical profiles, however, are not predicted accurately.

Furthermore, a post-processing method is developed to model NO formation in one- and two-dimensional laminar premixed methane/air flames (chapter 4). The detailed reaction mechanism, which includes nitrogen chemistry, is split into two parts. One part, which consists of the major combustion species, is solved first. In a post-processing step the second group of species, involved in the nitrogen chemistry, is computed. To reduce the system even more, steady-state assumptions are introduced for most of the intermediate species in the post-processing step. The results agree well with complex computations, and the computational effort is reduced considerably. Complex computations using detailed reaction mechanisms are used to investigate which reactions are most important for the production of NO . Furthermore, computations of NO in burner-stabilized flames are compared with measurements on a ceramic foam surface burner

and the agreement is satisfactory.

The post-processing method is also applied to two-dimensional flames. We consider a micro-slit burner and a single-slit burner. The flames on the first burner are nearly flat, which makes it possible to compare the results with one-dimensional computations. The results of the single-slit burner are used for example to investigate the accuracy of an empirical model for prompt *NO* formation. It has been found that this empirical model does not predict the prompt *NO* formation accurately.

Samenvatting

Het gebruik van gedetailleerde reactiemechanismen voor de modellering van verbrandingsprocessen vergt lange rekentijden. Daarom wordt er veel onderzoek verricht aan de ontwikkeling van gereduceerde reactiemodellen. De gereduceerde mechanismen kunnen voor de modellering van zowel laminaire als turbulente vlammen gebruikt worden. In hoofdstuk 1 worden verschillende methoden om een reactiemechanisme te vereenvoudigen gepresenteerd. Conventionele Reductie Methodes (CRM) zijn gebaseerd op partiële-evenwichtaannamen voor reacties en stationaire-toestandaannamen voor chemische componenten. De onlangs ontwikkelde Mathematische Reductie Techniek, welke Intrinsiek Laag-Dimensionale Manifolds (ILDM) in compositie ruimte bepaalt, wordt in hoofdstuk 2 uitvoerig behandeld. Deze Mathematische Reductie Techniek (MRT) veronderstelt dat de snelste reactiegroepen van de chemische bron term in stationaire toestand zijn; de chemie kan vervolgens beschreven worden met een gereduceerd aantal variabelen. De snelste reactiegroepen worden bepaald met behulp van een eigenwaarden analyse van de Jacobi matrix van de chemische bronterm. De reductie methode is toegepast op reactiemechanismen voor waterstof/lucht, $CO-H_2$ /lucht en methaan/lucht. Één- en twee-staps gereduceerde reactiemodellen zijn toegepast voor vlakke vlammen en de resultaten zijn vergeleken met gedetailleerde berekeningen. De resultaten geven aan dat een één-staps gereduceerd waterstof/lucht reactiemechanisme zonder HO_2 en H_2O_2 voldoende nauwkeurig is. Een twee-staps gereduceerd mechanisme is nauwkeurig voor waterstof/lucht reactiemechanismen die wel HO_2 en H_2O_2 bevatten. Voor waterstof/lucht en $CO-H_2$ /lucht reactiemechanismen zijn de resultaten van Conventionele Reductie Technieken vergeleken met de resultaten van de Mathematische Reductie Techniek. De resultaten geven aan dat de Conventionele Reductie Methodes nauwkeurig zijn voor hoge temperaturen, maar minder nauwkeurig voor lage temperaturen. Verder hangt de nauwkeurigheid sterk af van welke reacties en welke stoffen in partiële evenwicht of in stationaire toestand verondersteld zijn. Een twee-staps gereduceerd mechanisme voor methaan beschrijft de vlamstructuur redelijk goed. De adiabatische vlam snelheid en de profielen van enkele radicalen worden echter niet nauwkeurig door het gereduceerde schema beschreven.

Verder is een post-processor methode ontwikkeld voor de modellering van NO vorming in één- en twee- dimensionale voorgemengde methaan/lucht vlammen (hoofdstuk 4). De gedetailleerde reactiemechanismen die de complete stikstof chemie bevatten, worden opgesplitst in twee stukken. Een gedeelte dat bestaat uit de meest belangrijke stoffen in het verbrandingsproces wordt eerst berekend. In een post-processor stap worden de stoffen uit de tweede groep, die betrokken zijn in de stikstof chemie, berekend. Het systeem is verder vereenvoudigd door radicalen in stationaire toestand te veronderstellen. De resultaten komen goed overeen met gede-

tailleerde berekeningen en de reketijden zijn aanzienlijk korter. Resultaten van gedetailleerde berekeningen zijn gebruikt om te onderzoeken welke reacties het meest belangrijk zijn voor de vorming van NO . Berekeningen van brander gestabiliseerde vlammen zijn vergeleken met metingen aan een keramische oppervlakte brander en de resultaten komen goed overeen.

De post-processor methode is ook toegepast voor de modellering van NO -vorming in tweedimensionale vlammen. Vlammen op een micro-spletenbrander en een enkele-spleetbrander zijn gemodelleerd. De vlammen van op de micro-spleetbrander zijn bijna vlak en kunnen vergeleken worden met resultaten van één-dimensionale berekeningen. De resultaten van de berekeningen aan de enkele spleetbrander zijn gebruikt om te onderzoeken hoe nauwkeurig een empirisch model voor de vorming van prompt NO is. Het is gebleken dat het empirisch model voor prompt NO vorming niet erg nauwkeurig is.

References

- [Bat57] Batchelor, G.K., *Homogeneous Turbulence*. Cambridge University Press **1957**.
- [Bow92] Bowman, C. T., Control of Combustion- Generated Nitrogen Oxide Emissions Technology Driven by Regulations, *Twenty-fourth Symposium (International) on Combustion, The Combustion Institute*, **1992**, p. 859.
- [Bou93] Bouma, P.H., Goey de, L.P.H., Nieuwenhuizen, J.K. and Drift van der, A., Modelling of Twofold Flame Behaviour of Ceramic Foam Radiant Gasburners, *Proc. Second International Conference on Combustion for a Clear Environment, Lisbon*, **1993**, p. 36.3. (also in Combustion, Energy and the Environment, *Mc Graw-Hill Series*)
- [Bou95a] Bouma, P.H., Eggels, R.L.G.M., Goey de, L.P.H., Nieuwenhuizen, J.K. and Drift van der, A., A Numerical and Experimental Study of the NO-Emission of Ceramic Foam Surface Burners., *Combust. Sci. and Tech*, *108*, 1-3, p. 175. **1995**
- [Bou95b] Bouma, P.H., Eggels R.L.G.M. and Goey de, L.P.H., NO Emission of Ceramic Foam Surface Gas Burners in Radiation Mode, *Proc. Third International Conference on Combustion for a Clear Environment, Lisbon*, **1995**, p. 8.1.
- [Cor85] Correa, S.M., A model for non-premixed turbulent combustion of CO_2/H_2 jets. *Archivum Combustionis* **5**, 223, (**1985**).
- [Cor90] Correa, S.M. and Smooke, M.D., NO_x in Parametrically Varied Methane Flames, *Twenty-Third Symposium (International) on Combustion, The Combustion Institute*, **1990**, p. 289.
- [Dix68] Dixon-Lewis, G., Flame structure and Flame Reaction Kinetics (II). Transport phenomena in multicomponent systems, em Proc. Roy. Soc. A. **307**, p. 111, **1968**.
- [Dix75] Dixon-Lewis, G., Goldsworthy, F.A., Greenberg, J.B., Flame Structure and Flame Reaction Kinetics (IX), Calculation of Properties of Multi-Radical Premixed Flames, *Proc. Roy. Soc. Lond. A.* **346**, p. 261-278, (**1975**).
- [Dup93] Dupont V., Pourkashanian M. and Williams A., Modelling of Process Heaters Fired by Natural Gas. *Journal of the Institute of Energy, March*, **1993**, 66, p. 20.
- [Egg93] Eggels, R.L.G.M., Somers, L.M.T., Goey de, L.P.H. and Nieuwenhuizen, J.K., NO-

- Post Calculations for Flat Laminar CH_4 /air Flames, *Proc. Second International Conference on Combustion for a Clear Environment, Lisbon, 1993*, p. 12.2.
- [Egg94] Eggels, J.G.M., Direct and Large Eddy Simulation of Turbulent Flow in a Cylindrical Pipe Geometry, *Ph.D. Thesis, Delft University of Technology*, Delft University Press, **1994**.
- [Egg95a] Eggels, R.L.G.M., Goey de, L.P.H., Mathematically Reduced Reaction Mechanisms Applied to Adiabatic Flat Hydrogen/air Flames. *Combust. and Flame*, **100**:559 (**1995**).
- [Egg95b] Eggels, R.L.G.M., Goey de, L.P.H., Modeling of Burner-Stabilized Hydrogen/air Flames using Mathematically Reduced Reaction Schemes, *Combust. Sci. and Tech.* **107**, 1-3, p. 165 (**1995**).
- [Egg95c] Eggels, R.L.G.M., Louis, J.J.J., Kok, J.B.W. and Goey de, L.P.H., Comparison of Conventional and Low-Dimensional Manifold Methods to Reduce CO/H_2 -air Mechanisms for Turbulent Flame Modeling *Submitted to Chemical Engineering Science* **1995**.
- [Egg95d] Eggels, R.L.G.M., Goey de, L.P.H., Post-Processing Method for Predicting NO Formation in One- and Two-Dimensional Premixed Methane/air Flames, *Submitted to Combustion and Flame*, **1995**.
- [Egg95e] Eggels, R.L.G.M., Goey de, L.P.H., Formation of NO in One- and Two-Dimensional Laminar Premixed Methane/air Flames using Complex Reaction Schemes. *Proc. Third International Conference on Combustion for a Clear Environment, Lisbon, 1995*, p. 28.4.
- [Fen71] Fenimore, C.P., Formation of Nitric Oxide in Premixed Hydrocarbon Flames., *Thirteenth Symposium (International) on Combustion*, The Combustion Institute, **1971**, p. 373.
- [Gei94] Geist, G.A., Beguelen, A., Dongarra, J.J., Weicheng, J., Manchek, R., and Sunderam, V.S., *PVM User's Guide and Reference Manual*. Technical Report ORNL/TM-12187, Oak Ridge National Laboratory, September **1994**.
- [Gla92] Glarborg, P., Lilleheie, N.L., Magnussen, B.F., Kilpinen, P. and Hupa, M., A Reduced Mechanism for Nitrogen Chemistry in Methane Combustion, *Twenty-fourth Symposium (International) on Combustion, The Combustion Institute*, **1992**, p. 889.
- [Goe95] Goey de, L.P.H., Somers, L.M.T., Bosch, W.M.M.L. and Mallens, R.M.M., Modeling of the Small Scale Structure of Flat Burner-Stabilized Flames, *Combust. Sci. and Tech.* **104**, 4-6, p. 387, (**1995**).
- [Gou92] Goussis, D.A., Lam. S.H., A Study of Homogeneous Methanol Oxidation Using CSP. *Twenty-Fourth Symposium (International) on Combustion*. The Combustion Institute, Pittsburgh, **1992**, p. 113.
- [Ive73] Iverach D., Basden K.S. and Kiron, N.Y., Formation of Nitrogen Oxide in Fuel-lean and Fuel-rich Flames, *Fourteenth Symposium (International) on Combustion, The Combustion*

Institute, Pittsburgh, **1973**, p. 767.

[Jan 82] Janicka J., Kollmann W., The Calculation of Mean Radical Concentrations in Turbulent Diffusion Flames. *Combust. Flame*, **44**:319 (1982).

[Kee85] Kee, R.J., Grcar, J.F., Smooke, M.D. and Miller, J.A., A Fortran Program for Modeling Steady Laminar One-Dimensional Premixed Flames, *Sandia Report SAND85-8240*, Sandia National Laboratories, Livermore, CA 94550, **1985**.

[Kee91] Kee, R.J., Rupley, F.M. and Miller, J.A., The Chemkin Thermodynamic Data Base, *Sandia Report SAND87-8215*, Sandia National Laboratories, Livermore, CA 94550, **1989**.

[Lam88] Lam, S.H., Goussis, D.A., Understanding Complex Chemical Kinetics with Computational Singular Perturbation, *Twenty-Second Symposium (International) on Combustion*. The Combustion Institute, Pittsburgh, **1988**, p. 931.

[Lan92] Lange, H.C., Modelling of Premixed Laminar Flames., *Ph.D. Thesis*, Eindhoven University of Technology, **1992**.

[Lin92] Linan, A., Williams, F.A., *Fundamental Aspects of Combustion*, Oxford University Press, Oxford (1992).

[Maa89] Maas, U., Pope, S.B., Simplifying Chemical Kinetics: Intrinsic Low-Dimensional Manifolds in Composition Space. *Combust. Flame*, **88**:239 (1992).

[Maa92] Maas U., Pope, S.B., Implementation of Simplified Chemical Kinetics Based on Low-Dimensional Manifolds., *Twenty-Fourth Symposium (International) on Combustion*. The Combustion Institute, Pittsburgh, **1992**, p. 103.

[Maa94] Maas, U., Pope, S.B., Laminar Flame Calculations Using Simplified Chemical Kinetics Based on Intrinsic Low-Dimensional Manifolds. *Twenty-Fifth Symposium (International) on Combustion*. The Combustion Institute, Pittsburgh, **1994**.

[Mal95] Mallens, R.M.M., Lange de H.C., Ven van de, C.H.J. and Goey de, L.P.H, Modeling on Confined and Unconfined Laminar Premixed Flames on Slit and Tube burners, *Combust. Sci. and Tech*, **107**, 4-6, p. 387 (1995).

[Mav94] van Maaren, A., One-step Chemical Reaction Parameters for Premixed Laminar Flames. *Ph.D. Thesis*, Eindhoven University of Technology, **1994**.

[Mil89] Miller, J.A. and Bowman, C.T., Mechanism and Modeling of Nitrogen Chemistry in Combustion, *Prog. Energy Combustion Sci*, **1989**, Vol. 15, p. 287.

[Pet87] Peters, N., Williams, F.A., The Asymptotic Structure of Stoichiometric Methane-Air Flames. *Combust. Flame* **68**:185 (1987).

[Pet92] Peters, N., *Lecture Notes of Ercoftac Summer School on Laminar and Turbulent Com-*

bustion. Aachen, **1992**.

[Pet93] Peters, N. and Rogg, B., *Reduced Kinetics Mechanisms for Applications in Combustion Systems*, Springer Verlag, **1993**.

[Pop93] Pope, S.B., Maas U., Simplifying Chemical Kinetics: Trajectory-Generated Low-Dimensional Manifolds, *Cornell Report FDA 93-11*.

[Rie94] Riedel, U., Schmidt D., Maas U., Warnatz J., Laminar Flame Calculations Based on Automatically Simplified Kinetics. *Proceedings Euroterm Seminar No. 35, Compact Fired Heating Systems and Fourteenth Journées d'Etudes of the Belgium Section of the Combustion Institute*, **1994**

[San94] Sanders, J.P.H., Scalar Transport and Flamelet Modeling in Turbulent Jet Diffusion Flames. *Ph.D. Thesis, Eindhoven University of Technology*, **1994**.

[Soe74] Soete G.G., Overall Reaction Rates of NO and N_2 Formation From Fuel Nitrogen, *Fifteenth Symposium (International) on Combustion, The Combustion Institute*, **1974**, p. 1093.

[Som94a] Somers, L.M.T., The Simulation of Flat Flames with Detailed and Reduced Chemical Models. *Ph.D. Thesis, Eindhoven University of Technology*, **1994**.

[Som94b] Somers, L.M.T., Analysis of a Systematical Reduction Technique, *Twenty-Fifth Symposium (International) on Combustion*. The Combustion Institute, Pittsburgh, **1994**.

[Som95] Somers, L.M.T. and Goey de, L.P.H., A study of a Premixed Slit Burner, *Combust. Sci. and Tech*, **108**, 1-3, p.121, **1995**.

[Smo91] Smooke, M.D., Reduced Kinetics Mechanisms and Asymptotic Approximations for Methane Air Flames, *Lecture Notes in Physics*, Springer Verlag, **1991**.

[Str84] Stehlow, R.A., Combustion Fundamentals, *McGraw-Hill Book Company*, New York, **1994**.

[Ten72] Tennekes, H. & Lumley, J.L., *A first course in turbulence*. MIT Press. **1972**.

[Thi90] Thiart, G.D., Finite Difference Scheme for the Numerical Solution of Fluid Flow and Heat Transfer Problems on Nonstaggered Grids, *Numerical Heat Transfer Part B*, vol. **17**, p 43 **1990**.

[Wil92] Williams, A., Woolley, R. and Lawes M., The Formation of NO_x in Surface Burners. *Combust. Flame*, **89**:157 (**1992**).

Acknowledgements

During the research I performed the last four years at the Faculty of Mechanical Engineering (WOC) at the Eindhoven University of Technology, I could rely on the support of many people. I want to thank all these people at TUE, UT and KUN. However, some people I would like to thank in particular.

In the first place, I thank my copromotor Philip de Goey, whose support has been essential in order to perform the research as presented in this thesis. I also thank my colleagues, Rick de Lange, Peter Sonnemans, Bart Somers, Arjen van Maaren, Peter Bouma and Roel Mallens. They did not only share the same room in good and bad times, but also made computer codes and results of computations and measurements available, which made it possible to develop the reduction methods within relatively short time and provided experimental data for comparison.

Furthermore, I thank the members of my promotion committee, prof.ir. Nieuwenhuizen, prof.dr. Mattheij, prof.dr. D.J.E.M. Roekaerts and prof.dr. ir. M.E.H. van Dongen for carefully studying my thesis and useful suggestions.

I'm grateful that I had some discussions with dr. Ulrich Maas (University of Stuttgart and presently in Berlin), who could help me in several minutes more than other people in hours.

Finally, I want to thank drs. Jules Spaanjaars and dr. J.J. ter Meulen who made it possible to perform radical and temperature measurements in flames using LIF and LIPF techniques. Unfortunately, it was not possible to present these results in this thesis, as the last results, which are very promising, were obtained recently.

Curriculum Vitae

My name is Rudolf Leonardus Gerardus Maria Eggels and I am born on 30 July 1967 in Wessem. I went to primary school in Neer. Then I followed secondary school (Scholengemeenschap St. ursula) in Horn, where I graduated in 1984 for HAVO and in 1986 for VWO. From 1986 till 1991 I studied at the faculty of physics at the Eindhoven University of Technology. The last year I spend at the section of Transport Physics, where I studied the dynamical behaviour of the permeability and tortuosity of porous media supported by dr.ir. M.E.H. van Dongen. On June, 26, 1991 I graduated, receiving the title of Master of Physics. In September 1991 I started my Ph.D. research in the group of Laminar Combustion at the Faculty of Mechanical Engineering of the same University. Finally, I decided to move to Eindhoven, spending more time on combustion of gas in theory and laboratory conditions than on the road. I appreciate the opportunities I got to attend courses in Aachen (Germany, 1992) and Aussois (France, 1993) and to present results and meet colleagues at conferences in Sydney (Australia 1992), Lissabon (Portugal, 1993), Garmisch Partenkirchen (Germany, 1993), Irvine (U.S.A., 1994), Lissabon (Portugal, 1995), San Francisco (U.S.A., 1995) and Delft (The Netherlands, 1995).

Stellingen

behorende het proefschrift van

R.L.G.M. Eggels

Modelling of Combustion Processes

and NO Formation with

Reduced Reaction Mechanisms

1. De introductie van een compositieruimte maakt het mogelijk om door middel van een eigenwaarde analyse van de chemische bronterm van een reagerend systeem, deze op te splitsen in deelruimten corresponderend met snelle en langzame processen.
Hoofdstuk 2, dit proefschrift.
2. Het ontkoppelen van vlamberekening en NO vorming levert een grote verlaging van de rekentijd op, terwijl de berekende NO concentraties weinig afwijken van gedetailleerde berekeningen.
Hoofdstuk 4, dit proefschrift.
3. Hoewel de Mathematische Reductie Techniek als de meest nauwkeurige reductie methode voor reactiemechanismen beschouwd kan worden, zijn Conventionele Reductie Methoden voor sommige toepassingen meer geschikt.
Hoofdstuk 4, dit proefschrift.
4. Toepassing van de Mathematische Reductie Techniek leidt tot een essentiële verlaging van de rekentijd indien deze toegepast wordt in twee- en drie-dimensionale geometrieën. De tijd die nodig is om de Intrinsiek Laag-Dimensionale Deelruimten te bepalen is dan een fractie van de rekentijd voor de modellering voor het verbrandingsproces.
5. Experimenteel kan geen onderscheid gemaakt worden tussen thermische en prompt NO. Numeriek kan dit wel, de resultaten zijn echter sterk afhankelijk van het gebruikte reactiemechanisme.
6. Dikwijls wordt over NO_x gesproken terwijl eigenlijk alleen NO bedoeld wordt.
7. Het prompt NO mechanisme wordt vaak verwaarloosd. De rechtvaardiging hiervoor is meestal moeilijk te achterhalen.
8. Hoewel tabellering van gereduceerde reactiemechanismen gebruikelijk is voor de modellering van turbulente verbrandingsprocessen, wordt het toepassen van deze tabellen voor de modellering van laminaire verbrandingsprocessen in het algemeen sceptisch bekeken.
9. Het verlagen van de milieubelasting wordt als een goede reden beschouwd om snelheidsbeperkingen voor personenauto's in te voeren. Het verhogen van de maximale snelheid voor treinen en daarmee ook het energieverbruik, wordt echter niet als een probleem voor het milieu gezien.
10. Het zelf bedenken van een methode om een probleem op te lossen levert meer inzicht op en is vaak efficiënter dan toepassing van standaard methoden.
11. Het met overtuiging presenteren van een onvoldoende gefundeerde mening leidt slechts tot onbegrip in plaats van duidelijkheid.